The use of novel digital power supply to drive laser systems.

Doneddu, Daniele

The use of Novel Digital Power Supply to Drive Laser Systems

Daniele Doneddu

Submitted to the University of Wales in fulfillment of the requirements of the Degree of Doctor of Philosophy

Swansea University

2010

Abstract

Light-based therapies are becoming increasingly important and widely applied within the clinical practice. Their advantages over more traditional therapies have created an expanding market which is driving the development of more efficient and sophisticated devices. These devices allow a more precise control of the characteristics of the optical output to maximise benefits of the treatment. Although many studies have been conducted on light, and more specifically lasers, both from a therapeutic and a technological perspective, there is still much research to be undertaken. Laser systems have been used for more than two decades for the treatment of vascular lesions. Indeed the application of selective photothermolysis utilising the monochromaticity of the laser system has become the treatment of choice. However the treatment of larger blood vessels remains problematic. Many workers have, for theoretical and clinical reasons, elected to choose the YAG laser for the treatment of larger thread veins and vascular lesions containing larger vessels. The therapeutic output has been mixed and the need for further work identified.

This thesis describes the design of a novel approach to the control of the temporal profile of the YAG laser. The design aspect of the work includes a computer modelling study which shows that careful control of the temporal parameters can in principle improve the therapeutic output. A novel approach to the digital control of the flashlamps pumping the YAG crystal is also described. The digital control of the flashlamp translates to sensitive control of the temporal profile of the laser output in a way that has not been described to date. The thesis therefore concludes that control of the temporal output of the YAG laser, if possible, should give improved therapeutic output and that the necessary level of control can be achieved by advanced digital

techniques. Future clinical work should prove improved therapeutic results.

Declarations

DECLARATION

This work has not previously been accepted in substance for any degree and is not being concurrently submitted in candidature for any degree.

Signed..... (Candidate)

Date 10/09/2010

STATEMENT 1

This thesis is the result of my own investigations, except where otherwise stated. Where correction services have been used, the extent and nature of the correction is clearly marked in a footnote(s).

Other sources are acknowledged by footnotes giving explicit references. A bibliography is appended.

Signed..... (Candidate)

Date 10/09/2010

STATEMENT 2

I hereby give consent for my thesis, if accepted, to be available for photocopying and for inter-library loans ~~after expiry of a bar on access approved by the Swansea University.~~

27/09/2010

Signed... (Candidate)

Date. 10/09/2010

Contents

Acknowledgments

I would like to take the opportunity to thank the outstanding individuals I was lucky enough to work with on this research effort: Professor Marc Clement and Dr Mike Kiernan. Their friendship, the precious support throughout the proceedings of this work, the time they have taken off their *über* busy schedule and the many interesting discussions we had throughout have marked these years of my life in Wales indelibly. I will never be able to find great enough words to express my gratitude to them.

A special thanks to Professor Kelvin Donne and also to Dr Gwenaelle Daniels, for the invaluable support and the time they have dedicated to me to allow me to carry out the modelling investigations of my work.

A special thanks goes to the guys at CyDen for their help, patience and support during this development work. Amongst them: Kevin, Simon, Gareth. I would also like to thank Dr Caerwyn Ash for his support, especially with regards to aspects relating to the light-tissue interaction and broadband radiation technology.

I would also like to thank Steve Batcup at Swansea University for his helpful advice and support in relation to the circuit aspects of my work. Many thanks also to the guys at the Institute of Life Science at Swansea University for giving me the opportunity to carry out the work in the laboratories.

I cannot forget the support I received from my friend and colleagues especially during the finalisation of this work. Strictly in alphabetical order: Akshay, Bin, Jonny, Louisa, Sarah, Will. Thanks for putting up with my buzzing around like a "blue a***d fly": you are a great bunch,

guys.

And last but not least, my dear family: in *primis*, my "mamma", Maria Assunta, my sister, Giusy, my uncle Vincenzo; and those who are not with us anymore in the flesh, who are looking after us from up there: my father Luigino and my brother Luigi. The encouragement I received and the constant support throughout my life have been invaluable.

And, again, to you all, thanks for everything you have done and still do to make my life great.

Grazie!

List of Figures

List of Tables

Definitions and Abbreviations

AC/DC	Alternating Current / Direct Current
ADI	Alternating Direction Implicit
ANSI	American National Standards Institute
CT	Clinical Trial
DC	Duty-Cycle
DPSU	Digital Power Supply Unit
EMR	Electromagnetic Radiation
EMS	Electromagnetic Spectrum
FWHM	Full-Width Half-Maximum
IPL	Intense Pulsed Light
ISSVA	International Society for the Study of Vascular Anomalities
Kr	Kripton
KTP	Potassium-Titanyl-Phosphate
LASER	Light Amplification by Stimulated Emission of Radiation
MASER	Microwave Amplification by Stimulated Emission of Radiation
MOSFET	Metal-Oxide Semiconductor Field Effect Transistor
NIR	Near-Infrared Light
PDL	Pulsed Dye Laser
PDT	Photo-Dynamic Therapy
PWM	Pulse Width Modulation
PWS	Port-Wine Stain
SH	Strawberry Haemangioma
TDT	Thermal Damage Time
TRT	Thermal Relaxation Time
UV	Ultra Violet
Xe	Xenon
YAG	Yttrium-Aluminium-Garnet

Chapter 1

Introduction

1.1 The Laser - A Solution Looking for a Problem

The importance of lasers and their contribution to advancements of science, knowledge and technology within the past 50 years and for the years to come is often overlooked by many. The laser was reported by Townes to have initially been described as "a solution looking for a problem" [17], as initially the scientific community struggled to identify suitable applications: for many applications, it really was only a matter of thinking differently.

As we will see in the following chapters, the fundamental characteristics behind the concept of the laser are substantially shared among the various types of lasers, and lie under solid physics foundations. However, it is possible to distinguish between several families of laser devices, by excitation methods, and the characteristics of the laser medium.

At the heart of the principles governing the operation of lasers lies the process of stimulated emission. The existence of this process had first been theoretically proposed by Einstein in his 1917 paper "Zur Quantentheorie der Strahlung" (On the Quantum Theory of Radiation) [18] as a third process involved in the interaction between matter and radiation (together with the two processes of absorption and spontaneous emission). An overview of the physical processes in order to give a background to the proposed work will be given in chapter 4.1.

A categorisation based upon the type of active medium which is responsible for emitting radiation can identify the following main families of laser [19]

- Gas lasers
- Semiconductor Laser
- Solid-state lasers
- Liquid lasers
- Free-electron lasers
- X-ray lasers

The focus of this work is on Solid-state lasers for medical applications. In this type of lasers, the active medium is a non conductive solid, crystalline material which, as it will be explained in more details in the following chapter, through the incorporation of impurities within the crystal (a process called doping) can allow the emission of laser light. It is this doping species that dictates the spectral properties of the laser. Among the solid state lasers family, rare-earth-doped Yttrium-Aluminium-Garnet (YAG) crystal based laser is the type which has found the widest diffusion, due especially to the favourable properties of the material. By incorporating the element Neodymium as a dopant, we therefore obtain a Nd:YAG laser crystal, which will be used as the active medium in this work.

Technology behind the use and evolution of solid state lasers has been around for almost 50 years now; however there haven't been major developments in the last two decades. Sub systems which constitute the laser system, especially the power supply section and the electrical driving circuitry have not evolved significantly, and until recently, still rely on bulky components with little innovative developments in the control section of the system.

Lasers were initially confined to the laboratory environment, therefore features such as volume, weight and ergonomics were of relatively lower priority. However, soon an incredible number of applications started to flourish. Especially the military sector contributed to boost laser research with significant investments which in turn contributed to advance the knowledge in laser physics and technology. This also resulted in the demand for more compact systems,

which however was initially limited to very low power lasers (primarily finding applications as portable military range finders).

1.2 Applications in Medicine

The use of light for medical purposes dates back to the ancient Egypt, as early as 4000BC, when the use of light was coupled to photo sensitizers to promote pigmentation of the skin in individuals affected by vitiligo [20], whereas the use of light for material processing was described for the first time by Aristophanes in one of his comedies, "The Clouds", in 423 BC. Since then, light has been employed in both fields in a multitude of ways; however, it is not until the laser arrived that it became possible to use optical radiation extensively for therapeutic use.

Since the first appearance of the laser, its use for medical applications has flourished considerably. The first application in medicine dates from 1961, with the use of a ruby laser for eye surgery (specifically, retina reattachment) by Campbell [21], followed by use in dermatology in 1963 by Goldmann [22] [23].

Today, lasers have found applications in the medical field for both diagnostics and therapy, as well as a surgical tool, in applications, especially in dermatology [24] ranging from the treatment of a variety of diseases and cutaneous lesions [25] including vascular and pigmented lesions [26] [27] [28], adult port wine stains (especially through developments of the Pulsed Dye Laser - PDL, see [29] [30] [31]).

Extensive reviews to assess acne scar reduction and short term efficacy of treatments of acne vulgaris using a variety of sources and treatment modalities using both solid state lasers, broadband radiation and Photo-dynamic Therapy (PDT) have also been published [32].

As it will be shown in more detail within the following chapter, the discovery and first description of the mechanism of selective photothermolysis by Anderson and Parrish [33], the ability to selectively remove target structures without disrupting the surrounding skin, made it at least possible to treat areas of the skin to remove for example tattoos without destroying the surrounding skin leaving a scar. Theory predicted that pulse durations in the nanosecond

domain would be optimal for tattoo removal, which allowed for widespread use of the Q-switched Nd:YAG, alexandrite, and ruby lasers. Since then, the use of short pulsed solid state lasers has offered a safer alternative to the treatments thus far employed, such as thermal methods, surgical excision, chemical destruction and laser ablation with Argon or CO2 lasers, all of which methods inevitably give rise to scarring of the tissue treated, often resulting with significant residual tattoo pigments [34].

Therefore, wide spread use of solid state laser appeared for tattoo removal [35] [36] [37] [38] [39] [40]. Especially YAG lasers are effective in cosmetics surgery, for tattoo removal [41]. Dark tattoo pigments, especially blue and black, but also dark brown, effectively absorb the relatively long 1064-nm wavelength, but this radiation is less well absorbed by epidermal melanin pigment than shorter wavelengths. This enables effective treatment of darkly pigmented individuals with less risk of affecting epidermal melanin pigment than shorter wavelengths.

Studies have been published on the use of lasers to treat pigmented skin lesions in pediatric patients [42], and extensive reviews on the subject have been produced recently on port wine stains and hemangioma [43]. New opportunities to improve pediatric skin conditions are offered by new treatment modalities such as photodynamic therapy (PDT) to help avoiding redarkening of the lesions and newer types of lasers, such as pigmented lasers for treatment of pigmented lesions and Erbium fiber lasers for reduction of port wine stains [44].

Continuous wave and long-pulse solid state lasers such as Nd:YAG and Alexandrite are also subject of clinical studies in dermatology, for medical and cosmetic treatments such as hair removal [45] and specific studies and reviews have been published for hair reduction in specific parts of the body, such as, for example, legs [46] or axilla [47]. Clinical trials (CTs) and randomised clinical trials studies and reviews have also been published where solid state lasers are compared with Intense Pulsed Light (IPL) treatments [48]. Particularly, the difficulty and especially the short follow up period of most CTs makes it difficult to evaluate the real efficacy of laser and IPL treatments for the reduction and "'permanent"' reduction of unwanted body hair, as emphasised for example in [49]

Significant applications are also in dentistry, Ear Noise and Throat, gynaecology, endoscopic surgery, ENT, revascularisation, carcinoma therapy, plastic surgery, aesthetic medicine and surgery, sport medicine, medical digital imaging; and new applications are still being developed.

The main field of medical application that developments from this experimental work can help address lies however within the treatment of vascular lesions. Research on lasers, and more specifically on YAG lasers is active in this field, as shown for example by the recent clinical work of Civas and colleagues in [50], reporting efficacy of long-pulsed Nd:YAG laser treatment in a variety of vascular lesions.

In sum, the importance of lasers in the medical field is growing, as clinicians are embracing and supporting the application in the laboratory as well as pre-clinical and clinical trials of laser radiation for an ever increasing number of diseases. This phenomenon in turn is boosting the technological development of laser systems to equip the clinician with tailored and flexible solutions to more effectively target diseases.

The principles underlying the use of optical radiation in medical fields of relevance are explained in 1.3.

1.3 An Innovative Approach

As previously stated, Nd:YAG based laser systems, as well as other solid-state lasers, have however traditionally been cumbersome and bulky. The electronics, and the energy storage and delivery section of the power supply in particular, have evolved very little. Means of accommodating temporal variations of the laser output to achieve flexibility have traditionally relied upon employing and switching between a multitude of energy storage components within an electrical switching network, which leads to an heavy and voluminous system. Controllability in the time domain has traditionally been overlooked, in favour of achieving shorter pulses, and higher peak power.

Recent developments [51] in the power supply technology to drive Intense Pulsed Light (IPL)

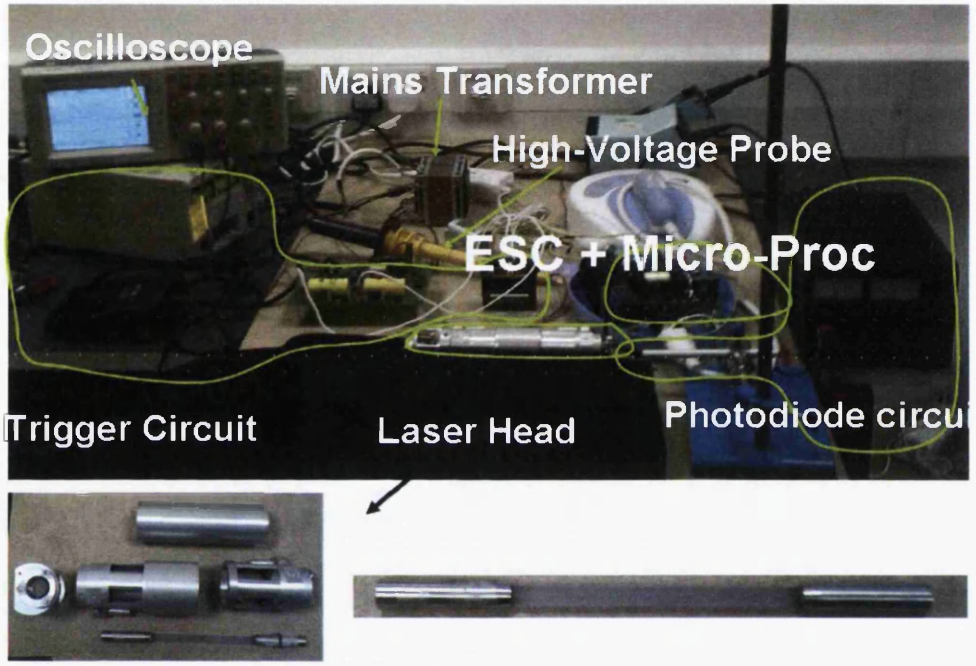

Figure 1.1: An experimental setup for laser measurements; the components are outlined in the picture

devices offer now the possibility of a step change in the approach and methodology of design to solve issues related to achieving control of lasers.

This work postulated and aims at demonstrating a novel method of controlling the output of a Solid-state laser for use in medical applications. Through digital control of the optical device used to provide the energy to the lasing medium (a so called laser pump), it will be shown that a controllable laser output can be achieved within a compact, efficient, flexible low-cost system to serve as a proof of concept.

The importance of this work lies in the novel approach that has been taken to solve the problem common to most traditional flashlamp-driven Nd:YAG laser systems, that being a fine

control of the laser pulse shape whilst avoiding multiplication of circuit elements and therefore considerably saving weight and volume. Compact units can be devised which can make use of extensively tested traditional components (flashlamps, capacitor, switch-mode power supply)

There are various reasons why the control of a laser pulse is of great importance from both technological and medical viewpoints, as it will be explained in the following two subsections.

1.3.1 The technology perspective

From a technology viewpoint, achieving a fine control of the temporal profile allows for a more compact system, as it removes the need for inclusion of several bulky components such as Capacitors of different values to accommodate for the different durations of pulses and energies of a laser pulse and gives inherent flexibility for developing the concept to provide diagnostic and therapeutic tools.

1.3.2 The medical perspective

From a medical viewpoint, the following considerations are relevant. Human tissues are complex media, whose characterisation, response to and interaction with radiative processes is still subject of active research, both from a modelling and medical viewpoints. In the next chapter, the interactions between light - and lasers specifically, and tissues will be detailed. However, in order to introduce the topic, the following considerations can be advanced.

Light is a form of electromagnetic radiation (EMR) which falls within the visible spectrum. When radiation is directed to a homogeneous medium, it will experience reflection and transmission to some extent, due to the difference in refraction index between air and the medium. Irregularities in the surface may also generate scattering and increase reflection. Within a complex medium such as tissue, due to inhomogeneities, radiation will also experience scattering and multiple internal reflections which will therefore influence its penetration through the tissue. In sum, mechanisms of:

- reflection

- scattering
- absorption by structures within the tissue
- transmission

happen when radiating a living tissue.

The way radiation interacts with a given living tissue is in first approximation a function of the wavelength of the radiation. Reflection and scattering, together with the absorption behaviour of matter are primarily important in diagnostics. From a clinical and therapeutic point of view, absorption - which consists in the transformation of radiant energy in to another form of energy, usually heat, or acoustic energy, or molecular excitation - mechanisms are of great importance, together with parameters such as exposure time and effective power density applied to a tissue with a specific absorption. Interaction therefore is intimately linked to the mechanism of absorption, and it's shown through specific absorption spectra. However, as it will be shown in the following chapters, the penetration depth of incident radiation is influenced by the scattering of light.

From the definition of absorption, therefore, it is implied that when a radiation of appropriate wavelength is applied to a tissue, the tissue will respond by exhibiting variations in temperature, thermacoustic effects, or molecular vibrations, which then revert back to the original level according to a characteristic relaxation curve, characterised by a coefficient which varies according to each tissue and other factors.

To be able to precisely control shape and duration of a laser pulse allows for the ability to precisely control at each moment the amount of energy delivered to tissues, and to change it accordingly to the desired interaction with the tissue. In this way, it is possible to ensure that, for example:

- if pain threshold is exceeded, pain is kept to a level which is bearable by the patient,
- permanent damage is not caused to the surrounding tissue, etc.

whilst ensuring that the right amount of useful radiation is administered to the area to be treated.

The next chapter will expand on the rationale for this work from the medical perspective. Specifically, the therapeutic area of choice - blood vessels and associated vascular lesions, together with outlined laser-tissue interaction mechanisms will be described.

1.4 The Research Question

This thesis addresses a research question which is split into two parts:

- Can the accurate control of the temporal profile of a YAG laser in principle deliver improved therapeutic benefit when analysed theoretically?
- Can the necessary level of control of the optical output of the YAG laser be achieved utilising sofisticated digital control techniques?

Chapter 2

The Medical Need

2.1 Introduction

In this chapter the medical needs for the development work undertaken within this thesis will be detailed, following on from the previous chapter. The chapter will start with providing background on the basic light-tissue interaction phenomena, with emphasis on those tissues specifically related to this work. The following sections will then describe the specific field of operation of the proposed technology outlining the use of the specific technology as a therapeutic medium within the aforementioned therapeutic field. Finally, initial concepts of the technology in relation to the therapeutic field outlined will serve as a introduction to the subsequent chapter.

2.2 The Human skin

Skin is the surface layer of tissue surrounding the human body [2]. It is the body's largest organ, and it protects tissues from variation in temperature, water, micro-organisms and physical damage. The skin has 3 main layers; the epidermis, the dermis and the subcutaneous layer (superficial fascia). These all protect and regulate the body's temperature as well as store water, fat and vitamin D. The sense of touch, pain, heat and cold are all networked through this complex surface layer to the central nervous system.

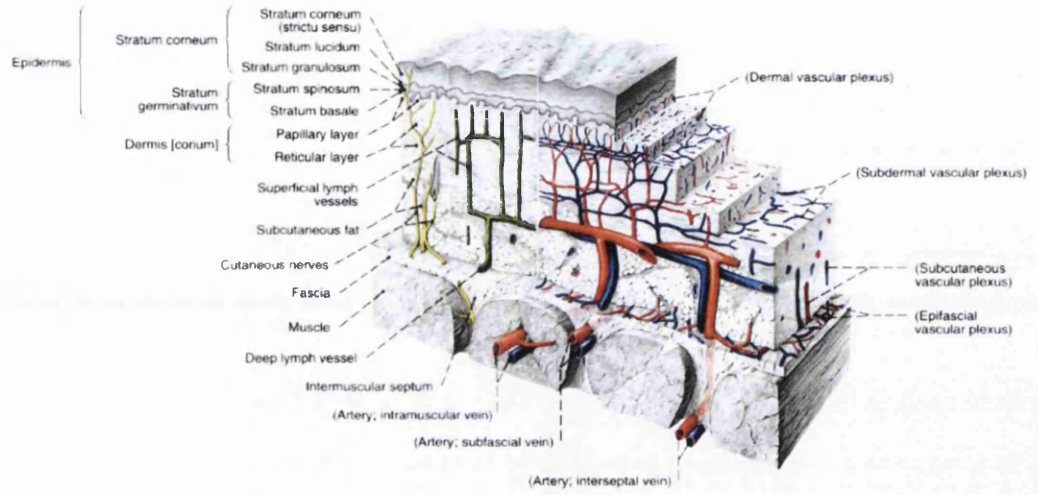

Figure 2.1: Section of skin. Mag. 10X (From [1])

2.2.1 Epidermis

The epidermis is the outermost layer of the skin; it forms the waterproof, protective wrap over the body's surface. The epidermis is a thin avascular layer composed of cells containing keratin in different stages of growth and degeneration. The presence or absence of this layer, by use of micro dermabrasion or exfoliation, dramatically alters the amount of light necessary to create change in the layers below the epidermis. Therefore, Tretinoin therapy or micro dermabrasion, like other similar methods that remove or thin the horny layer, compensates for a reduction in light energy due to the reduction in optical resistance and scattering of ageing or photo damaged skin. The epidermis is broken down into five layers, stratum-corneum, stratum-lucidum, stratum-granulosum, stratum-spinosum, and the stratum-germinativum also called stratum-basale. The first challenge of light transmission is successful penetration of these first 5 layers of the epidermis without stimulating the tissue or losing a significant amount of energy. Each of the 5 layers produces unique obstacles, however the most difficult layer for visible light to penetrate is the keratinized horny layer commonly known as the stratum-

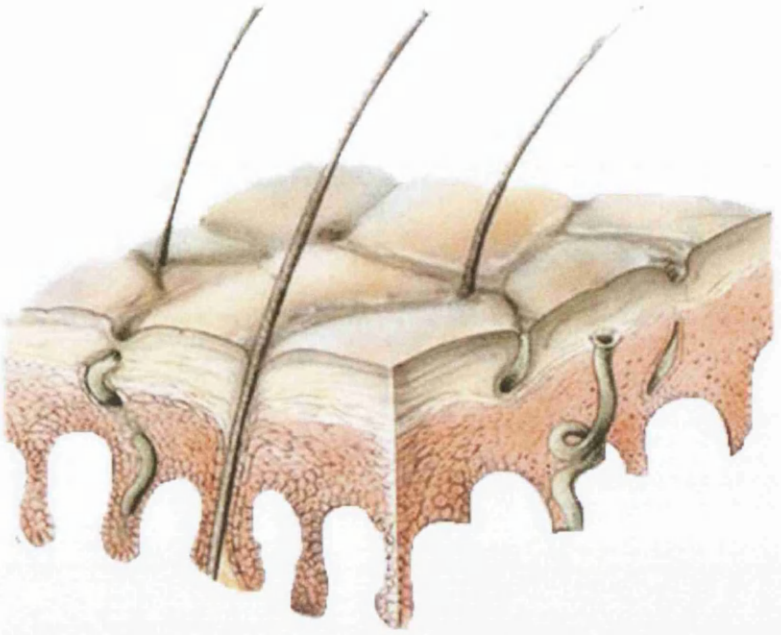

Figure 2.2: The epidermis is the upper or outer layer of skin. The deepest part of the epidermis contains melanocytes. These cells produce melanin, which gives the skin its colour. (image source: www.scf-online.com)

corneum. Melanin production responds to ultra violet exposure and gives us our intrinsic skin colour and the degree of tan on our skin. Melanocytes reside in the basal layer of the epidermis. These dendritic cells make up about one in ten of the cells in this layer, and are in contact via their dendrites with about 30 surrounding keratinocytes. Melanocytes produce melanosomes, which travel along the dendrites carrying melanin granules and drop them off, via synapses onto surrounding keratinocytes, where they enter the cell and sit over the nucleus protecting it from ultra violet (UV) light. The stratum corneum is produced by the transformation of epidermis and, for reasons of simplification; the optical coefficients of the epidermis and stratum corneum are regarded as the same.

2.2.2 Dermis

The dermis is the layer of skin beneath the epidermis that consists of connective tissue and cushions the body from stress and strain. The dermis is tightly connected to the epidermis by a basement membrane. It also harbors many nerve endings that provide the sense of touch and heat. It contains the hair follicles, sweat glands, sebaceous glands, apocrine glands and blood vessels. The blood vessels in the dermis provide nourishment and waste removal to its own cells as well as the stratum basal layer of the epidermis.

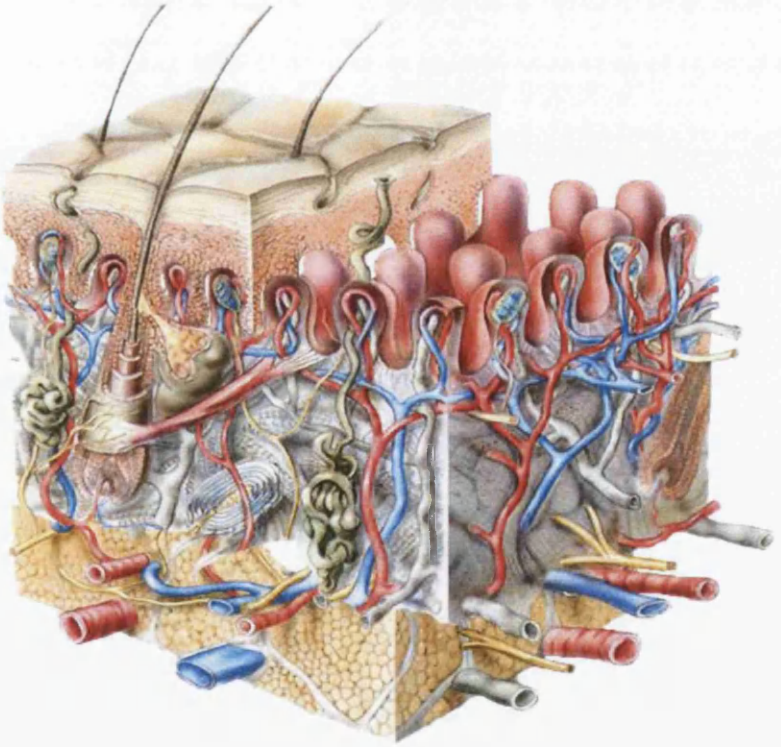

Figure 2.3: The dermis is below the epidermis that make up human outer skin. The dermis contains blood vessels, lymph vessels, hair follicles, and glands that produce sweat. (image source: www.scf-online.com)

The dermis area contains the targets for the light in hair removal application, namely the bulb of the hair follicle and the matrix. The dermis consists of fibrous collagen mixed with

elastin fibers that support the epidermis. Fibers give skin its pliability as well as its ability to return to normal state after deformation. Hyaluronic acid (glucoseaminoglycans) are present throughout the entire dermis, and fill the space between the other skin structures. This gel like substance accounts for the skin's ability to accommodate changes in body weight and size. Often the target sought is in the central layers of the dermis, below the optically translucent layers of the epidermis and above the support structures of the subcutaneous layer.

2.2.3 Subcutaneous tissue

The subcutaneous layer of the skin lies beneath the dermis and is composed primarily of adipose fat cells. It serves as mechanical and thermal protection to the body.

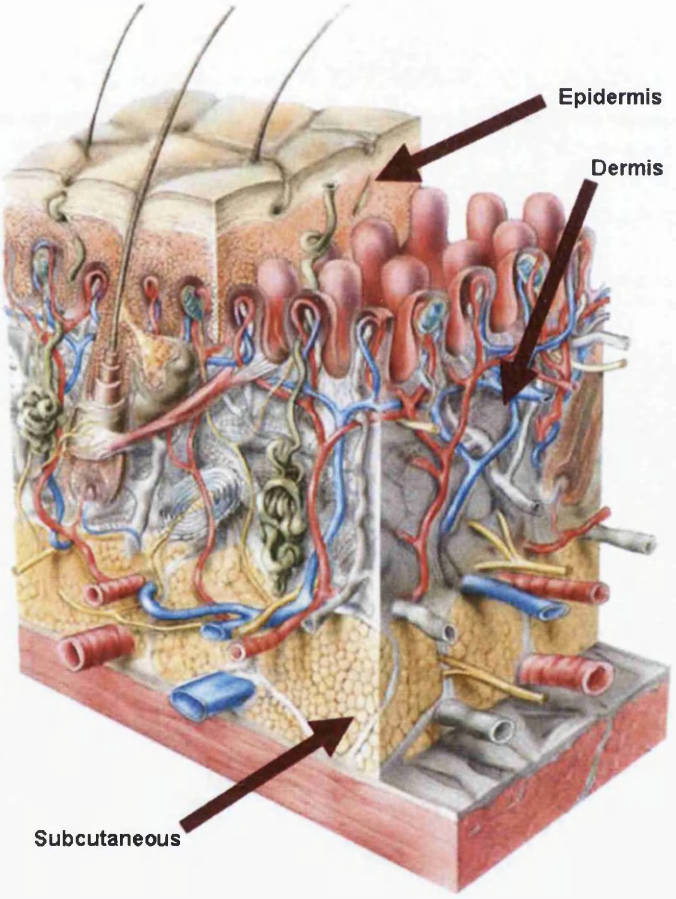

Figure 2.4: The subcutaneous tissue is a layer of fat that lies between the dermis of the skin and underlying fascia. (image source: www.scf-online.com))

Correct wavelength selection will seek an ideal target and not affect the deep subcutaneous layer, this choice will affect penetration depth and amount of forward scattering involved as the subcutaneous fat is assumed to diffuse all visible light because there are no relevant chromophores in subcutaneous fat.

2.2.4 Fitzpatrick Scale

In 1975 a Harvard Medical School dermatologist, Thomas Fitzpatrick, developed the Fitzpatrick Classification Scale for skin types. This scale classifies a person's complexion and their tolerance of sunlight. It is used by dermatologists and beauty therapists to determine how skin will respond or react to UV light exposure.

Skin Type	Ethnicity	Description
I	Caucasian:	Very light complexion, light eyes, freckles, usually blonde or reddish hair colour.
II	Caucasian:	Light complexion, light eyes, occasional to frequent freckles, blonde, reddish, light brown hair colour.
III	Darker Caucasian, light Asian:	Medium complexion, light to dark eyes, hair colour usually brown to dark.
IV	Mediterranean, Asian, Hispanic:	darker complexion, dark eyes, dark brown to black hair colour.
V	Middle Eastern, Latin American, light-skinned black, Indian:	Dark complexion, dark eyes, usually black hair colour.
VI	Dark-skinned black:	Black complexion, black eyes, black hair colour.

Table 2.1: Describes the 6 skin types known as the Fitzpatrick skin type classification. This classification denotes 6 different skin types, on skin colour, and reaction to sun exposure.

Skin type is often categorized according to the Fitzpatrick skin type scale which ranges from very fair (skin type I) to very dark (skin type VI). The two main factors that influence skin type and the treatment program devised for laser or IPL treatment are:

1. Genetic disposition - Skin Types I to III should add one Fitzpatrick level when you have blood relatives with darker skin type IV or higher.

2. Reaction to sun exposure and tanning habits.

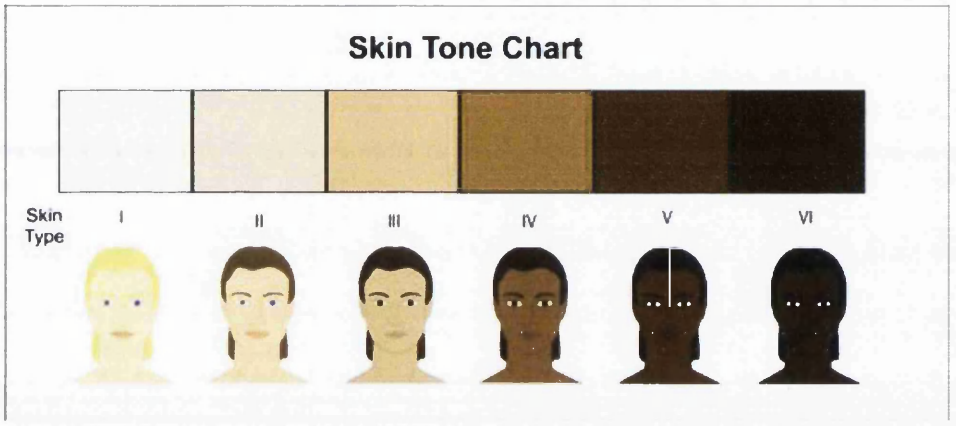

Figure 2.5: A visual representation used for categorising Skin types I-VI.

Skin type is determined genetically and is one of the many aspects of overall appearance, which also includes colour of eyes, hair, etc. The way skin reacts to sun exposure is the important factor in correctly assessing your skin type. Recent tanning (sun bathing, artificial tanning or tanning creams) has a major impact on the evaluation of skin colour. People often confuse Fitzpatrick with active sun tan, however Fitzpatrick skin type is determined at birth and does not change through lifespan, but the degree of tan can change.

2.3 Vascular Lesions

2.3.1 Vascular Lesions

Vascular lesions, and more specifically those that could be treated with a non-invasive procedure - cutaneous vascular lesions, can constitute a significant source of psychological distress especially if they occur within visible (un-covered) areas of the skin [6] [52].

A classification is useful, for the purposes of understanding and guiding the choice of the most appropriate laser - or combination thereof, and laser settings to be used for treatment.

The International Society for the Study of Vascular Anomalies (ISSVA) recently adopted a classification scheme, clearly separating vascular tumours (hemangiomas of different types) which result from active cell proliferation, from vascular malformations, which are inborn defects in vascular morphogenesis. These two types of lesions have different clinical behaviour and require different diagnostic and therapeutic strategies [53] [54]. Criteria that can be used for classification can encompass composition and structure of the lesion well as its natural history and evolution. Perhaps the most useful classification system is based on the characteristics of the endothelium. Vascular lesions can be either congenital or acquired [55].

Congenital lesions can be subdivided in to:

- hemangiomas (with endothelial cell hyperplasia)
- vascular malformations (with normal endothelial cell turnover and variable degree of vessel ectasia)

Of these, Port Wine Stains (PWS) are the most common type of congenital vascular malformations. Hemangiomas, and Infantile hemangiomas are the most common tumor of infancy. They are a uniquely dynamic form of "birthmarks", as they are absent or barely evident at birth and develop within few weeks to months of life. The involution phase normally lasts several months to years [56].

Acquired vascular lesions of interest to laser therapy and characterised by vessel ectasia are:

- telangiectasias

- spider and cherry angiomas
- venous lakes
- leg vein abnormalities

Although abnormalities can obviously occur in any component of the vascular system, the area of primary interest is where the malformations in the vessels are visible or impact on the upper layers of the skin surface, i.e in the deep or superficial plexus.

The vessels in the plexus principally consist of the smaller distributing arteries, arterioles, capillaries, venules and veins, along with the associated meta-arterioles and shunts. Figure 2.6 shows the vascular structure of the skin. The function of the plexus is both to supply the tissues with nutrients and to maintain the thermal stability of the body.

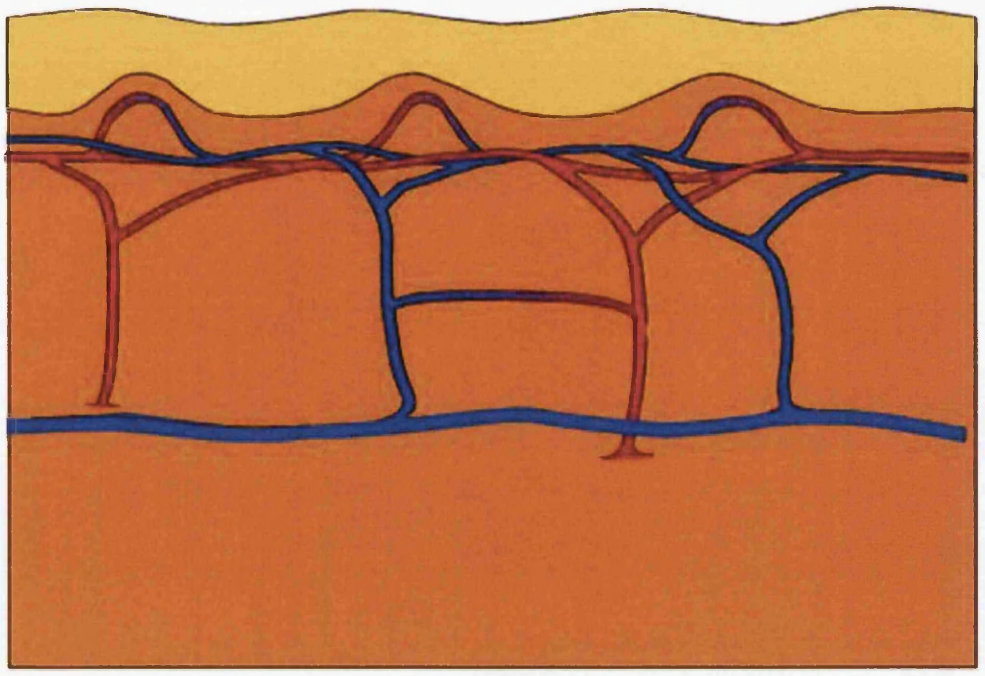

Figure 2.6: The vascular structure of skin.

Opening and closing the pre-capillary sphincters, in conjunction with the operation of the shunts, regulates the amount of blood distributed to the capillaries. The skin has a complex

network of shunts and meta-arterioles continually varying the amount of blood flowing within the capillary beds. The blood flowing through this network determines the amount of heat given out or retained by the body.

When the body is warm, increasing the blood flow to the skin's capillary beds, known as the superficial plexus, dissipates excess heat. When the body is cold, the pre-capillary sphincters supplying the superficial plexus contract and reduce the amount of blood flow thereby limiting heat loss.

An anomaly occurring within the plexus would typically be manifested as a change in either the normal skin colour or surface appearance. These types of abnormalities are referred to as Vascular Lesions.

In the majority, the commonest types of vascular lesions are not of a serious nature and are not caused by any medical disorder. There are some exceptions where the lesions are secondary indications of an underlying condition or the lesion proliferates to such an extent that it interferes with vital organs. The characterisation of a number of common vascular lesions is given below.

Port-Wine Stains (PWS)

Port-Wine Stains (PWS) are low-flow capillary malformations, primarily occurring in face and neck. Their evolution accompanies the growth of the individual and can lead to formation of nodularity and hypertrophy in adults.

Port-wine-stains (PWS) are manifested as a deep red to purple discoloration of the skin, caused by a malformation primarily in the superficial plexus. Whereas in normal skin the vasculature accounts for approximately 2% of a given volume, in a PWS the vasculature may account for up to 8%. This increase in vascular volume gives the skin in a PWS its characteristic red appearance.

PWS are present at birth and grow proportionally with the individual, i.e. PWS are non-proliferating. There is a rarely seen condition known as 'Acquired Port-Wine Stains' where a lesion identical in appearance to a congenital PWS can form in adulthood. Possible causes for

the formation of acquired PWS have been suggested as mechanical or thermal damage to the skin, excess exposure to sunlight, hormonal imbalances or neurological disorders.

Although PWS are not classified as life threatening and are benign in nature, their cosmetically unsightly appearance can lead to psychological trauma to the sufferer. There are notable exceptions to this where PWS are secondary indications of an underlying condition, an example of this being Sturge-Kalischer-Weber syndrome where the visible superficial lesion overlays a disturbance in the sub-surface vasculature. This is commonly associated with facial lesions and in cases where the periorbital and eyelid regions are involved, there is an increased likelihood of Glaucoma being present. The various syndromes account for approximately 5% of PWS.

In a typical PWS, the skin vasculature does not form correctly, the cause of which is unknown although some authors have postulated that the nerve functions controlling the vessels have not matured correctly. Attempts have been made to characterise the different types of vessel malformation and a number of distinct types have been classified according to how the affected vessel structure differs from the norm, although a single PWS commonly contains more than one type of malformation. The types of PWS range from simply an increased number of normal vessels to dilation of the vessels and thickening of their wall structures. The majority of PWS only affect the superficial plexus however in some cases, complex interconnections between the superficial capillaries and the deeper plexus are seen. Although PWS are non-proliferating, the lesion does have a definite life cycle. At birth, the PWS tend to be light pink to red in colour with the surface of the skin appearing normal in texture. Throughout the ageing of the sufferer, the vessels within the PWS tend to gradually increase in size, becoming more dilated giving the lesion a darker appearance. In middle to old age, the vessels have expanded to such an extent that they protrude upwards appearing as nodules on the skin surface. It has been suggested that as the lesion ages, the supporting collagen structures around the vessels lose their strength, as is normal in ageing, hence allowing the vessels to further dilate.

Strawberry haemangioma

Strawberry haemangiomas (SH) (Fig. 2.7) are not present at birth, tending to appear as a small, pin-head sized spot in the first few weeks of infancy. The SH undergoes a rapid proliferation phase where it will transform into a raised, sponge-like lesion many cubic cm in volume within as little as a few weeks since first appearing. The majority of strawberry haemangioma tend to appear in the head and neck region and themselves do not present a threat to life, however they do have serious secondary implications where the lesion can interfere with vital functions such as vision or respiration. The lesions often ulcerate and bleed leading to risk of infection.

There are two distinct types of SH, capillary and cavernous haemangiomas, although a single lesion may have components of both types. Capillary haemangioma appear as a deep red discoloration and slight raising of the skin surface. Cavernous haemangioma have a deeper component that can raise the skin surface many centimetres and give the skin a blue-red appearance.

Whereas Port-wine-stains are permanent, strawberry haemangioma do undergo spontaneous regression, up to 70% completely disappear before the sufferer reaches 10 years of age, although there are no precursors to indicate which lesions regress or remain. Where the lesion does regress, the affected area can undergo pigmentary changes and scar tissue can remain.

Telangiectasia

There are a number of different forms of telangiectasia, the most common appearance is as a raised, red spot in the order of 1mm in diameter. Figure 2.8 shows a picture of telangiectasia. This is caused by a permanent dilation of existing superficial vessels, either arteriole, capillary or venule. If the primary vessel is a venule or arteriole, in many cases an extensive network of feeding or draining capillaries is also seen giving the lesion a 'spider' like appearance.

This form of lesion is typically non congenital and is relatively benign in nature, often occurring in adolescence or pregnancy, tending to randomly resolve. However, in the case of Osler-Weber-Rendu syndrome, the lesions are hereditary and significant haemorrhaging occurs from the affected areas. This can lead to complications such as infection.

Figure 2.7: Strawberry Haemangioma.

Thread Veins

The term 'thread veins' applies to the form of 'red-linear' telangiectasia found most often on the legs and has a higher incidence of occurrence in females. Thread veins are non-congenital and although being cosmetically unsightly, they are classed as non-threatening. They have a tendency to occur in pregnancy, or have a gradual emergence in middle age and remain for life.

Thread veins are an enlargement of the vessels in the superficial plexus, appearing on the skin as networks of fine red or blue strands up to 2-3mm in diameter. In a relatively small incidence of cases, the overlying thread veins are associated with an anomaly in the deeper plexus.

Figure 2.8: Telangiectasia.

2.4 Traditional Treatments

Prior to the advent of laser therapy for the treatment of vascular lesions, in the majority of instances the lesions were effectively left without any form of intervention. Various therapies were attempted to either remove or disguise the lesion with varying levels of success, and in some cases, the result of the therapy left the sufferer with a significantly deteriorated appearance.

This section will outline the various therapies or treatment modalities that were most commonly attempted.

2.4.1 Camouflage

By applying skin coloured pigments to the surface of the skin, the lesion could be disguised to appear as normal. This is only a temporary measure and is very time consuming. Obviously this only gives acceptable results where the lesion is flat with no raised nodules. Hence generally it is only useful for covering PWS.

2.4.2 Excision

Excision of vascular abnormalities is commonplace where the lesion is endangering vital bodily functions although it is not considered appropriate for purely cosmetic purposes. Therefore this is only a viable option when the lesion involved is of the proliferating haemangioma type.

Excision involves removing the affected area and, if necessary, grafting normal healthy skin onto the excised area. This is a very complex operation and the resultant graft or scar tissue may appear more unsightly than the original lesion.

2.4.3 Radiation Therapy

This is a radical approach and has proved to be of little or no effect. This involves bombarding the lesion with radiation to destroy the vasculature. Cases have been reported where the radiation therapy has induced the formation of skin cancer.

2.4.4 Drug Therapy

The use of drug therapy has been widely used in the treatment of vascular lesions. Strawberry haemangiomas have been successfully controlled via the use of steroids to slow down or stop the proliferation of the lesion. Although this technique is of considerable use, there is the risk of secondary complications affecting body organs when high doses of steroids are used.

The treatment of thread veins with drug therapy is very commonplace and is widely regarded as the treatment of choice for the removal of veins of typically 1mm diameter and above, although it is not suitable for the treatment of varicose veins. By injecting an appropriate compound

directly into the vein, thrombosis is induced locally leading to disruption of the blood flow and ultimately the vein will collapse and no longer be a viable structure. This technique is termed Sclero-therapy.

Most recently, the use of beta-blockers has been proposed and successfully carried out. The effect of the use of drugs such as propanolon (a generic beta-blocker), serendipituously discovered by Laut-Labrze et al. [57] represents the most important discovery in recent times regarding treatment of haemangiomas.

2.5 The Blood Vessel

2.5.1 Introduction to the anatomy of the blood vessel

The human circulatory system is an extremely complex structure estimated to contain approximately 60,000 miles of arteries, veins and capillaries ranging in diameter from 10's of mm to a few microns [58].

The purpose of the circulation system is three fold. Firstly, oxygen- and nutrients-rich blood to be pumped by the heart needs to be transported throughout the human body for it to survive. Diffusion of oxygen and nutrients through the vessel membranes nourishes the bodily tissues and vital organs.

Secondly, the waste products from the normal cellular and overall body metabolism need to be expelled from the body and are therefore absorbed into the blood stream for disposal.

The third, and often overlooked, function of the circulatory system is thermal regulation of the body. By controlling fluctuation of the blood flow within the skin the amount of heat released or held within the body is influenced [59].

The vessels that constitute the circulatory system vary dramatically depending upon their intended interaction with the body's tissues. In first approximation, we can subdivide the vessels in arteries and veins. Although vessels differentiate substantially one from the other both physiologically and functionally, they all share a basic underlying structure.

The primary differences for all the vessel types is their bore, or lumen, diameter and the construction of the vessel wall. There are a finite number of common building blocks that constitute the vessel wall. However, depending on the function of the individual vessel, all or only some of these blocks are present. The vessel wall consists of three discrete layers (see Fig. 2.9), namely the *Tunica Intima*, *Tunica Media* and the *Tunica Adventitia* [60].

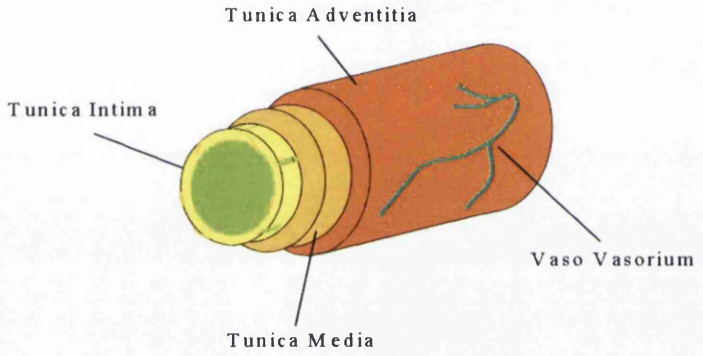

Figure 2.9: Typical vessel structure

Tunica Intima

This is the innermost coating of the vessel wall. The tunica intima of all vessels contains an internal layer of endothelial cells surrounded by the basal membrane. The endothelial cells play a key role in the process of exchange of nutrients from the blood to the surrounding tissues. The basal membrane bonds the endothelial layer to the outer layers of the wall or to the external tissues. The wall of the larger vessels has additional layers of collagen based connective tissues

and an elastic lamina.

Tunica Media

The tunica media consists of two concentric layers of smooth muscle fibres and elastin, a protein based tissue component that is highly flexible. The presence of smooth muscle both strengthens and allows flexibility of the vessel wall. The muscles of the vessel wall have a blood supply of their own, delivered via the Vasa Vasorium, which provides them with the nutrients. The products of the metabolism within the vessel walls are disposed of via the lymphatics system.

Tunica Adventitia

Where present, the tunica adventitia consists of further layers of smooth muscle and connective tissues. Again, if the smooth muscle is present, both the Vasa Vasorium and lymphatics are required. Typically the tunica adventitia is only found within the larger vessels for strengthening and flexibility.

2.5.2 Basic Physiology of the vessel

The walls of the larger vessels are high in elastin and muscle tissue content. This allows these vessels to freely expand under the varying blood pressure during the phases of the heart beat. As the ventricle contracts, the blood is expelled from the heart under high pressure (the systolic pressure) and passes through the largest of the vessels, the aorta. The elastic nature of the aorta allows it to expand and allow the increased blood to pass through unrestricted. When the ventricle relaxes, the blood pressure drops accordingly and the aorta recoils. This recoil of the aorta has the effect of maintaining the blood pressure at a suitable level (known as the diastolic pressure).

The arteries that distribute the blood to the various parts of the body have a different wall structure to the large aorta. The amount of blood required by the body organs and extremities varies constantly, therefore a method of controlling this blood flow is incorporated into the

Vessel Name	Bore Diameter	Wall Thickness	Tunica Intima	Tunica Media	Tunica Adventitia
Elastic Artery (Aorta)	**25mm**	**2mm**	Endothelium Basal lamina Elastic lamina Smooth muscle	Elastic lamina Smooth muscle Vasa Vasorium	Elastic fibres Collanogenic fibres Vasa Vasorium Lymphatics
Muscular Artery	**4mm**	**1mm**	Endothelium Basal lamina Elastic lamina	Smooth muscle (Multiple layers) Elastin Elastic lamina	Elastic fibres Collanogenic fibres Vasa Vasorium Lymphatics
Arterioles	**30μm**	**6μm**	Endothelium Basal lamina Elastic lamina in larger arterioles	Smooth muscle Elastic lamina in larger arterioles	Elastic fibres Collanogenic fibres
Meta-arterioles	**10μm**	**2μm**	Endothelium Basal lamina	Smooth muscle - discontinuous	Traces of connective tissue
Capillaries	**8μm**	**0.5μm**	Endothelium Basal lamina	Absent	Traces of connective tissue
Venules	**20μm**	**1μm**	Endothelium Basal lamina	Absent in small venules Single layer of smooth muscle	Collanogenic fibres
Veins	**5mm**	**0.5mm**	Endothelium Basal lamina Traces of elastic lamina	Smooth muscle Elastic lamina Smooth muscle Vasa Vasorium	Elastic fibres Collanogenic fibres Smooth muscle Vasa Vasorium Lymphatics
Large Veins (Vena Cava)	**30mm**	**1.5mm**	Endothelium Basal lamina Connective tissue Elastic lamina	Smooth muscle Elastic lamina Vasa Vasorium Lymphatics	Smooth muscle Elastic fibres Collanogenic fibres Vasa Vasorium Lymphatics

Table 2.2: Vessel types and structure

distributing or 'muscular arteries'. The wall of these muscular arteries is constructed from small amounts of elastic material surrounded by layers of smooth muscle. Depending upon the stimulus applied to the wall muscle signalling the amount of blood required by the tissue the vessel is supplying, the effective diameter of the vessel is increased or decreased and the blood flow is varied accordingly.

Prior to entering the smallest of the vessels, the capillaries, the blood pressure must be reduced. This is due to the fact that the relatively thin capillary walls are not able to withstand the blood pressure found within the arteries. A series of vessels known as Arterioles are responsible for reducing the blood pressure to a level which can be safely maintained within the

capillaries. Arterioles are characterised by their relatively thick vessel wall in comparison with their internal bore diameter. The wall is constructed from the normal thin innermost layers surrounded by multiple layers of smooth muscle. These layers of muscle ensure that the blood flow prior to entering the arteriole passes though the small bore without expanding the vessel. This reduction in bore diameter reduces the blood flow.

A second type of arteriole is also present within the circulatory system and is known as a 'meta-arteriole'. These differ from the common arterioles in so much as their wall only consists of a single layer of smooth muscle concentrically surrounding the endothelial and basal lamina at discrete intervals. These muscle bands can locally vary the diameter of the meta-arteriole and hence influence the blood flow through the vessel. The meta-arterioles are direct connections from the arterioles to the venules with multiple connections to the capillary beds. The capillaries are fed via minute valve-like structures, called pre-capillary sphincters, located along the length of the meta-arterioles.

The arteriole and capillary beds can be bypassed further 'up-stream' in the circulatory system via the Arteriovenous Anastomoses (known as Shunts) acting as direct connections from the arteries to the veins. They operate in a method similar to the meta-arterioles and control the flow of blood into the smaller vessels.

Capillaries are the finest, and most extensively distributed, vessels of the circulatory system. The wall structure of capillaries consists of only the endothelial cells and the basal lamina, hence their inability to withstand anything other than the lowest of blood pressures. Although the capillaries are small, the expansive networks and thin wall structures allow for rapid diffusion of essential nutrients and fluids from the blood to the tissues. There are three classifications of vessels, namely continuous, fenestrated and discontinuous. These capillary types differ in the structure of the endothelial layer. The continuous type capillaries are characterised by the very minute intra-cellular gaps in the endothelial layer for the exchange of fluids across the vessel wall. Fenestrated and discontinuous capillaries are characterised by the significant spacing of the endothelial cells. This larger spacing of the cells allows the diffusion of larger protein molecules

and in the case of the bone marrow, liver and spleen tissues, the gaps are large enough for the diffusion of blood corpuscles.

The venules are the first stage in the return path of the blood to the heart, draining blood from both the capillary beds and the meta-arterioles. Venules have a relatively thin wall however the amount of connective tissue in their outer tunicae gradually increases as the venule bore diameter increases.

After traversing the venules, the blood is then transported via the veins which can be differentiated from the venules by their increased internal bore diameter, increased wall thickness and modified endothelial structure. The endothelial lining of the veins is formed into 'folds' protruding out into the vessel lumen which act as valves. These valves stop the blood from draining back away from the heart.

The superficial veins of the limbs have an increased muscle content in the vessel wall for additional strength. This thickening of the walls is necessary to counteract the tendency of the veins to expand or distend under the gravitational influence of the blood pressure. The vena cava is the final component of the circulatory system prior to the blood returning to the heart and completing a full 'circuit'. The vena cava has substantial layers of smooth muscle in it's tunicae for strength. This stops the vena cava from collapsing under the suction pressure from the contraction of the heart ventricle.

2.6 Light-tissue interaction

2.6.1 Basic Light Tissue Interaction

Understanding the transfer of optical radiation within skin is important to develop new therapies based on photothermal and photochemical reactions in skin. There have been many studies focused on understanding and describing models for photon transportation through skin, being the most extensively studied tissue to date because of its importance in photobiology (Anderson and Parish 1981, Barton et al 1998, Jacques 1987b, and Miller et al 1993). These models have also been needed in other medical fields such as diagnostic evaluation and monitoring. Detailed information about the propagation of light using fluorescent, scattered, or transmitted light through tissue are used to measure parameters such as drug concentration or blood oxygenation in-vivo. The propagation of light within tissues is an important problem that confronts the dosimetry of therapeutic laser delivery and the development of diagnostic spectroscopy.

2.6.2 Definition of Light

Light is a very complex form of radiant energy that is composed of energy packets known as photons that move at $2.99 \times 10^8[m/s]$. James Clerk Maxwell first postulated a set of equations governing photons until Plank, Bohr, De Broglie, Einstein and others created quantum theory, where photons possess a function of duality acting as a particle and a wave. The variety of photons is arranged into the electromagnetic spectrum (EMS) according to the wavelength of those photons from short cosmic gamma rays to long radio waves (Figure 2.10). The distance between two successive troughs or crests of these waves, determines the wavelength. The brightness of visible light is determined by the number of photons, and the colour of visible light is related to the energy contained in each photon. The energy relationship of each photon is shown in the following Plank Einstein equation.

$$Energy(J) = h \times f = h \times \frac{c}{\lambda} \tag{2.1}$$

Where h is the Planks constant, f is the frequency, c is the speed of light, and λ is the wavelength The first application of photospectroscopy was when Isaac Newton used a prism in 1666 to

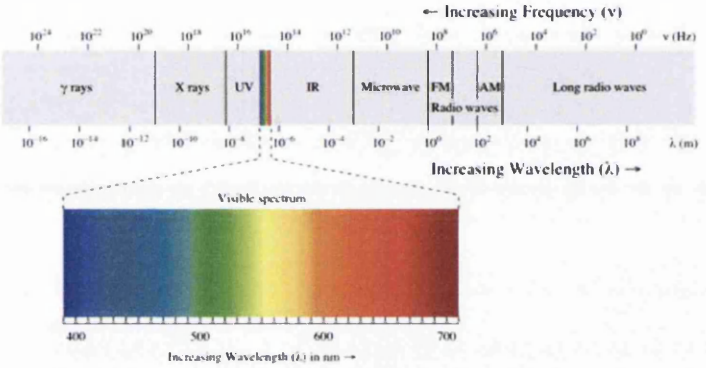

Figure 2.10: The electromagnetic spectrum ranges from gamma rays on the left to radio waves on the right. A small section of this range is called light, which is visible to the human eye. (image source: www.wikipedia.org)

identify that white light is composed by a spectrum of colours and opened up a new era in the scientific investigation of light. In 1800, Sir William Herschel had demonstrated the existence of radiation beyond the red end of the visible spectrum, a component now known as infrared radiation. In 1801 Johann Ritter discovered the ultraviolet (UV) region of the solar spectrum by showing that a chemical action was caused by some form of energy in the dark portion beyond the violet. Other such discoveries include the detection of the element helium from spectroscopy of sunlight by the unknown yellow spectral line signature, first observed from a solar eclipse in 1868 by French astronomer Pierre Janssen. The electromagnetic spectrum extends from below the frequencies used for modern radio through gamma radiation, covering wavelengths from thousands of kilometers down to a fraction the size of an atom. The term light generally refers to the portion of spectrum with wavelengths between 400 nm and 700 nm, which can be seen by the naked eye.

2.6.3 Light Tissue Interaction

The earliest recorded use of light was discovered in ancient Egypt dating back to approximately 4000 B.C. It was at that time that sunlight united with psoralen containing herbs (like parsley), a natural topical photo sensitizer, to help re-pigment individuals suffering from vitiligo, where the skin had become depigmented through an autoimmune reaction.

It is important to first understand how light produces a biological effect in skin. The four mechanisms for interaction between light and tissue can be described as

- Photochemical: absorption of light by chromophores in or added to tissue creating a chemical reaction upon light exposure. An example of this is the absorption by light of Porphyrin within Acne, creating singlet oxygen destroying the host bacteria.
- Thermal: the deposition of thermal energy in tissue causing biological changes, such as changes in blood chemistry in superficial blood vessels or thermal denaturising of follicular stem cells.
- Photo-ablative: photons of sufficient energy cause vaporisation of external layers of skin, removal of keloid scars by carbon dioxide (CO2) lasers are such an example.
- Electromechanical: a laser can induce a dielectric breakdown of tissue leading to the formation of focused plasma, generating a shock wave rupturing surrounding tissue.

95% of incident radiation exposed to skin may be absorbed or scattered within any of the layers of skin, thus 5% is typically reflected. Figure 2.11 shows a model of light-tissue interaction with the associated mathematical relationships. The first interaction at the surface of skin is the probability of a photon to reflect from the interface or refract into the multiple layers of skin. The directions of the resultant photons are governed by Fresnel's law and Snell's law, respectively, and their impact on the loss of intensity are determined by the relative values of their refractive indices.

The two main physical phenomena affecting light propagation in biological tissue are absorption and scattering. This interaction of light with living tissue is generally a function of the wavelength and energy delivered. In order for light to produce any biological effect in skin

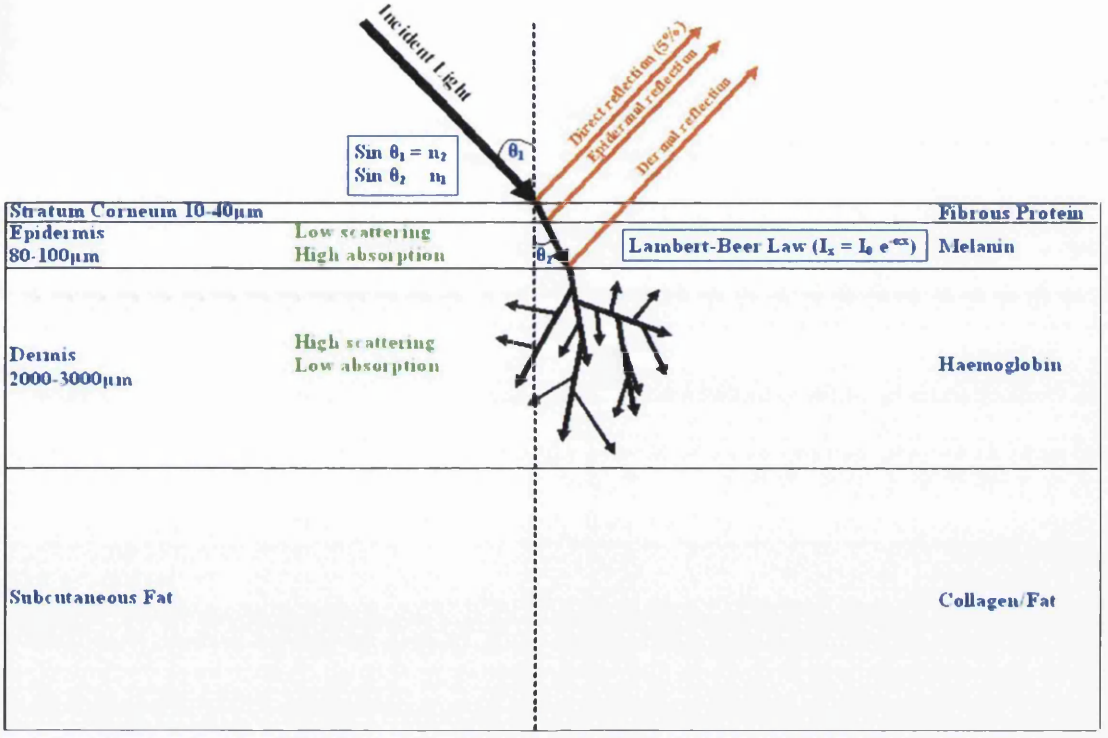

Figure 2.11: Illustration shows emitted broadband light from an IPL is reflected, absorbed and scattered by human skin (from [2]).

it must first be absorbed, where transformation of radiant energy to a different form of energy (usually heat) occurs by the specific interaction with tissue. If the light is reflected from the surface of the skin or transmitted completely through it without any absorption, then there will be no biological effect. If the light is imprecisely absorbed by any target or chromophore in skin then the effect will also be imprecise. It is only when the light is highly absorbed by a specific component of skin that there will be a precise biological effect.

While this reaction may seem difficult to anticipate accurately, in fact, there are only four main components of skin that absorb light energy: melanin, haemoglobin, and intracellular or extra cellular water, and their absorption spectra have been well investigated. Many researchers have reported the optical coefficients of each layer of human skin and the molar absorption

coefficients spectra of chromophores such as melanin and blood (Anderson & Parrish). Excellent experimental methods have been described by Barton et al. [61] and Sardar et al. [62] for determining absorption, scattering and scattering anisotropy coefficients. Manufacturers of light based equipment have taken this information and designed technological devices that produce light which are of the correct wavelengths to be precisely absorbed by one of these components of skin, while minimising collateral injury to the surrounding normal skin.

2.6.4 Selective Photothermolysis

Selective photothermolysis describes the uses of selected wavelengths to destroy particular targets in skin proposed by Anderson and Parrish in 1983. With the correct combination of wavelength, energy density and pulse duration, it is possible to precisely target and damage an absorbing biological target without causing injury to the surrounding structures.

In tandem with the principle of selective photothermolysis is the concept of thermal relaxation. Thermal relaxation is used to describe the limitation of thermal damage when a desired target absorbs a particular wavelength in an amount of time that is equal or less than that target's thermal relaxation time. One way to achieve greater injury to the biological target is by increasing the pulse duration of light exposure. The thermal relaxation time (TRT) for hair follicles that are $200\mu_m$ to $300\mu_m$ in diameter is approximately 40 to 100 milliseconds (figure 3.7). If pulse duration were the only factor, then the ideal pulse duration should lie between the thermal relaxation time for epidermis, which is approximately 3 to 10 milliseconds, and the thermal relaxation time for hair follicles.

2.6.5 Absorption

The probability of light absorption by tissue molecules is described by the absorption coefficient $\mu_a[m^{-1}]$ which is defined as the probability of absorption per unit length. Photons interact with molecules in their path, and if the energy of the photons is resonant with the energy levels in molecules, a photon may be absorbed and cause an excited energy state in the absorb-

ing molecule. Absorption of light in tissue is strongly wavelength dependent, since absorbing molecules called chromophores absorb in different wavelength regions. The absorbed energy is most often converted into heat, but can also be re-emitted as fluorescence or be used for a photochemical reaction. Most commonly the absorption in homogeneous, non-scattering medium can be expressed by the use of the Lambert-Beer law

$$I(x) = I(0) \exp(-a(x)) \tag{2.2}$$

Where I(0) is the incident intensity, and a is the absorption coefficient of the medium.

2.6.6 Scattering

Scattering is a process in which the direction of propagated light changes by refraction at boundaries of differing refractive indexes resulting in a widening of the light beam and a loss of energy density or fluence (Plaetzer et al [63]). Scattering of light in any media has the most pronounced effect on light intensity and directionality. Scattering has been thoroughly studied in biological tissue by many and in experiments scattering has been shown to be strongly forward directed.

The scattering of photons within media is described by two mechanisms, namely Rayleigh and Mie. Unfortunately neither Rayleigh nor Mie scattering completely describes the effects observed in tissue however they are conditionally used in photon transport models. Experimentally observed scattering shows weaker wavelength dependence than that predicted by Rayleigh's theory, but the effect is stronger than that explained by Mie scattering [33] [64].

Rayleigh scattering occurs if the scattering particle is smaller than the wavelength; subcellular biological structures like mitochondria are Rayleigh scatterers. If the size of the particle is larger than the wavelength, the scattering can be described by Mie theory. In Mie theory the electric and magnetic fields within the particle must be considered. The Mie scattering cross section is inversely dependent on the square of the particle radius and depends weakly on the wavelength. Mie scattering is strongly forward directed. Scattering by fat droplets in milk and

scattering by water droplets in clouds are typical examples of Mie scattering.

Considering a cloud floating on a clear blue sky provides an excellent example of Mie and Rayleigh scattering. The sky is blue due to the strong inverse dependence of Rayleigh scattering with wavelength. The shorter (blue) visible wavelengths are scattered much more intensely by the atmosphere whereas the longer (red) wavelengths have a tendency to penetrate through the atmosphere. Clouds consist of small water droplets appearing white or grey against the blue sky, because of the independence of Mie scattering with wavelength, even though the cloud is smaller with much less material than the sky. Mie scattering is immense within the water droplets thus the cloud casts a shadow on the ground as light is scattered into all directions by the cloud.

Depending on the amount of scattering particles and their scattering efficiency, photons will travel a given distance between scattering events. This distance is called the scattering mean free path l_s and is given by the scattering coefficient as $ls = 1/\mu_s$.

In the case of multiple scattering it is useful to know the scattering angular anisotropy of the scattering events. Each time light is scattered it will change direction and move in the new direction until it once more is scattered or absorbed. The angular distribution of the scattering angles can be described by the anisotropy factor g, i.e. the cosine of the average scattering angle. Where ϑ is the scattering angle, scattering in skin is strongly forward directed, and the value of g is approximately 0.8 to 0.9.

$$g = \cos\vartheta \tag{2.3}$$

Scattering by collagen fibres appears to be of major importance in determining penetration of optical radiation within the dermis whereas the epidermis provides an optical barrier primarily by absorption of radiation and to a much lesser degree by optical scattering. Dermal scattering, at least in the visible spectrum, is largely forward projected, with the mean scattering angle per scattering event being 20o using a 632 nm helium-neon (HeNe) laser wavelength.

An observed effect through computer modelling is the effect of back-scattering, where photons move from an absorbing epidermis into highly scattering dermis, many of these forwardly moving photons are reflected with a high angle and absorbed within the melanin rich basal layer within

the epidermis, thus a band of greater absorption occurs on the epidermis side of the junction with the dermis.

2.6.7 Optical Properties of Various Tissue Types

Knowledge about skin optical properties is essential to reveal information from measured reflectance spectra and visual changes of skin post treatment. The visual appearance of skin is attributed to both the scattering and absorption properties. Tissue scattering is caused by water, fats and proteins like collagen, described by a combination of Rayleigh and Mie scattering previously described. The main chromophores of interest when considering absorption are melanin, haemoglobin, water, and porphyrin.

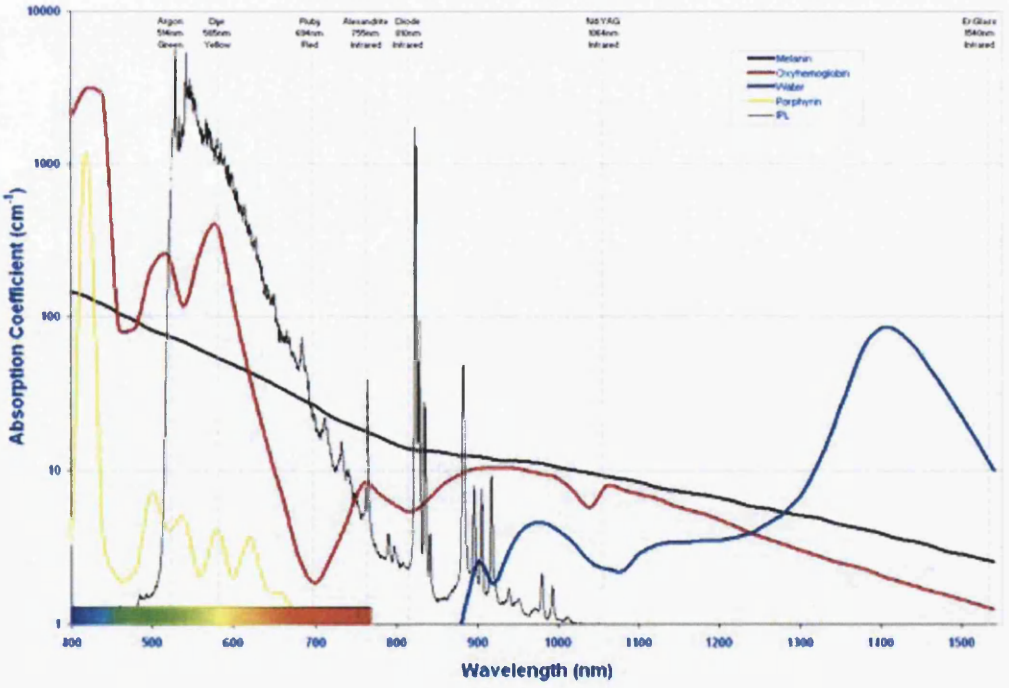

Figure 2.12: Absorption coefficients of melanin, oxyhaemoglobin, water, and porphyrin. (From [2])

Melanin

One of nature's elegant defense mechanisms is to protect cellular DNA from exposure to ultraviolet wavelengths originating from sunlight by shielding such cells with a highly ultraviolet absorbing material. In humans, melanin is the primary determinant of skin colour, hair colour, pigmented tissue, and assigning eye colour by melanin within the iris. Some individual animals and humans have very little or no melanin in their bodies, a condition known as albinism.

The absorption of melanin is not a "neutral density filter" in skin, as its absorption is greatest in the UV region, tailing off logarithmically into the longer less damaging wavelengths (figure 4). There has been a great amount of research into optical properties of melanin, of which there are two main types, pheomelanin and eumelanin that can be found in human skin. The optical properties probably do not differ significantly between eumelanin and pheomelanin [65] [62]. Pheomelanin is a red-brown polymer of benzothiazine units largely responsible for red hair and freckles. Pheomelanin is particularly concentrated in the lips, nipples, glands of the penis and vagina. Eumelanin is found in skin and hair, typically found within melanosomes in the epidermis [66], that colour hair grey, black, yellow, and brown. In humans, it is more abundant in people with dark skin. Eumelanin are black or brown nitrogenous protein-polymer pigments. The increased production of melanin in human skin is called melanogenesis resulting in a lasting tan. Studies on skin type's I-III have shown a trend for increased epidermal eumelanin content with higher Fitzpatrick skin types but no correlation was observed with pheomelanin (Thody et al 1991).

Figure 2.13 shows the increasing amount of melanin found in skin for the Fitzpatrick skin types taken from two studies. This fits the grading difference between a light tan between skin types I and II and the step difference between skin type V (Indian skin) and skin type VI (Afro-Caribbean). Although there is peer reviewed data on epidermal concentrations of all skin types, there is no data on follicular melanin concentrations for various hair colours.

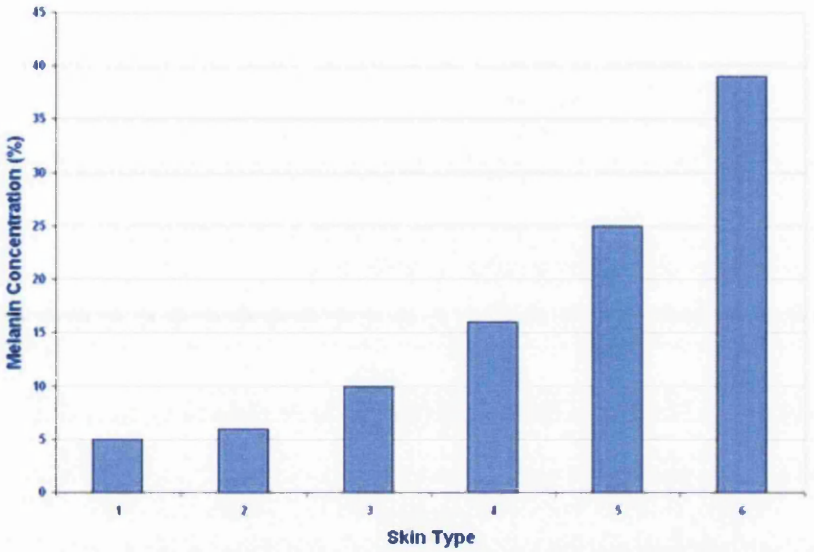

Figure 2.13: Data of increasing Epidermal Melanin Content (EMC) for the 6 Fitzpatrick Skin Types. Data was extrapolated from [3] and [4].

Haemoglobin

Haemoglobin is designed to transport oxygen (O_2) from the lungs to vascular tissues throughout the body, and return carbon dioxide (CO_2) back to the lungs. The oxygen binding capacity of the haemoglobin molecules is due to the four heme groups found within each haemoglobin molecule. The heme consists of a porphyrin ring with a central Fe atom in the 2+ oxidation state. Figure 2.12 shows haemoglobin possessing a roller coaster absorption characteristic with respect to wavelength. However, the absorption characteristics of blood differ with haemoglobin species shown in Fig. 2.12. Oxyhaemoglobin (HbO_2), shows a bright red colour, deoxyhaemoglobin (Hb), without bound oxygen has a dark red, bluish livid colour, and methaemoglobin where the oxidation state of the blood is 3^+ and cannot bind with oxygen (Ash 2008b) has a chocolate-brown colour.

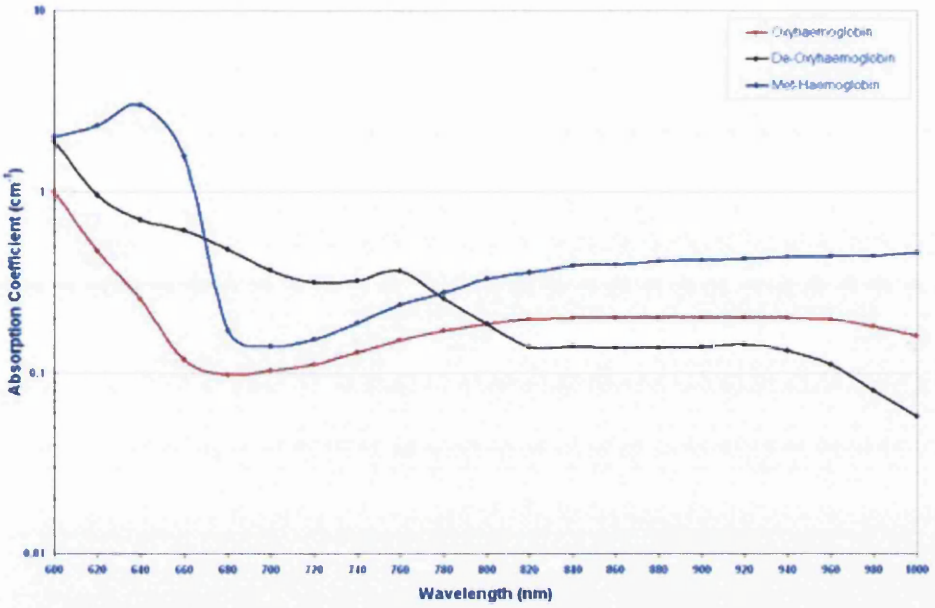

Figure 2.14: Absorption coefficients of oxyhaemoglobin, deoxyhaemoglobin and methaemoglobin. Diagram shows that the absorption of methaemoglobin is 10 times greater than oxyhaemoglobin at 632nm and generally deoxyhaemoglobin have a higher absorption than oxyhaemoglobin (from [2])

Water

Skin is composed of approximately 70% water and the volume of water presents a large absorption target even for wavelengths of light that have a fairly low water absorption coefficient. The absorption of water is insignificant below 800 nm, and within wavelenghts around 800nm it is still very low in comparison to the other two chromophores (melanin and haemoglobin). Increasing to much longer wavelengths, the absorption coefficient at 1320 nm is circa 2 cm-1, which is almost fourteen times the absorption coefficient for water at 1,064 nm. This translates to 1400% better absorption of water at 1,320 nm than at 1,064 nm.

Porphyrin

The treatment of acne differs from melanin and haemoglobin as the primary target is not the dominant chromophore. Bacteria within an acne lesion contain a photosensitive compound called porphyrin. When porphyrin is illuminated with certain wavelengths of light, a photochemical reaction is initiated where singlet oxygen is created that kills the bacteria leading to suppression of the acne. To achieve long-term suppression of acne, the light has also to trigger the body's natural wound healing response.

Selecting wavelengths to target the high absorption peak in the blue region will only destroy superficial bacteria as the light will not penetrate to the full extent of the lesion, in addition the wound healing response will not be initiated. Red light may have anti-inflammatory properties by influencing the release of cytokines from macrophages or other cells. Macrophages exposed to low intensities of 660 nm wavelength release cytokines which stimulate fibroblast proliferation and the production of growth factors, thus influencing the inflammatory process, healing and wound repair.

Using wavelengths that target the secondary porphyrin absorption peaks in the Q-band (500 - 620 nm) will destroy the host bacteria with free radical oxygen and trigger the healing process thus inducing long term acne suppression. It is important to note that out of the five absorption peaks of porphyrin the largest of the peaks at 408 nm (soret band) has the greatest absorption coefficient.

Chapter 3

Optical Therapy

3.1 Introduction

As outlined in 1.2, the use of light to treat a variety of medical conditions has a long history. However, as previously mentioned, a systematic and experimental-scientific approach to the matter has much more recent foundations. A description of the fundamental principle of selective photothermolysis is given.

As mentioned in the previous chapter, the principle of photothermolysis has been originally described by Anderson and Parrish in their seminal paper in Science (1983) [33]. The principle defined how energy from a laser source was absorbed by a particular target component of a molecule or tissue - a chromophore, within the skin leading to a specific biologic effect; collateral structures are spared during the process. Description of chromophore was given in 2.6. However, as mentioned in the previous chapter, tissue absorption is not the only factor influencing therapeutic performance and biologic effects. Phenomena such as scattering of the incident radiation influence the penetration depth of the radiation, as described in [67]. In particular, collagen is mainly responsible for scattering phenomena which decrease as the wavelength of the incident radiation increases. Choice of a specific laser will be therefore dependent upon the depth at which the target is located. Therefore, in first approximation we can consider the two

phenomena to be the main factors responsible for the penetration of laser light.

A chromophore is a chemical group which causes coloration in a dye or molecule. The molecule will therefore have a color if absorption of a radiation of a certain wavelength by said molecule and reflection or transmission of other wavelengths happen. In a chromohore, the energy difference between two different molecular orbitals happens to be within the range of the portion of the spectrum of the incident radiation. The absorbed radiation in the chromophore causes an electron to get to an excited state (from its original ground state). The light energy absorbed by the chromophore is usually converted in to heat. Heat generated during this process is used for a variety of therapeutic purposes. Excitation then usually falls according to a specific exponential decay time, which is characteristic of the specific target structure.

In the skin, the main chromophores which are of interest for therapeutic purposes when targeting human tissues and especially vascular tissues are:

- Melanin
- Haemoglobin (oxy-haemoglobin and deoxy-haemoglobin)
- Water

The characteristic absorption curves for melanin and haemoglobin are found in Fig. 3.1. Absorption in water starts to appear for radiation of wavelengths higher than 1000nm circa, and becomes dominating for increasing wavelengths in the infrared spectrum (water absorption characteristic is not shown in the picture). This limits the use of longer wavelength for vascular therapy applications.

As we can see from the figure, the characteristic for melanin is a monotonal curve showing the decrease in absorption coefficient for increasing wavelengths.

Melanin is the preferred target chromophore for laser hair removal treatments. However, its presence constitutes a major factor in determining the viability of vascular laser therapies compared to others. In fact, scattering phenomena in the skin, which are dependent upon the average scatterer size, are influenced by a number of factors. Firstly, the concentration and cluster size of melanin and melanin fragments pertaining to different skin types as well as to

different areas of the body. Secondly, differences in scatterers such as collagen and elastin for different (exposed and un-exposed) areas of the body. Furthermore, concentrations of scatterers have been shown to vary for different layers (epidermis and upper dermis, lower dermis) of the skin. Particularly, sun-exposed areas such as the dorsal forearm, have shown to have a smaller mean scatterer size than normally un-exposed areas such as the upper inner arm in the lower dermis, but larger mean scatterer size in the upper dermis and epidermis. The former has also been linked, other than to the concentration of melanin, also to possible photoaging effects which may be responsible for a decrease in collagen and elastin bundle size, as hypotesised by *Tseng et al.* [68]. These considerations, whilst being very useful from a diagnostics perspective (and this is indeed the original purpose of the work described in [68], are also very interesting from a therapeutic point of view, as they can inform development of product which couple imaging and parameter extraction within a feedback loop to calibrate the therapeutic laser source parameters.

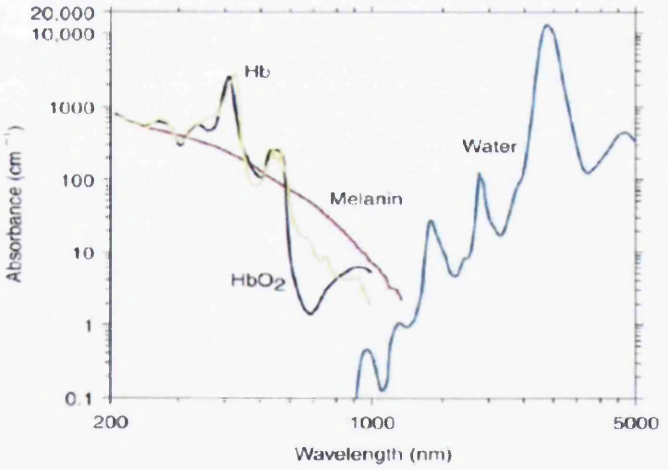

Figure 3.1: Characteristic absorption spectra for the three main skin chromophores: melanin, haemoglobin, oxyhaemoglobin and water (adapted from *Kauvar and Khrom*, 2005 [5]

3.2 Mechanisms of Necrosis

The reaction of the tissue on absorption of the incident laser energy can be classified into photothermal, photochemical, and photomechanical effects, as summarised in 2.6.3.

Photothermal reaction occurs where the energy absorbed by the tissue chromophores is converted into heat, which then causes hyperthermia, coagulation, carbonisation or evaporation of tissue depending on the temperature reached.

Photochemical reaction occurs when absorption of light by chromophores in or added to the tissue creates a chemical reaction upon light exposure.

Photomechanical reaction is caused where absorbed photons induce stress gradients and pressure waves to destroy biomolecules by breaking their bonds rather than by thermal means.

In-depth description of the three above-mentioned effects is available in relevant literature. Only a basic overview will be provided in this study with an emphasis on photothermal reactions as blood vessels can be permanently destroyed by this effect.

Photothermal Reactions

The thermal reaction of a laser in a living tissue is a complex process resulting in three distinct phenomena, being (i) the conversion of laser light into heat at the site where the impinging optical radiation has been absorbed by tissue chromophores, (ii) the transfer of heat to surrounding cells / tissue, and (iii) the tissue reaction to heat depending upon both temperature and time.

Hence long exposure time at moderate temperature will cause delayed necrosis of the tissue to be achieved while high temperature for short time will achieve coagulation with immediate visible effects such as whitening / blanching of tissue. Schematically, the photothermal reaction comprises of three main mechanisms, namely hyperthermia, coagulation and volatilisation.

Hyperthermia can be subdivided in to two groups, the first one concerning phenomena occurring at low temperature where there is no significant change in the tissue, even if the irradiation time is long.

The second group concerns phenomena generally involving significant (typically greater than

$10^{-4}s$) exposure to a mildly elevated temperature, typically above $42°C$. Above that temperature, enzymes and other molecular components are affected, oedema of the cells is formed and the structure of the membrane is loosened, causing denaturation and irreversible aggregation of macromolecules within the cell. Consequently, there is eventual cell death.

These effects are not immediately apparent to the eye but usually require up to 24 hours to develop into necrosis.

Above $60°C$ the process of photocoagulation begins. Much like hyperthermia, the mechanism of coagulation is centred around the denaturation of protein. Generally photocoagulation requires only a short exposure to a high temperature and the effects are immediate and visible, such as whitening of the tissue. It is therefore a more obvious form of thermal injury than hyperthermia. Of particular interest to us is the denaturation of the collagen fibres which make up the walls of blood vessels. It is currently accepted that in order to destroy a blood vessel its wall has to be injured in such a way that it will not recover. As the vessel wall does not have a suitable chromophore to absorb light, the (oxy)haemoglobin within the vessel is targeted. When the red corpuscles are heated to a high temperature, the heat diffuses away from the vessel wall, whose temperature is subsequently raised. Current opinion has it that if this temperature is raised to above $70°C$ and held for about $1ms$, the collagen fibres of the vessel will denaturate and die. Hence the blood vessel can no longer be sustained. The ectatic vessels destroyed in that way are replaced by blood vessels normal in size, number and structure, and the skin normally returns to its normal colour.

When tissue is heated to $100°C$, the cell water starts to boil. The subsequent conversion of water in to steam causes the cell walls to be ruptured explosively to allow the steam to escape. Blood vessels may also be destroyed via this process if the vessel walls are ruptured under the pressure caused by vapourisation of the intra-vessel serum. Once the water has completely evaporated from a cell, rupture of the tissue, also known as the *popcorn effect*, is observed. The subsequent debris are rapidly raised to a higher temperature until around $300°C$ is reached. At this point, there is a further decomposition of the molecules causing the tissue to blacken

and become carbonised. At still higher temperature (over $500°C$) the residue will burn and evaporate.

Photochemical Reactions

Photochemical effects are caused when photons absorbed by a molecular chromophore convert that molecule to an excited state which subsequently participate in a chemical reaction. Hence the photon essentially behaves as a reagent that is stoichiometrically consumed in the photochemical reaction as a photochemical product is produced. A variety of photochemical reactions can occur such as photoinduction, photoactivation, photoradiation, photochemotherapy (photodynamic therapy, or PDT) and photoresonance. Photochemical reactions may occur at low power densities and long interaction times(from minutes to hours).

Photomechanical Reactions

The production of photomechanical effects is limited to high power short pulsed beams such as those achieved with Q-switched or mode-locked lasers. At such intensities, extreme heat is produced in a very tight space, temperatures rises very rapidly and molecules and atoms are structurally altered. As electrons are ejected from their orbits, tissue material is ionised to form a confined plasma. This plasma generates mechanical shock waves which can break tissues.

Photomechanical reactions are used beneficially in a number of clinical applications such as opthalmology, urology and dentistry.

3.3 Selective Photothermolysis - Description

According to Anderson and Parrish's original definition, the process was only dependent upon the fluence utilised. *Altshuler and Anderson* would then revisit the concept in 2001 and propose what they would call Extended theory of Selective Photothermolysis [69]. The extended theory was formulated to account for non-uniformly pigmented structures in biological tissues; which would also take in to account dependency of the treatment parameters upon the power, pulsewidth

and shape of the Electromagnetic Radiation (EMR); dependency not just upon target size, absorption and thermal properties, but also on geometry, is discussed as a means for achieving a successful treatment. In addition, another important factor is discussed: in contrast with the standard Selective Photothermolysis theory, the target is destroyed by heat diffusion from the pigmented area to the target rather than by direct heating from EMR.

The revisited Extended Selective Photothermolysis principle accomoddates for the more complex phenomena occurring within complex tissues, where heat diffusion phenomena from a heater target to the target tissue are instead responsible for the delivery of the energy to said target tissue.

In the case of blood vessels, the radiative energy from a laser source of a suitable wavelength would hit the preferred chromophore - haemoglobin present in erythrocytes (red blood cells) thus causing an increase in their temperature. This heat would then be transferred through diffusion to the surrounding endothelial cells of the blood vessel. The heat would cause damage to the vessel wall. If the pulse time of the radiation is less than or equal to the TRT, heat is confined to the target - the vessel walls.

Selective Photothermolysis

Photothermolysis is based upon the principle of using radiative energy to selectively destroy the abnormal vessels within a vascular lesion whilst leaving the healthy surrounding tissue structures intact. The premise is therefore to irradiate the skin surface with a suitable laser source which only deposits its energy in the vasculature, the light passing harmlessly through the epidermis and dermis. As shown previously, many of the conventional treatment modalities include a substantial risk of side effects or complications. By determining a suitable treatment protocol and an optimum set of laser parameters, selective photothermolysis provides an efficacious method of removing vascular lesions with minimal risk, discomfort and trauma for the patient.

Selective photothermolysis is only feasible, with an acceptable clinical outcome, when a number of criteria are met. An acceptable clinical outcome is defined as being a complete

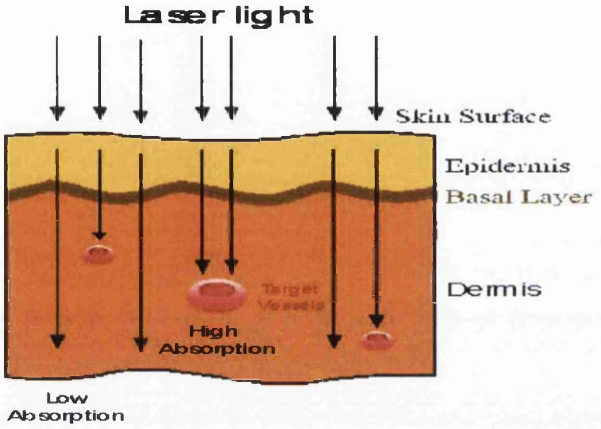

Figure 3.2: Basic Theory of Selective Photothermolysis (adapted from [6])

clearance, or a noticeable improvement in appearance of the lesion, with no pigmentary or textural changes to the skin surface. In the case of proliferating lesions such as Strawberry Haemangiomas, a favourable result is a retardation or ceasing of the growth phase and/or possible resolving of the lesion.

For selective photothermolysis to be achieved, the following criteria have to be taken into consideration;

- the target vessel must have a chromophore which can absorb laser light;
- the surrounding healthy tissues must have a minimal amount of the target chromophore, allowing light to be transmitted;
- the absorption of laser energy in the healthy tissues does not produce any irreversible or long term damage;
- the laser light incident at the target vessel is sufficient, in both intensity and duration, to induce the desired clinical effect, namely necrosis.

An analysis of the above four points generates a theoretical set of laser parameters for optimum treatment efficacy.

Firstly however, it is necessary to understand the mechanism of vessel necrosis induced by the absorbed laser energy as this has a direct bearing on the choice of laser parameters used.

As previously outlined, in order to permanently destroy a typical blood vessel, the wall structure has to be 'injured' in such a way that it cannot recover.

When a blood vessel is injured, the following sequence of events will occur when enough of the vessel wall structure is breached:

- blood cells (platelets) congregate at the site of wall injury;
- a blockage in the vessel is created at the wall injury site;
- a thrombotic reaction occurs stopping blood flow in the vessel;
- the vessel structure collapses on itself;
- fibroblasts are created in the region of the vessel collapse;
- recollegenation of the area, giving the tissue a normal histological appearance.

The injury can be achieved either photo-thermally, photo-mechanically or by a combination of both effects. However, as will be made clear, the treatment of vascular lesions by laser is complicated by the fact that the vessel wall does not have a suitable chromophore to absorb the laser energy. Therefore, the chromophore that is targeted is the oxyhaemoglobin of the red corpuscles circulating within the vessels.

The process by which the endothelial layer is destroyed photo-thermally is that of utilising laser energy to heat the corpuscles to such an extent that, through a process of secondary heating, the endothelial cells are raised to $70 - 80°C$. If this temperature is held for approximately $1ms$ or more, the protein-based cellular structures denature and die. If enough of the endothelial cells undergo this denaturing, the vessel can no longer be sustained.

To destroy the endothelial cells by a photo-mechanical process, the rate of change of temperature within the vessel and the peak temperature reached is of importance. If the rate of temperature increase within the vessel is large enough, and the energy delivered is sufficient to raise the water-based intra-vessel serum to greater than 100oC, micro-vaporisation occurs and the corresponding pressure increase will rupture the vessel wall. This can only occur if the pressure rise can overcome the elastic nature of the vessel wall components.

This understanding of how vessel necrosis is achieved, combined with an examination of laser-tissue interaction, allows an in-depth analysis of the optimum laser parameters required.

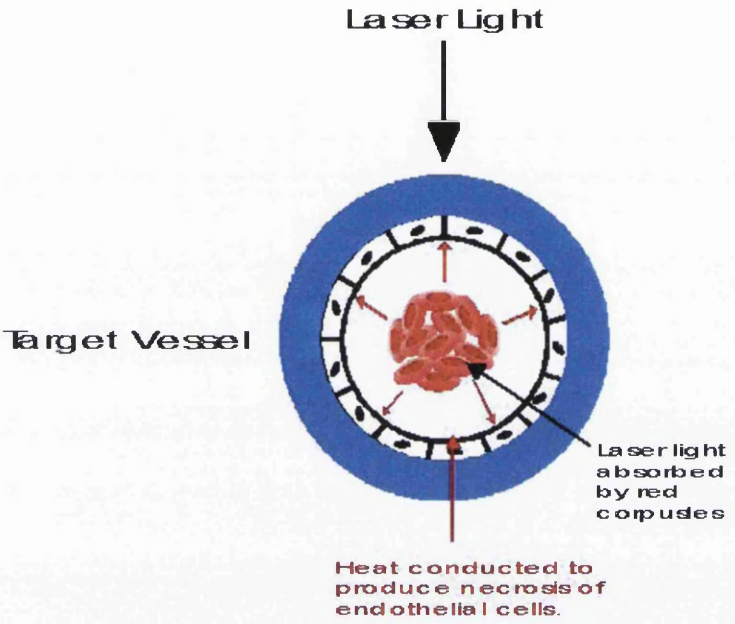

Figure 3.3: Photothermal Secondary Heating of the Vessel Wall (adapted from [6])

The key laser parameters are traditionally wavelength, pulse duration and energy.

3.3.1 Wavelength Selection

The two primary factors which influence the choice of laser wavelength for the treatment of vascular lesions are:

- How does the light interact with the skin ?
- How does the light interact with the target vessels ?

Understanding both these interactions will lead to the definition of the optimum laser wavelength for the treatment of vascular abnormalities.

Once the ideal wavelength has been selected, a third and highly significant factor must be introduced, namely:

Is there a laser capable of producing the optimum wavelength?

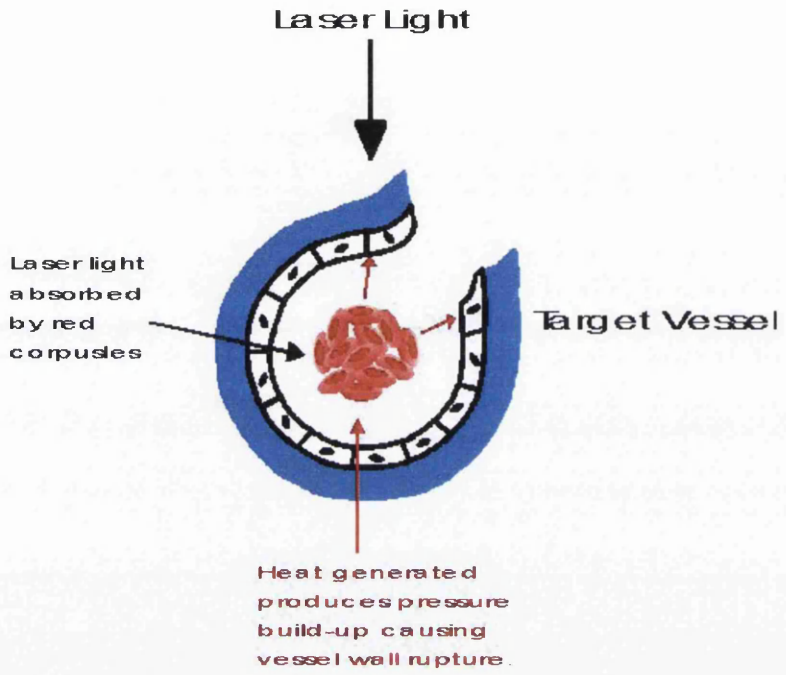

Figure 3.4: Photomechanical Destruction of Vessel Wall (adapted from [6])

How does the light interact with the skin ?

The vascular structure of skin lies typically a minimum of 0.5mm beneath the skin surface. Some vascular abnormalities are shallower and situated at a depth within the skin close to the skin surface but, in general, the light must pass through the epidermal and upper dermal regions of the skin to interact with the underlying vasculature.

A simplified model, previously shown in fig. 2.11, is useful in understanding how the laser light interacts with the skin. When light is incident at the skin surface, any or a combination of four possible actions can take place, namely reflection, scattering, absorption or transmission.

Reflection at the surface accounts for only a small proportion of the incident light. The amount of reflection is highly wavelength and incident angle dependant and is due to the change of refractive index between air and the stratum corneum. In the visible and near-infrared region of the spectrum, the skin will tend to reflect 4-7% of a normal incident laser beam.

The absorption, transmission and scattering of light all determine how deep the light penetrates into the skin, which like all soft tissues in the human body, is a highly water based structure. By examining the light-water absorption profile of tissue, from the far-infrared (FIR) to the ultra-violet (UV), a suitable spectral window for selective photothermolysis is defined.

Light with a high water absorption coefficient will have minimal penetration into the skin. Far infra-red light, such as is produced by the CO2 laser at $10.6\mu_m$, is highly absorbed in water and hence all the energy is deposited in a very thin layer, typically $30\mu_m$, at the uppermost surface of the skin. Moving to the shorter wavelengths, the absorption coefficient gradually decreases, however there are noticeable peaks such as that at approximately 2000nm where the absorption is higher than that at $10.6\mu_m$.

Wavelengths in the ultra-violet (UV) region of the spectrum introduce a two-fold problem regarding their suitability for use in this application, namely water absorption and reactivity. Again, UV light has a high water absorption coefficient therefore the light does not penetrate sufficiently into the skin to reach the vasculature.

Shorter wavelength ultra-violet light has considerable reactivity when interacting with biological tissue. The photon energy of UV light is high enough to cause the breakdown of the molecular bonds of DNA. Breaking of these bonds can lead to the production of free radicals. Free radicals are highly reactive, short lived particles which have been shown to be possible pre-cursors to the development of cancerous cells.

Taking into account the above factors, the suitable wavelength range is reduced to a window consisting of visible and near-infrared (NIR) light.

Scattering of the visible light in tissue is forward dominated hence only a very small proportion is re-emitted from the skin. The impact of scattering is to diffuse the light as it penetrates deeper into the skin. If a collimated laser beam is used to illuminate the skin, when the photons interact with the components of the skin they can have their angular direction altered and the beam expands. The energy density present at the vasculature will often result in higher energy densities below the skin surface.

In the visible and NIR region of the spectrum the skin has two primary chromophores, namely Melanin and Oxyhaemoglobin. Melanin is the skin's natural barrier preventing excessive exposure to UV light. Melanin therefore has a very high absorption coefficient in the UV spectrum, gradually decreasing through the visible region and becoming negligible in the NIR.

For light to penetrate far enough into the skin to reach the vasculature, and hence the haemoglobin, the light must first pass through the basal layer, the melanin bearing region within the lower epidermis and upper dermis.

The optimum conditions for selective photothermolysis to take place is where the absorption in the oxyhaemoglobin dominates over that in the melanin. The absorption coefficient of melanin peaks in the shorter wavelength region with a gradual decrease with increasing wavelength. This is also the general trend for oxyhaemoglobin and it is therefore clear that the NIR region is not optimal.

Moving down the spectrum, a suitable window opens up in the yellow-red region (570 - 600nm) corresponding to a peak in the oxyhaemoglobin absorption curve. In the 570-590nm band, the difference in absorption between oxyhaemoglobin and melanin is significant and is theoretically optimum for selective photothermolysis to take place.

With this spectral band selected as an appropriate starting point, fine tuning of the wavelength choice can only take place by considering how the light interacts with the vasculature.

How does the light interact with the target vessel

If we consider PWS, typically the abnormal vessels within a PWS are between $30 - 100\mu_m$ in diameter and are full of red corpuscles circulating within them. Surrounding the corpuscles is the plasma, a clear water-based substance. Light incident on the vessel wall is transmitted and absorbed by the corpuscles generating heat. A simplified model is useful to understand the thermal profile produced by the laser energy within the vessel.

Although the absorption coefficient of oxyhaemoglobin is relatively constant throughout the 570-590nm region, the small variations impact on the thermal profile generated within the target

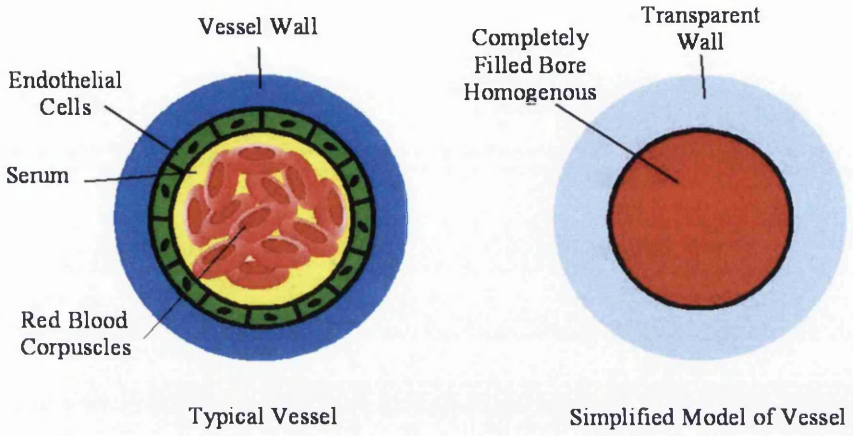

Figure 3.5: Simplified Model of Vessel (adapted from [6])

vessel.

The Lambert-Beer law is suitable to determine the absorption profile, and hence the thermal profile, within the target vessel. [50]. Figure 3.6 below shows how the light is absorbed in a vessel for a range of wavelengths, the light being applied perpendicularly to the vessel. This simplified approach does not take into account scattering into the sides of the vessel. As can be seen, light at the lower end of the spectral range is absorbed in a very small volume at the top of the vessel. This therefore produces a highly localised temperature rise near the upper vessel wall and a maximum peak value for a given energy density.

For the longer wavelengths, the absorption becomes more evenly distributed throughout the vessel leading to a more uniform temperature rise with a lower peak value. For a given energy fluence reaching the target vessel, the thermal profile is highly dependent upon wavelength which will determine which interaction mechanism is dominant.

The shorter wavelengths can produce the necessary temperature increase, in a localised region in the vessel, to cause micro-vaporisation to occur. It is therefore likely, under these circumstances, that the photo-mechanical process will be of more significance but with only a small portion of the wall structure affected.

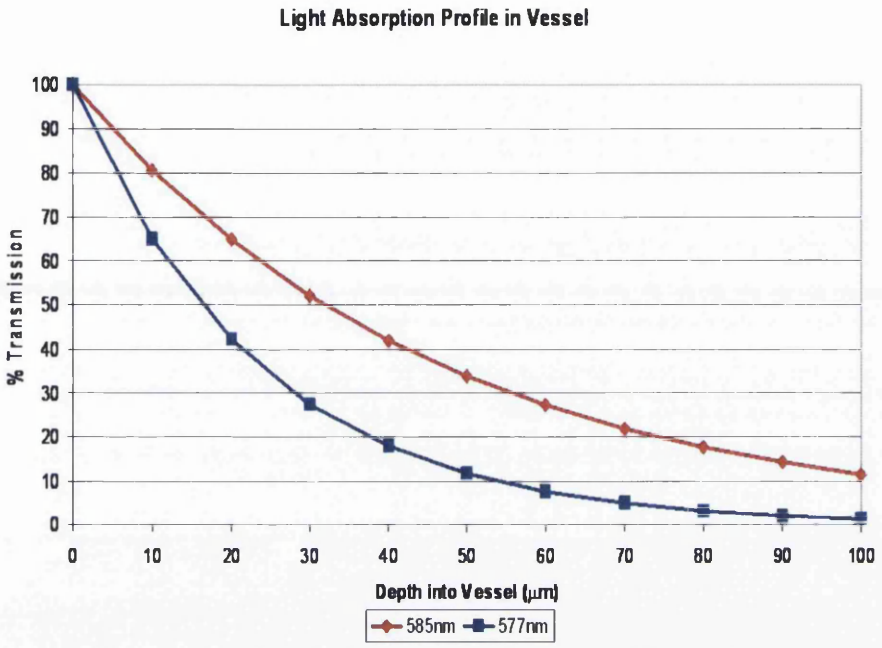

Figure 3.6: Wavelength Dependency on Vessel Absorption Profile (adapted from [6])

On the other hand, when the longer wavelength is utilised, there is a more volumetric heating of the vessel and hence more of the wall structure is affected. However, to raise this larger volume to the cell necrosis threshold, a relatively high energy fluence would be required.

Another factor to consider is the varying range of vessels within a typical PWS. For a vessel diameter of approximately $30\mu_m$, light at the longer wavelengths of 580nm and above will be partially absorbed, a significant amount passing harmlessly through the vessel into the lower dermis.

Therefore a balance has to be reached whereby the absorption profile within the vessel, and the depth of penetration of the light into the skin, is matched to a single suitable wavelength for treatment of the majority of PWS.

Initial clinical procedures were carried out using a wavelength of 577nm. This proved most effective on the lighter, more superficial PWS where the target vessel was of relatively small

diameter. When treating the more mature, darker PWS where the vessel diameter was larger, it was found that moving to a longer wavelength was more beneficial.

The current general consensus is that using a wavelength of 585nm will be the most effective for the varying physiology of PWS. [51] At this wavelength, the light will penetrate slightly deeper into the skin than at 577nm and will produce a more volumetric distribution of energy in the vessel.

3.4 The Pulse

3.4.1 Pulse duration analysis

For maximum effectiveness and safety of the applied laser pulse, the heat must be confined to the target vessel. This is also necessary to reduce the possibility of thermal damage to the healthy structures around the vessel. Therefore the energy must be applied in a duration where the temperature for vessel necrosis is reached and held for the optimum time.

What also must be considered is that the vessel contains the absorbing chromophore and the process of necrosis of the wall structure is a secondary effect, i.e. either by wall rupture, thermal denaturing of the endothelial cells or a combination of both.

To derive a suitable pulse duration, the physical properties of the target vessel are of importance. The theory of selective confinement of the generated heat depends upon the thermal relaxation time (TRT) for a given vessel dimension. The TRT is defined as that time taken for an object to decrease to 50% of its maximum temperature. [52]

The thermal relaxation time τ for a vessel is given by:

$$\tau = \frac{d^2}{16\chi} \tag{3.1}$$

where d is the vessel diameter and χ is the thermal diffusivity (taken as $1.4 \times 10^{-7}[m^2][s^-1]$, equivalent to water). Figure 3.7 shows the TRT for the typical vessels found within a PWS.

Laser pulses shorter than the thermal relaxation time will provide the maximum temperature

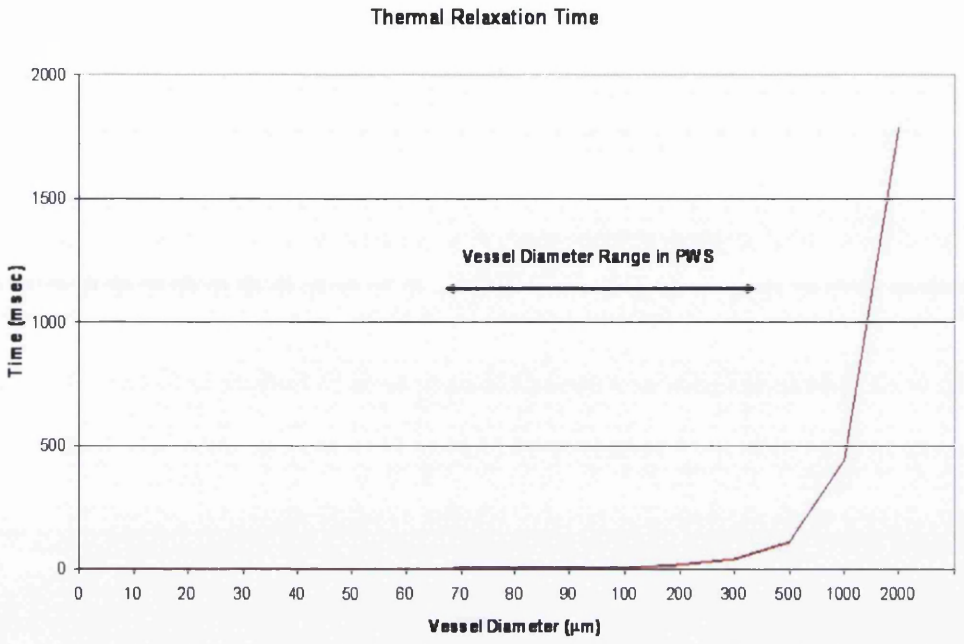

Figure 3.7: Thermal relaxation time for varying vessel diameter

rise in the vessel. This will increase the likelihood of photo-mechanical damage occurring through micro-vaporisation because the heat is confined with little time to diffuse away.

Laser pulses which are equal to or slightly less than the thermal relaxation time will provide conditions where the heat is confined to the vessel, hence allowing a significant local temperature rise, and maximising the time for the heat to diffuse to the vessel wall.

Laser pulses longer than the thermal relaxation time will induce non-specific damage to the surrounding tissue through heat out diffusion. It is apparent that the optimum pulse duration is approximately equal to the thermal relaxation time for a given vessel size. This argument leads to the fact that in a PWS where the target vessels are of varying diameter, no single pulse duration meets the ideal criteria. When using a long pulse duration on small diameter vessels, for a given fluence, the heat generated can be conducted away at a rate such that the necrosis temperature is not reached, leading to ineffective treatment. The opposite case is where

short pulses are used on large vessels, namely the volumetric heating only induces very localised necrosis, not enough to permanently damage the vessel.

From figure 3.7 above, the optimum pulse duration for PWS is in the 1-3 milli-second range. This allows for maximum treatment efficacy for a wide range of vessel dimensions whilst minimising the possibility of non-specific thermal damage.

3.4.2 Thermal Relaxation time (TRT) and Thermal Damage Time (TDT)

When a photon corresponding to a radiation of a certain wavelength hits a target, it would cause it to increase its temperature. The increase in temperature follows an exponential decay with time constant which is characteristic of the specific chromophore targeted. The period of time necessary to lower the temperature to one-half of the peak temperature is referred to as the Thermal Relaxation Time (TRT). Therefore, TRT refers to the time for the target to cool sufficiently through dissipation of heat to surrounding structures. TRT is characteristic of the specific target, and its value is directly proportional to the square of the size of the object and inversely proportional to thermal diffusivity. According to the standard Selective photothermolisis principle, the target's temperature increases due to the EMR to which it is exposed. However, some uncertainty still currently exist as to how precisely calculate the time necessary to obtain a therapeutically meaningful result in laser therapy and laser treatments. The Extended theory of photothermolysis has tried to address this issue. According to this theory, in order for selective photothermolysis to take place, the energy delivery time has to exceed a specific threshold time, called Thermal Damage Time (TDT), after which irreversible damage occurs to the target. TDT has been defined as the time needed for the outermost part of the target to reach damaging temperature by heat diffusion from the absorber. Still these findings are object of controversy [70] and an exact mathematical construct to precisely match in vivo behaviour has not yet been developed.

Photochemical reactions	**Interactions**
Photoinduction	Biostimulation
Photoactivation of drugs	
Photoradiation	
Photochemotherapy	Photodynamic therapy
Photoresonance	

Photothermal reactions	**Biological effects**
Photothermolysis	Thermal-dynamic effects Microscale overheating
Photohyperthermia	37 - 43°C No irreversible damage of normal tissue 45 – 60°C Loosening of membranes; tissue welding: Denaturation of enzymes
Photocoagulation	60 – 100°C Coagulation; necrosis
Photocarbonisation	100 – 300°C Drying out; vaporisation of cell water; rupture of tissue (pop-corn effect)
Photovaporisation	>300°C Carbonisation and pyrolysis of tissular residues

Photomechanical reactions	**Biological effects**
Photoablation	Fast thermal explosion
Photodisruption	Optical breakdown; mechanical shockwave

Table 3.1: Classes of laser-tissue interaction

Chapter 4

The LASER system

4.1 History of the first LASERS

The acronym LASER stands for Light Amplification by Stimulated Emission of Radiation. It is worth observing that research on LASERs started as an investigation of stimulated amplification in the microwave region of the spectrum. The first LASER was therefore a MASER (standing for Microwave Amplification by Stimulated Emission of Radiation). The first MASER was built in 1954 by C. Townes, utilizing the property of inversion population (more detailed explanation will be given in Section 4.3) between two molecular levels of ammonia to amplify radiation at around 1.25 cm. Other work was carried almost simultaneously by N. Bloembergen, A.M. Prokorov, and N.G. Basov on the optical excitation scheme for masers. In 1958, Schawlow and Townes filed the first patent on lasers, by extending the working principles to optical frequencies, and using a Fabry-Perot resonator for feedback. Other than filing a patent [71], Schawlow and Townes also published their findings on [72]. Those years saw research on laser and the race to build the first laser flourish and become important (patents disputes lasted for thirty years after) amongst several groups in US and Soviet Union. However, the first laser to be built was attributed to T. Maiman who in 1960 developed, demonstrated and patented a system based on a pink ruby crystal optically pumped by a helical flashlamp surrounding the cylindrical laser

crystal [73].

For about ten years, ruby-based lasers were used. Subsequent key discovery was that of the method of Q-switching for the generation of high peak pulse powers [74]. However, the laser was still, apart from its use in the military field (for applications such as military range finders), primarily a research tool. An intensive search of other lasing materials began soon, with research groups around the world investigating a variety of solid-state materials. The first lasers utilizing neodymium as an ionized impurity appear in 1961, using calcium tungstate as a host material. In 1964, the key discovery was made in identifying the Yttrium Aluminium garnet (YAG) as a best choice host material for neodymium ions. Since then, the Nd:YAG laser has proved to be the most versatile of the solid-state lasers. A Nd:YAG-based laser system is the subject of the present work.

Subsequent evolutionary steps in solid-state lasers concerned research on generating shorter pulses. This was accomplished first with the introduction of the techniques of Q-switching - as mentioned in the previous paragraph, and subsequently of Cavity Dumping. If by the and of the 1960s most of the inventions relating to solid-state lasers were made, efforts in the coming years had to be put towards improving reliability and simplify operation to allow commercial use of laser systems. In the mean time, other types of lasers were also investigated and developed, such as carbon-dioxide and argon lasers. Strong competition from these other simpler and more reliable types of lasers was faced by solid-state lasers during the 70s. In the latter part of the 70s, new discoveries led to the development of tunable solid-state lasers, such as Ti:sapphire, which, coupled with ultrafast modulation techniques, allowed to achieve very low pulse durations in the order of femtoseconds. Recent developments in laser diode technology has paved the way for more efficient and compact solid-state laser systems. As it will be shown in the proceedings, different means for providing the energy required to operate the laser are possible, and are primarily divided between Broadband pump sources (arc lamps, flashlamps), and monochromatic pump sources (semiconductor laser diode). The use of Laser diodes offer some advantages over more traditional flashlamp technology in terms of efficiency and lower thermal load of the solid-state

material, both to be attributed to the spectral match of their output with the absorption of the Nd:YAG. The work subject of this research has made use of a Xenon (Xe) flashlamp as the energy source to the Nd:YAG crystal. A more detailed description of a flashlamp and its typical circuit arrangements will be given in the proceedings of this chapter.

4.2 Performance parameters

Lasers are characterized by a set of physical and performance parameters. Traditionally, by varying these parameters, we can tailor the laser characteristics to suit a particular application. Solid state lasers are, amongst all types of lasers, those which offer the highest flexibility of use, due to the large range of output parameters that can be obtained with them. In fact, by choosing size, shape type of the lasing material, and by adding extra active and passive components such as amplifiers, filters, etc, performance parameters such as Average output power, Peak Power, Pulse Width, Pulse Repetition Rate, Linewidth can be controlled. Spatial beam characteristics can be varied to produce different spot sizes and lower the beam divergence . Also, by using tunable lasers, or using optical parametric oscillators it is possible to achieve tunable output.

4.3 Theory and principles of the LASER

4.3.1 Physical explaination

Although the term LASER (or, what is now more commonly referred to as laser) applies to a wide range of devices, and some types are quite distinct from other types, it still is possible to identify common physical principles underlying their operation.

Laser physics, the discipline that studies lasers, is a science which encompasses fields as diverse as quantum mechanics, optics, gas dynamics, semiconductor, atomic and molecular physics and electronics.

In order to understand how a laser works, it is worth focusing on some important concepts, which play a critical role in the design of a laser. One of these concepts is that of the Energy

Transfer among atoms and molecules. Another concept very useful to keep in mind is that factors such as the optical design of the resonator have a major role in the characteristics of the laser output, but they are also influenced by the physics of the laser medium itself (for example, a gas laser would require a completely different setup and design of the cavity than a solid state or a semiconductor laser). As previously anticipated, much of the theory of LASERs involves Quantum Mechanics. Indeed, the original name for laser physics was Quantum Electronics, and this originated from the first lasers built, and the maser research carried out at that time.

4.3.2 Interactions of radiation with matter

In order to understand the behavior of a laser it is fundamental to analyze the basic interactions of radiation with matter. Assuming:

- A laser system can, to the first approximation, be considered as an aggregate of many identical atomic systems;
- At the start (t=0) our systems are at thermal equilibrium, i.e., lower energy states in the medium are more populated than the higher energy states.

According to quantum mechanics, energy transfer between atoms and molecules in a system happens according to transitions between discrete energy states. This change is associated with the emission or the absorption of a photon. This phenomenon obeys to the Bohr's frequency relation:

$$E_2 - E_1 = h\nu_{21} \tag{4.1}$$

where E_1 and E_2 are two discrete energy levels, ν_{21} is the frequency, and h is Planck's constant. The difference in energy between the two levels is called a quantum. Only electromagnetic waves whose frequency is ν_{21} and whose energy corresponds to the energy difference of such an atomic system can interact with.

In order to make the operation of the laser possible, we need to perturb the equilibrium by raising the atoms (or molecules, or ion, according to the different types of lasers) to higher energy levels through interaction with waves and absorption of energy. This energy is applied externally, and it is called a "pump" source - therefore, the process of applying energy in laser physics is called "pumping a laser". When there are more atoms in a higher - excited - level than in the lower level, a situation called "population inversion" happens. When the laser medium is under inversion conditions, a wave incident on the medium will cause the atoms to emit other photons thereby dropping to a lower energy level. The wave will therefore be amplified through this process called Stimulated Emission and supplied to the radiation field. Fig. 4.1 shows the Energy level diagram for a typical 4-level system such as Nd:YAG.

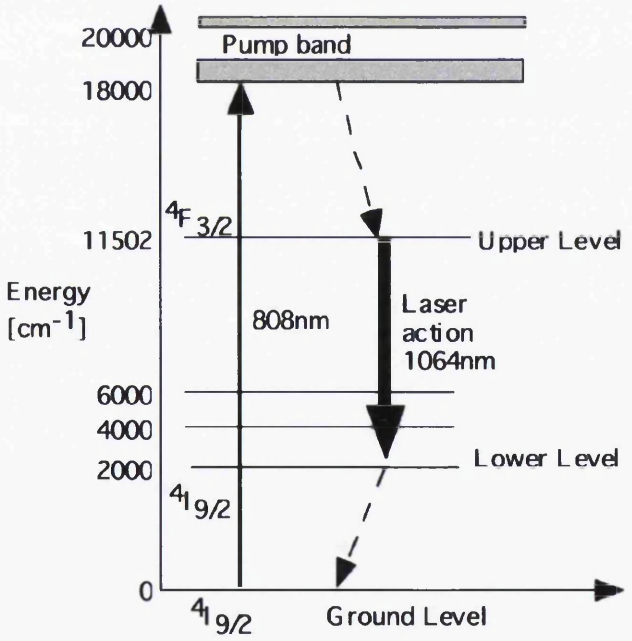

Figure 4.1: Energy level diagram for Nd:YAG (solid line indicates the transition with light; dashed line indicates the non-radiative transition without light). Adapted from [7]

4.3.3 From amplifier to oscillator

The initial emission of radiation - which, in the visible spectrum, would be not dissimilar to having a coherent monochromatic light bulb, provides an output of photons at low energy levels. A further step is necessary in order to benefit from most of the useful characteristics of lasers. When a radiation amplifying medium is coupled to a feedback mechanism in such a way that oscillation is made possible, then the system produces an output at much higher energy levels.

Most laser systems (with the exception of some types of lasers with such a high gain that they do not need mirrors and therefore do not operate in as an oscillator - they are said to operate in "superradiant mode") behave in a way similar to an electronic amplifier that is excited to oscillations by positive feedback. From amplifier theory we know that an amplifier oscillates with positive feedback when the gain becomes greater than the losses. Similarly, in a laser oscillator, the positive feedback is provided by the insertion of two mirrors at the two ends of the laser medium (see Fig. 4.2). This constitutes the basic structure of a so-called laser cavity. Stimulated emission occurring on the axis between the mirrors will therefore travel back and forth between the mirrors, thereby stimulating again emission from the atoms in the medium. In section 4.5, detailed description of concepts of a laser cavity and of a laser head, together with the principles underlying their operation, is given.

4.4 Laser types

A variety of lasers is currently available in the market as valuable tools for the clinician and the surgeon, for use in dermatology and specifically to treat vascular lesions and malformations. As previously outlined, the type of laser used depends on the particular lesion to be treated as location depth and vessel caliber dictate the efficacy of one type compared to another. In the case of vascular lesions, the target chromophore is always the haemoglobin. Although the range of superficial lesions that can be treated is continuously expanding [75], there is still a wealth

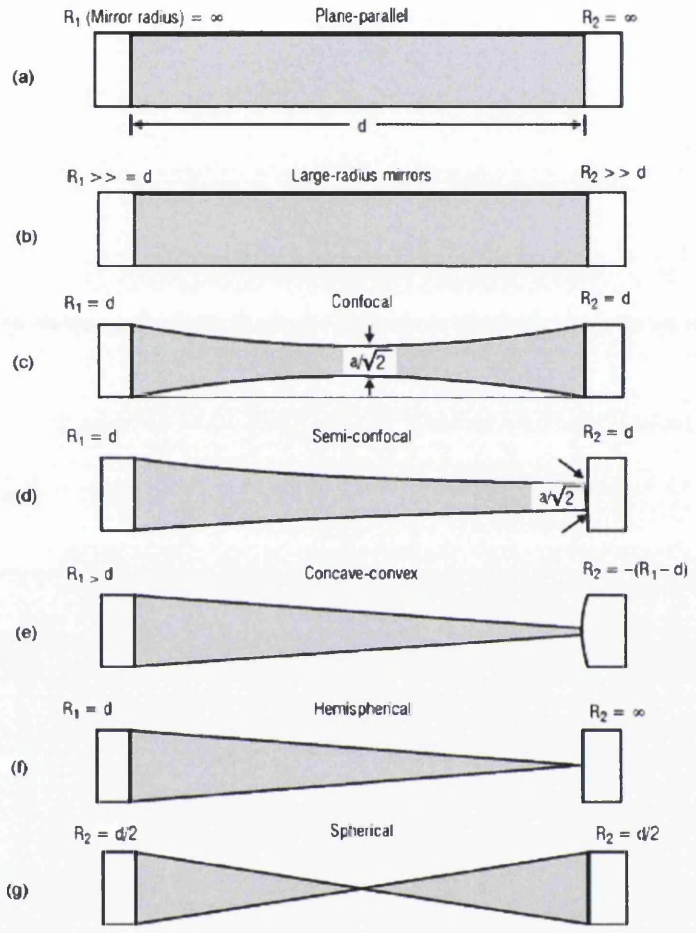

Figure 4.2: Common configurations of laser resonators - the intracavity radiation pattern is shaded (source: [8])

of research currently active on optimising methods and treatment modalities which can even make use of one or more lasers, often in combination. The main types of lasers currently used to target blood vessels are:

- solid state lasers: Nd:YAG, Alexandrite, KTP
- chemical lasers: Pulsed-Dye Laser (PDL)
- semiconductor lasers: laser diodes at 810nm, 940nm

Other than lasers, other light based devices are currently being used, such as Intense Pulsed Light (IPL) devices. IPLs use broadband spectrum flashlamps, which are often filtered to select

a certain wavelength band to allow treatment of specific target vessels superficially (shorter wavelength band) or more deeply (longer wavelength band). Most modern IPL s have been used to treat telangiectasia in the face. Although their usually large spot size offers the advantage of treating a large area, it can also pose the risk of large side effect, as well as sometimes, in some physical implementations, limit maneuvrability in tight concave areas [76].

KTP

By passing Nd:YAG laser light through a Potassyum-Titanyl-Phosphate (KTP) crystal, the wavelenght of YAG light halves (i.e., the frequency doubles), therefore we obtain a 532nm (green) light, which is very close to the 542nm absorption peak of haemoglobin. Systems available have spot sizes of 1-10mm, and pulse widths up to 100ms. Due to the shorter wavelength, depth of penetration through the skin is limited, therefore this laser can be used for small superficial lesions (face, neck and chest). Its use at high fluences often produces scars, and contact cooling is always necessary (through the use of sapphire windows and conduction gel). The KTP laser can also be used to target the epidermal melanin in combination with haemoglobin of superficial small vessels (use in photorejuvenation).

Alexandrite

The Alexandrite laser possess a wavelength of 755nm. The absorption in haemoglobin is less than for the KTP, however, the penetration is much deeper. Treatment encompasses the medium size (0.4-1mm) vessels. Its intermediate wavelength makes it less viable to treat deep vessels than Nd:YAG, however, the near-infrared spectrum at 755nm bypasses the smaller superficial vessels, thus making it not ideal to treat the very superficial smaller lesions.

Nd:YAG

In the general scenario, where absorption phenomena dominate over scattering, the peneration depth of radiation can be defined by using the Lambert-Beer law as the point where the radiation

intensity drops to $1/e$ of its value at the surface. However, for Nd:YAG near-infrared laser light at 1064nm in dermis, because scattering is significantly greater than absorption, photons penetrate more deeply than suggested by the simple application of the Lambert-Beer law. The accurate estimation of the penetration depth can only be obtained by the solution of the Radiative Transport Equation. Hence the need for using the Monte Carlo method in the present thesis rather than a Lambert-Beer-based method. A simple calculation for Nd:YAG reveals that by neglecting the scattering coefficient the penetration depth would be $\approx 4mm$. In practice, the value would be greater than this (between 6 and $7mm$) due to the aforementioned high scattering. Nd:YAG light can therefore penetrate deeply in the skin [77] and this characteristics makes it a good candidate for treating leg veins together with conditions such as Port-Wine Stains. The deep penetration means that often cooling (cryogen spurts, sapphire windows, force cold air) is required of the treatment area to counteract pain caused by heating. However, as the long wavelength is weakly absorbed by melanin, risks for epidermal damage whilst treating vascular lesions especially in patients with higher pigmentation is reduced.

PDL

PDL was originally developed primarily for the treatment of Port-Wine Stains. Current commercial systems have wavelengths of 585, 595nm, and especially the latter allows much deeper tissue penetration. Novel technology designs allow reduced number of treatment sessions through the use of a more gentle irradiation provided by particular arrangements in the subdivision of the pulse within shorter pulses. Reported clearance of small telangiectases greater than 90% have been reported [78]. Other recent advances for PDL are the availability of $3mm \times 10mm$ elliptical spot sizes, with marked improvements in the treatment of some spider veins conditions.

Laser diode

laser diodes at the wavelength of 810nm and, more recently, the longer 940nm, are successfully used to treat venous venous malformations such as venous lakes and telangiectatic leg veins

of diameters between 0.8-1.4mm, thanks to the relatively deep penetration. Often, immediate vessel clearance is achieved. It is relatively safe for patients with skin type I to IV [79].

4.5 Laser system - Components

Explanation of the traditional laser technology and components with primary reference to solid state lasers systems and YAG in particular is provided in the proceedings of the chapter.

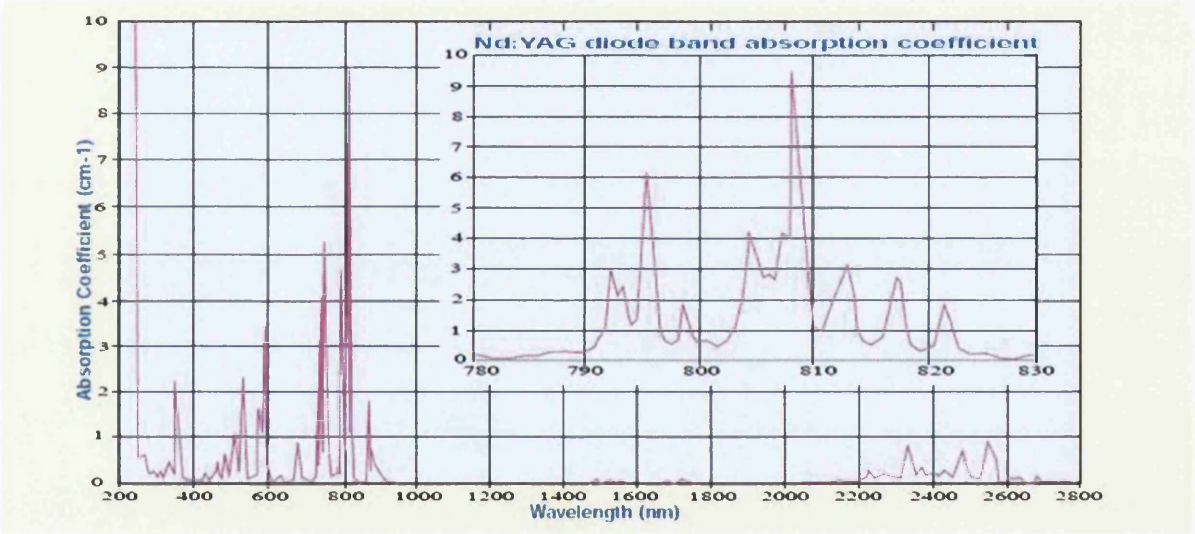

Figure 4.3: Absorption spectrum of Nd:YAG (from [9])

4.5.1 Laser cavity and laser head

As outlined in 4.3.3, in order to constitute a laser cavity, a lasing medium, an excitation medium, and a mechanism to provide feedback are the essential constituents of a laser cavity. Several approaches have been proposed over time for the design of such a cavity. They can be divided in to two main categories, namely, focussing and non-focussing pump cavities. The first configuration historically made use of a helical flashlamp placed around the laser rod, within a cylindrical reflective cavity. This approach has been supplanted by more modern approaches -

with reference to our categorisation such as an elliptical reflective cavity where a linear lamp and the laser rod occupy the two foci of the ellipse, respectively (see Fig. 4.4). A variation of this design makes use of two intercepting elliptical cylinders with the laser rod as the common focus between the ellipses and two linear flashlamps occupying the other foci. Another approach to building the cavity is the so-called *closed-coupling* configuration, which sees the lamp and the rod to be placed next to each other within a reflective cavity.

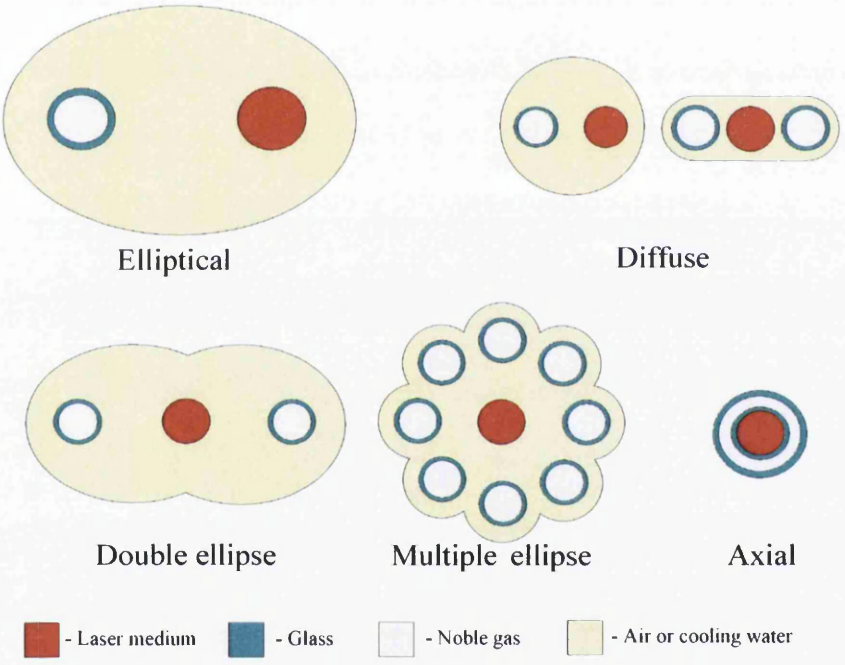

Figure 4.4: Common configurations of laser pump cavities (source: [10])

4.6 Flashlamp system

4.6.1 Flashlamp principles and technology

In order to pump a laser, technology based on flashlamp has traditionally been used, as it constitutes a relatively mature technology nowadays. A type of long arc flashlamp makes use of halogen gases such as Xe and Kripton (Kr). Xe and Kr flash lamps are confined arc flashlamps which produce microsecond to millisecond duration pulses of broadband light of high radiant intensities. Capable of operating at high repetition rates, these flashlamps generate light over a continuous spectrum from ultraviolet to infrared [80].

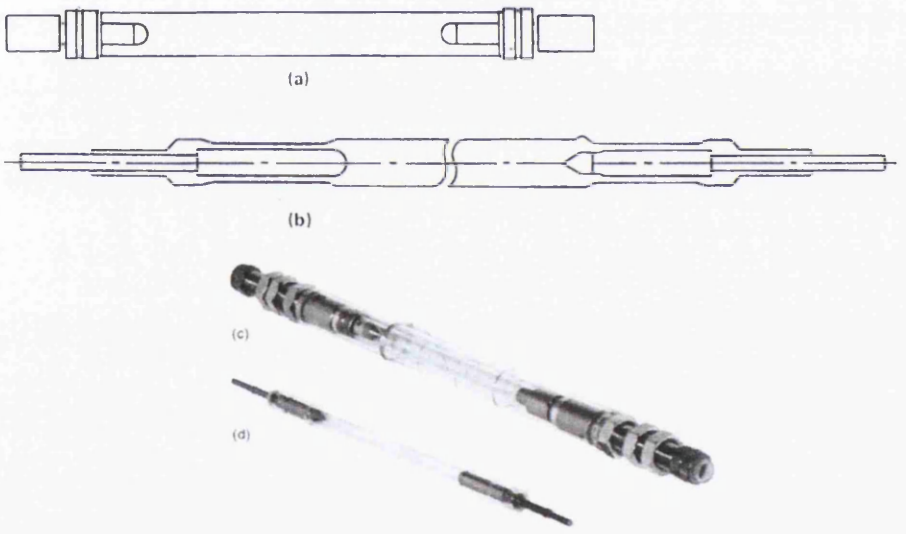

Figure 4.5: Drawing of (a) a flashlamp and (b) a continuous wave Kr arc lamp, (c) arc lamp with cooling jacket and (d) without cooling jacket (from [11])

Their use varies from the pumping of small lasers to the megajoule regime of solid state lasers used for inertial confinement fusion research experiments. Fig. 4.5 shows typical commercially available flash lamps to pump solid state lasers. Their use also extends to pump dye lasers. Flash lamps are manufactured in either helical or linear shape, and a number of paramenters,

among which:

- Type of lamp seal
- Envelope material and size
- Electrode style
- Power density
- gas
- fill pressure

dictates their output performance.

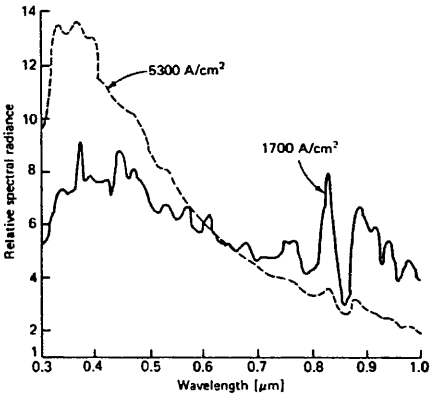

Figure 4.6: Spectral Emission from Xe Flash lamp with gas fill pressure=0.4atm. (EG&G, model FX-47A), at high current densities, and related black body approximated temperature values (source: [12])

From Fig. 4.6 we notice that the typically pulsed output of a flash lamp is for high current levels masked by a strong continuum. Moreover, it is possible to notice an apparent shift of the spectrum towards shorter wavelengths as the current intensity is increased. This is taken in to account by the emissivity of the flashlamp. The emissivity in general is greater at longer wavelengths than at shorter. Therefore, since the emissivity depends on both temperature and wavelength and increases for increasing power density, the end result is that the shorter wavelength band experiences an increase in emissivity greater than the longer wavelength band (for which the emissivity is already ≈ 1) with a resulting shift in intensity for shorter wavelengths.

Physics of flashlamp

When a flashlamp is designed, the gas fill type and pressure can be varied to suit the specific application for which the flashlamp is to be used. The spectral output of a flashlamp is determined by the current density i.e. the amount of current flowing per unit of cross sectional area of the lamp. Current density through a flashlamp is given by the expression:

$$J = \frac{4I}{\pi d^2} \tag{4.2}$$

where d is the bore diameter, I the current through the flashlamp; J is expressed in $[Acm^{-2}]$.

Current density is therefore proportional to the inverse square of the internal bore diameter of the flashlamp. Thus, a flashlamp of 8 mm diameter requires four times as much current as a 4 mm diameter flashlamp to deliver the same energy density. Hence a system, which uses narrow flashlamps uses far less energy than its large diameter counterparts.

An expression which does not take into account the time dependence of current change is called the $E_0 : T_A$ ratio. This is used to describe the loading rather than current density of a pulsed lamp and does not include a term for time dependence with respect to the current. The unit of measurement of this ratio is Watts per square centimetre $[W/cm^2]$ and so it is a measure of power density rather than current density. E_0 is the pulse energy in Joules supplied to the flashlamp and T is the pulse duration in seconds. The area A in this ratio refers to the internal surface area of the lamp envelope in the discharge region. The area is approximately $\pi d L_A$ where L_A is the arc length of the lamp and not the cross sectional area of the lamp bore, which is the area used in measuring current density.

The efficiency of energy conversion will increase with gas fill pressure in the Xe lamp up to a saturation point, but the disadvantage is that the lamp requires a higher trigger voltage and if a simmer current is used it will be more difficult to create and sustain. Default fill pressures in pulsed flashlamps are approx. 450 Torr in Xe lamps and approx. 700 Torr in krypton lamps.

The internal impedance of a flashlamp changes over the duration of the plasma discharge.

This is a direct result of the almost instantaneous heating of the gas plasma within the flashlamp bore. When a flashlamp has no potential difference across the tube it is non-ionised and thus has very high impedance, around 10^7 ohm or more, and thus initially, the entire power supply unit current flows into capacitor C, illustrated in Figure 4.7. If the voltage across the capacitor reaches a value equal to the breakdown voltage of the flashlamp, ionisation of the lamp gas starts to occur and so its impedance begins to decrease. A low impedance path quickly forms directly between the electrodes of the flashlamp as more gas atoms are ionised. Current now starts to flow from the capacitor into the flashlamp and the impedance of the lamp continues to fall, dropping down to about 1 ohm or less. If sufficient energy is available, the plasma of ionised gas in the lamp completely fills the internal bore. Eventually all the energy stored in the capacitor is expended and the lamp returns to a deionised state. Conduction through the lamp ceases and the power supply unit begins to recharge the capacitor and thus the process continues.

Assuming the plasma growth is instantaneous and completely fills the entire envelope in contact with the inner walls, the impedance is described by having the following relationship with time:

$$K_0(t) = \left| V(t)\,[I(t)]]^{-1/2} \right| \tag{4.3}$$

where $V(t)$ is the voltage across the lamp at time t, in Volts, $I(t)$ the current through the lamp at time t, in Ampere, $K_0(t)$ is the arc impedance parameter at time t, in $\Omega A^{1/2}$ and $K_0(t)$ is a function of the time dependant size of the arc and the nature and fill pressure of the gas in the lamp.

$$K_0(t) = \left[\frac{1.28 L_A}{dA(t)}\right]\left[\frac{P}{N}\right]^{-1/5} \tag{4.4}$$

where L_A is the arc length, in mm, $dA(t)$ the arc diameter at time t, in mm, P is the gas fill pressure in the lamp, in $Torr$ and N is a constant dependant on gas type [Xe = 450]).

A good approximation can be reached without dealing with the time dependant equations above, by assuming that the diameter of the arc is always equal to the diameter of the bore of

the flashlamp d and by assuming dA(t) is not time dependant. In general the time taken to reach wall-confined stabilization is less then one hundredth of the pulse duration:

$$K_0 = 1.28 \left[\frac{L_A}{d_A}\right] \left[\frac{P}{N}\right]^{-1/5} \tag{4.5}$$

K_0 can now be referred to as the impedance constant of the flashlamp. This is constant as it depends only upon the flashlamp's physical dimensions and the type and pressure of gas fill. K_0 is a critical parameter in describing a pulsed flashlamp. In systems using constant current power supplies, designers are primarily concerned with the K0 of the flashlamp as this determines the flashlamp's power output and hence the power of the flashlamp itself.

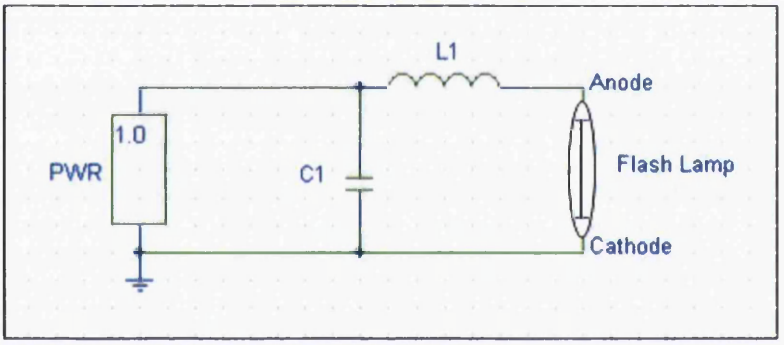

Figure 4.7: Basic schematic showing the components responsible for providing and delivering the energy to the flashlamp (adapted from [13])

The approximation for K0 based on bore diameter, arc length, gas type and cold fill pressure equation C still remains for lamps used under constant current operation. In considering a constant current in terms of both lamp current and lamp voltage, and where the discharge is fully wall-confined, reference to the timing within the pulse is no longer relevant, as it is the same at all stages during the wall stabilised pulse. This simplifies some of the theory, and the relationship between voltage, current, and K_0 previously described can now be expressed as:

$$V = K_0 I^{1/2} \tag{4.6}$$

$$PulsePower = K_0 I^{3/2} \tag{4.7}$$

$$I = \left[\frac{E_0}{K_0} T\right]^{2/3} \tag{4.8}$$

where T is the Pulse width in seconds.

Flashlamp technology

As described previously, flashlamps essentially consist of a quartz tube, two electrodes sealed within the envelope, and a gas fill. Xe provides a higher radiation output for a given electrical input energy, whereas Krypton offers a better radiation spectrum match with Nd:YAG, but lower radiation output, and it's best suited for low energy devices. As mentioned, the gas fill pressure has been shown to influence the performance of the flashlamp-pumped solid state lasers (see, for example, [81]) through the change in temporal profile of the current pulse through the lamp through changing the impedance of the lamp. However, for the purpose of these studies, the fill pressure is of secondary importance, as it will be shown in the following chapters.

In the proceedings of this work, focus has been put on demonstrating controllability of a solid state laser through digital control of the flashlamp. Operation of the lamp within this work has always been kept in the low current spectrum of operation (i.e., well below the physical limits of the flashlamp), therefore such parameters are of less importance and of no contribution to the experiments.

4.6.2 Driving electronics - the flashlamp driving circuit

Flash lamp devices used to pump solid state lasers are generally embedded within a so- called flash lamp trigger circuit. Flash lamps are normally operated within high-voltage / high-current / high light intensity vs power conditions. It is therefore of paramount importance to be able to provide the necessary energy to the lamp, and this is accomplished through the use of an

energy storage element, i.e., a capacitor. The capacitor is embedded within a circuit which allows the capacitor to charge thereby storing the energy; circuitry is also provided to allow a desired current pulse shape to be delivered to the lamp, as well as components to allow the lamp to be triggered and switched. Therefore, in general terms, a traditional flash lamp driving circuitry can be described as to be constituted by three main parts, namely:

- capacitor charging circuit
- pulse forming network
- flashlamp trigger circuit

Description of the triggering will be now carried out as this constituted the subject of a design choice for the system.

Flashlamp triggering

In order to trigger a flash lamp devices to fire lasers several different ways or topologies can be implemented.

The main topologies for triggering most in use are:

- external (parallel) triggering
- series (and pseudo-series) triggering
- simmer (and pseudo-simmer) mode
- overvoltage triggering

The flashtube discharge is initiated by means of a high voltage pulse Vz (trigger voltage) which must be higher than the static breakdown voltage of the tube [14] For most manufacturers, see for example, Perkin Elmer, V_z ranges between 2kV and 20kV. The difference between V_z and V_0 must be sufficient to avoid spontaneous triggering.

It is recommended that V_z is generated by a pulse transformer (trigger coil) at a transformation ratio of 1:20 to 1:100. A thyristor (or mechanical switch) discharges a trigger capacitor C_z via the primary side of the trigger coil. On the secondary side a damped high voltage oscillation is produced, the form of which greatly depends on the trigger coil and the external circuitry.

Among the types that may be referred to be Parallel triggered, the Capacitive external triggering (see Fig. 4.8) is the simplest form of triggering. In this case, the trigger electrode of the tube has been insulated from anode and cathode. However, it extends over the entire arc length.

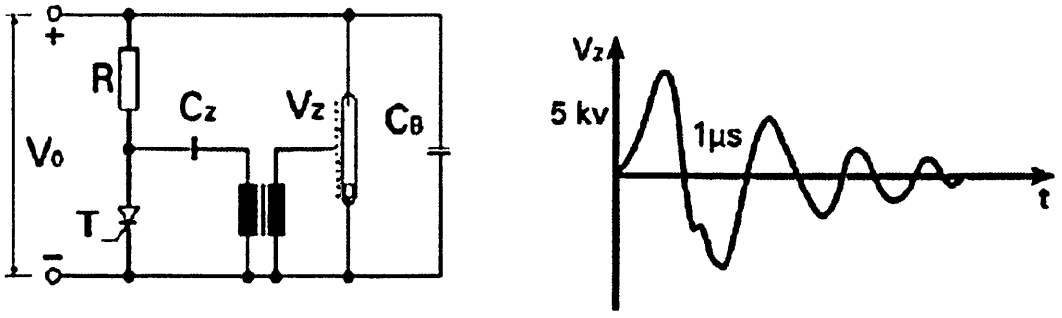

Figure 4.8: Capacitive external triggering circuit (from Perkin-Elmer, Inc. [14])

Advantages of this solution are normally a compact size of the coil, since the capacity of the trigger electrode is approximately $10pF$ against the cathode and anode and therefore the secondary side of the trigger coil can be highly resistive.

Disadvantages of external triggering are a relatively high trigger delay time (approximately $10 \pm 5\mu s$) and electromagnetic interferences in case of long wires in circuit.

The polarity of the first half wave of the trigger circuit can influence the trigger ability.

Another very common design is to have the secondary winding of the trigger coil either on the anode or cathode side of the tube to conduct, in any case, the entire discharge current. The optional trigger electrode H can be connected with anode or cathode. In comparison to the capacitive external triggering, the advantages of direct series triggering are: short trigger delay time ($< 1\mu s$) - with minimum jitter; low emission of electromagnetic interferences. Normally, however, direct series triggers are large size and high cost components.

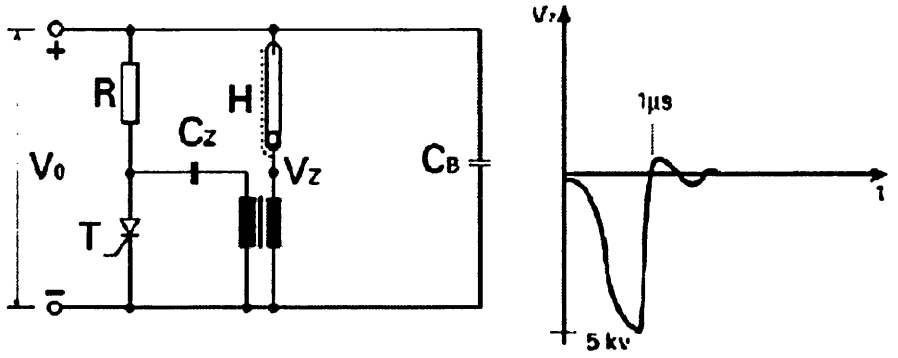

Figure 4.9: Direct Series triggering circuit (from Perkin-Elmer, Inc. [14])

4.7 Operation

Operation of a typical power supply unit to drive flashlamp can be described as follows.

A previously outlined, flash lamps, or discharge tubes as they are also known, typically comprise a sealed glass chamber in which a low pressure gas is contained. The chamber further comprises an electrode at each end thereof for providing an electrical discharge within the chamber and a further external electrode for ionising the gas to create a conduction path or arc between the electrodes. The electrodes extend from the interior of the chamber to the exterior of the chamber and thus permit external connection to a circuit for controlling the operation of the discharge.

The voltage difference across the electrodes must be significant and in order to maintain an ionised state of the gas, the voltage is stepped-up using a suitable charging circuit. The initial ionisation is triggered with the application of a trigger voltage across the electrodes, which requires the use of a timing circuit for timing the application of the stepped-up voltage with the trigger voltage.

Pulsed output flash lamps are conventionally used for intense pulsed light radiation treatment of skin or other tissue (typically mammalian tissue), for example, for medical purposes such as treatment of collagen, or for "optocosmetological" purposes such as depilation, wrinkle removal

or treatment of skin blemishes such as port wine stains. In operation, such intense pulsed light flash lamps give out discrete intense pulses of light, as opposed to conventional fluorescent lighting apparatus which is intended to operate in a quasi continuous manner.

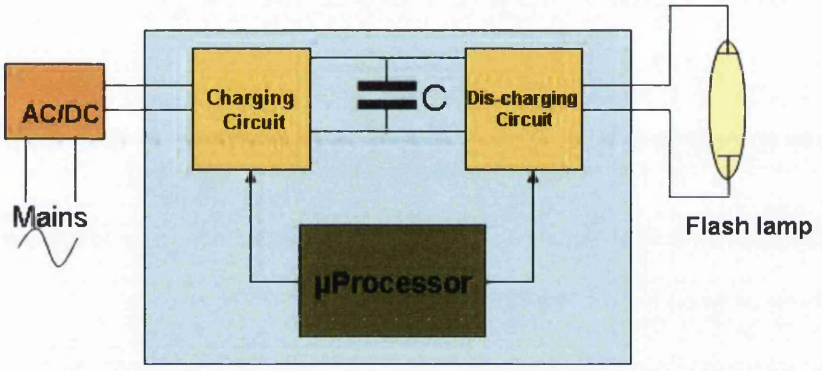

Figure 4.10: Conventional control circuit

A conventional control circuit for a flash lamp is shown in Fig. 4.10 and comprises a charging circuit and a discharging circuit. The flash lamp is powered from a mains supply via an Alternating Current / Direct Current (AC/DC) converter, which provides a low direct current (dc) voltage to the charging circuit. During charging of a main capacitor, the charging circuit boosts the low dc voltage up to a significantly higher voltage.

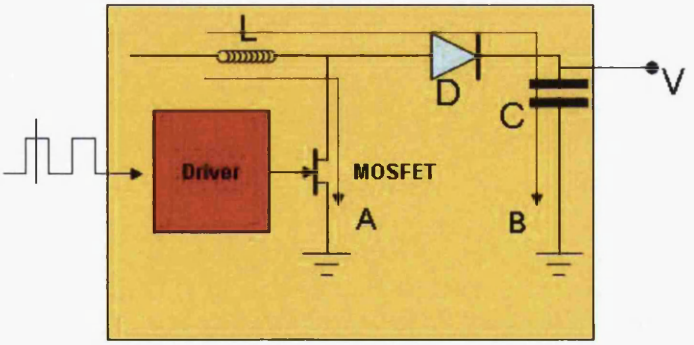

Figure 4.11: Conventional charging circuit part of the control circuit shown in Fig. 4.10

The charging circuit is pivotal to the correct operation of the flashlamp. The circuit is shown

in more detail in Fig. 4.11. The microprocessor of Fig 4.10 can deliver a square wave control signal of variable "ON" and "OFF" durations to a driver circuit, which converts the signal from the microprocessor to a voltage level suitable for driving a Metal Oxide Semiconductor Field Effect Transistor (MOSFET).

When the MOSFET is switched "ON", current flows according to path A, as shown in Fig. 4.11. As the current increases, energy becomes stored in the inductor L in the form of increasing magnetic field. When the MOSFET is switched "OFF", the inductor magnetic field energy is converted by the inductor into current to charge the capacitor via a diode, as shown by current path B. The value of this current starts at the level immediately before the MOSFET is switched "OFF" and decays linearly to zero. The whole cycle then repeats.

The current "I" is initially zero when the MOSFET is first switched "ON", but increases to a value given by the following formula:

$$I = V \times \frac{t}{L} \tag{4.9}$$

where t is the time in seconds, V is the input voltage (typically $19V$), and L is the inductance of the Inductor, in Henrys.

The microprocessor controls the "ON" and "OFF" times of the MOSFET such that during the "ON" time the current does not increase to a level where the inductor L would saturate or other circuit parts would operate in excess of rated current values. Also, during the "OFF" period, the inductor must be allowed to decay to zero before the cycle is restarted in order to prevent the inductor current going to saturation or the entire control circuit overloading over a number of cycles - a process commonly referred to as "walk to saturation". In addition, the microprocessor should minimise the circuit dead time, namely the time between zero inductor current and the start of a new charging period.

The circuit begins the charging sequence with the MOSFET in the "ON" state such that the capacitor voltage begins at a low dc voltage. The MOSFET is then switched "OFF" for

sufficient time to ensure that the inductor current completely decays to zero. The collapse of the inductor current generates a voltage spike which is used to add charge to the capacitor. The voltage spike is greater than the potential difference across the terminals of the capacitor when fully charged. However, during the collapse of the inductor current only an incremental charge and voltage are applied to the capacitor. Accordingly, after the inductor current has completely decayed to zero, the MOSFET is then switched back "ON" for a pre-determined time and then "OFF" again, so as to add more charge to the capacitor and thus increase the voltage across the capacitor terminals. This process is repeated until there is a sufficient potential difference across the capacitor terminals to create an optical output from the flash lamp.

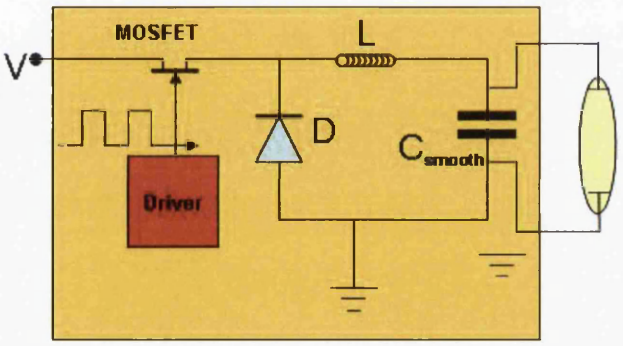

Figure 4.12: Discharge circuit within a typical flashlamp driving circuit

In Fig 4.12, the capacitor (not shown) discharges across the flash lamp via a discharge circuit. The discharge circuit utilises a step down, or buck converter circuit, arranged in a configuration where the source terminal of a further MOSFET is connected to an inductor via a diode. The discharge is provided when the further MOSFET is switched "ON" and this is again controlled by the microprocessor which thus controls the timing of the application of the discharge to the flash lamp.

With the further MOSFET switched "ON", the capacitor discharges across the flash lamp and current flows in the inductor. However, the MOSFET is only switched "ON" for a limited time to prevent the inductor current going to saturation. Before the inductor current reaches

saturation, the MOSFET is switched "OFF", thereby preventing further discharge of the capacitor, and the current in the inductor subsequently decays so as to create a voltage spike in an attempt to maintain the optical output from the flash lamp. The MOSFET is then switched back "ON" to further discharge the capacitor and thus maintain the voltage across the flash lamp. This process is repeated with each successive step involving a small reduction in the charge stored on the capacitor. In order to smooth the voltage waveform applied across the flash lamp, a capacitor C_{smooth} will typically be placed across the output terminals of the discharge circuit.

When the capacitor has fully discharged across the flash lamp, the entire process may then be repeated by switching the MOSFET in the charging circuit "ON" and "OFF" as described above to recharge the capacitor C.

The main trend has been towards utilising two separate circuits for charging and discharging the main Capacitor for operating a flash lamp. Therefore, each of the circuits comprises of separate components for their charge/discharge function, respectively. Accordingly, these charge/discharge circuits add to the size and weight of the resulting control circuit.

In addition, the above-mentioned charge/discharge sequence has been found to be complicated - it involves critical timing and relatively long charge times which are longer than the discharge time.

4.8 Design Considerations of traditional technology

Flashlamp devices, especially Xe lamps have the capability of being rapidly pulsed. This characteristics make them desirable in devices as varied as reprographic copiers as well as light based medical devices and a myriad of other applications. Traditional designs of flashlamp-based devices suffer from a number of significant disadvantges. As explained, for flashlamp operation, it is necessary that a dc voltage source be present to enable charging of one or more storage elements in the system (i.e., capacitors) to a desired voltage. The storage elements are then discharged through the lamp creating the flash illumination. The energy requirements for flashlamp operation can be quite substantial (for certain applications, such as for example reprographic

copy, up to 500-800J are normally needed to provide fusing of the toner). Since the design trend was towards providing energy storage of at least equal to the requirements of the operation of the devices, technology made traditionally use of large capacitors. Large capacitors add considerably to the weight and size of the system, and ultimately to the cost. Since the mid 80's there have been few propositions towards improving the energy delivery within flashlamp based devices, for example, techniques employing principles of switched capacitances have been proposed to enable the use of capacitances with values smaller than the required energy to be delivered. Techniques such those described in [82] make use of more than one capacitor to decrease the overall size of the system. Such design makes use of a variable output power supply with small internal capacitance and high voltage, and two capacitors. By using an automatic switching and control unit, the capacitors, each of them embedded within a capacitor charging circuit, are alternatively charged and discharged, thus each of them providing a burst of energy to the lamp, and increasing incrementally the total amount of energy to the lamp, until the energy required for the particular application is reached. In order to increase the efficiency of such systems, often implementation of techniques of so-called switching at zero-current crossing through the use of dc resonant circuits for the charge of the capacitor are employed.

4.8.1 Limitations of traditional technology

There are severe limitations in the traditional technology and in the flexibility of operation of traditional flashlamp and flashlamp-pumped laser power supply units.

First of all, limitations in weight and size have generally made the in field deployment of flashlamp pumped solid state laser units problematic. Utilisation of portable low power, low energy solid state units has traditionally been limited to the military field for very specific applications.

Solid state lasers for all the other applications, such as medical, have suffered from having to utilise a bulky and heavy technology.

The on-and-off operation of the capacitors is generally accomplished by using tyristors and

transistors. Tyristors, albeit being reliable and fairly components, have the main disadvantage of creating contention against turning off - they remain on until the storage element has fully discharged.

On a related matter, until very recently [83] technological developments did not provide capability of producing programmable pulse shapes for the flash lamp output that could have a fast change rate (quickly changing). Furthermore, in order to limit the size of the capacitors to reasonable values (it is worth noting that the size of the capacitors in the traditional circuit design would increase linearly with increasing the pulse width) the duration of the flashlamp pulse was severely limited in time to a few milliseconds. This situation was also made worse by the fact that in traditional circuit design, the utilisation of the Capacitor was extremely low, generally never exceeding 50% of the total available energy storage capacity. This latter factor clearly indicated that traditional designs were hampered by a poor utilisation efficiency of components. Large capacitors also pose important safety issues as an increased amount of stored energy also increases the risk of shock hazards when handling lamp drive circuit voltage and current levels which can be prohibitive for some applications an market audience.

In parallel, circuits techniques have also been developed to avoid premature failure of the flash lamp, thus increasing the mean time between failure of the system, therefore reducing maintenance costs. A most common technique employs a subcircuit to provide a low current density simmer mode to the lamp prior to transfer to an arc mode, which is the mode of operation during which the flash is produced. The simmer current maintains discharge within the lamp after the breakdown is initiated through triggering of the lamp (operation this to be accomplished by a triggering circuit), thus avoiding to have to initiate breakdown every time before a flash has to be produced. In this fashion, however, the circuitry for the main discharge mode is kept separate from the simmer mode circuitry, thus increasing again size and weight due to the duplication of components within the system.

Chapter 5

Modelling

5.1 Introduction and theoretical background

In order to understand how the incident laser light interacts with the tissues of a typical vascular lesion, a theoretical model was constructed. This model was based upon a two-stage process.

The first stage used a simplified model of vascular lesion skin to generate a fluence map of the irradiated zone. By using the optical parameters of the skin, namely the absorption and scattering coefficients, the individual photons of the incident laser light were tracked throughout their progression through the various upper layers of the skin and vasculature. The fluence map produced indicated how the laser light was distributed throughout the lesion site.

The second stage of the model used a geometrical representation of the temporal profile of the laser pulse, coupled with the fluence distribution map, to produce a time-dependent thermal profile of the irradiated site.

The tissue was represented by a simple two-dimensional, multi-laminar structure incorporating the various skin layers and vasculature (Fig. 5.1). The physical dimensions of both the skin layers and blood vessels were taken as representative of a typical venous malformation. It was assumed that the laser light was perpendicularly incident to the skin surface thereby reducing the amount of light lost through reflection at the air-skin boundary, this being the normal clinical

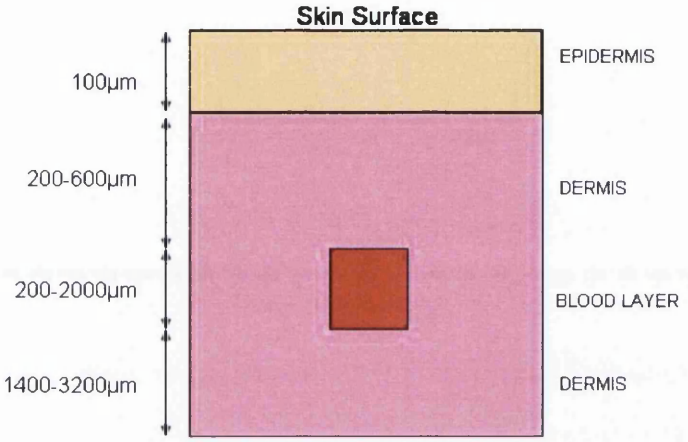

Figure 5.1: Representation of the 2D Monte Carlo model

operating procedure. However, this reflection was taken into account by reducing the amount of incident laser light by 4%, this being typically the value of reflection of a normally incident beam of visible light. The tissue to be modelled was represented as a two-dimensional array of cells, each cell having an absorption and scattering coefficient, shown in Fig. 5.2. Photons are released at the left hand boundary and their progress through the cells is recorded. Those photons that reach the right boundary determine the percentage of light transmitted by the tissue layer, photons scattered out of the mesh are not considered in the final total of transmitted photons.

For any given cell, a photon can be absorbed or scattered, the weighting of the direction of scatter being determined by the anisotropy factor g of the tissue.

The probability of absorption is given by the *albedo*:

$$\frac{\mu_a}{\mu_a + \mu_s} \tag{5.1}$$

Where μ_a is the absorption coefficient and μ_s is the scattering coefficient. The probability

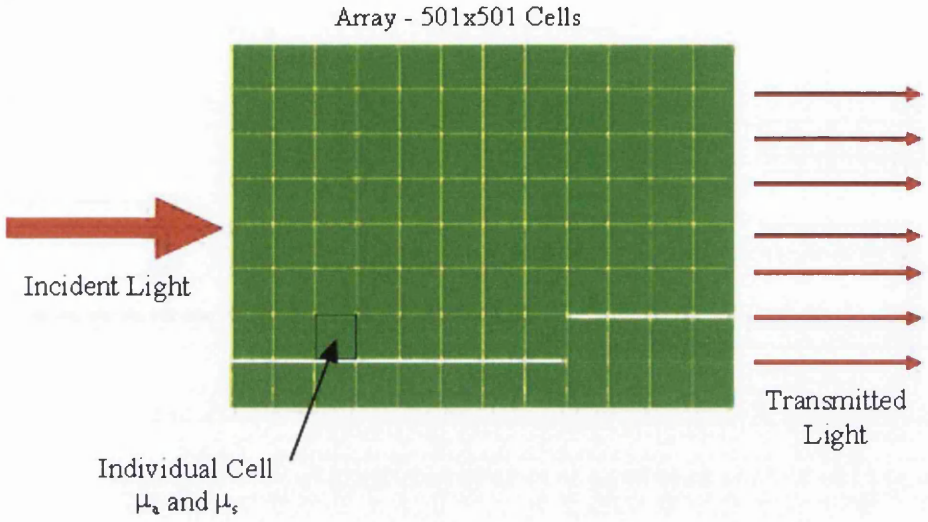

Figure 5.2: Two-dimensional Array Representing Tissue

of scattering is given by:

$$\frac{\mu_s}{\mu_s + \mu_a} \tag{5.2}$$

A photon in any given cell could be scattered into any one of 8 adjacent cells as per Fig. 5.3, the direction of scattering being determined by the Phase Function (see Eq. 5.7.

The anisotropy factor g is the mean cosine of the scattering angle. Where $g = 0$ the scattering is isotropic, $g = 1$ scattering is purely forward and $g = -1$, the scattering is purely backwards. Fig. 5.4. The anisotropy factor g is wavelength dependent and is derived from:

$$g \approx (\lambda 0.29^{-3}) + 0.62 \tag{5.3}$$

where λ is in nanometers and is only applicable for highly scattering, non vascular tissues. The scattering was defined by the Henyey-Greenstein phase function, namely:

$$p(\theta) = \left(\frac{\mu_s}{\mu_s + \mu_a}\right) \frac{(1 - g^2)}{(1 + g^2 - 2g\cos\theta)^{\frac{3}{2}}} \tag{5.4}$$

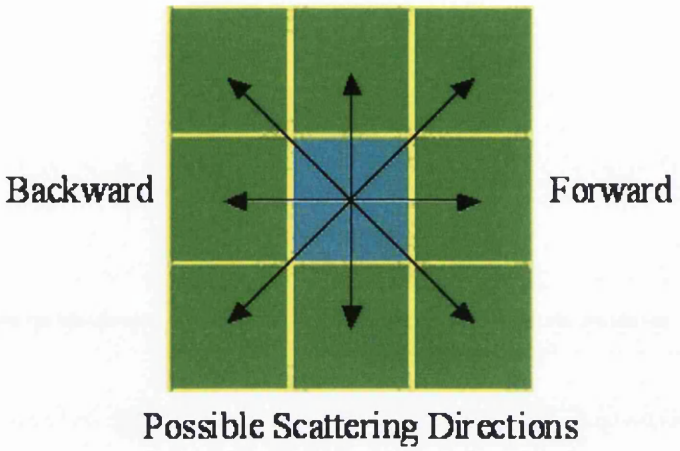

Figure 5.3: Model for the possible scattering directions

of which the generating function is

$$\cos\theta = \frac{1}{2g}\left\{1 + g^2 - \left[\frac{1-g^2}{1-g+2g\xi}\right]^2\right\} \tag{5.5}$$

where ξ is a pseudo-random number uniformly distributed over the interval zero to one. ξ is, for an isotropic distribution, related to the angle θ by the relationship: $cos\theta = 2\xi - 1$, with the azimuthal angle, $\phi = 2\pi\xi$ (if there is no azimuthal dependence ϕ is uniformly distributed between 0 and 2π). When a photon is scattered with angle (θ, ϕ) from a direction of travelling (μ_x, μ_y, μ_z), the new direction will be specified by a new vector (μ'_x, μ'_y, μ'_z) [15]:

$$\begin{aligned}
\mu_x{}' &= \frac{sin\theta}{\sqrt{1-\mu_z{}^2}}(\mu_x\mu_z cos\phi - \mu_y sin\phi) + \mu_x cos\theta \\
\mu'_y &= \frac{sin\theta}{\sqrt{1-\mu_z{}^2}}(\mu_y\mu_z cos\phi + \mu_x sin\phi) + \mu_y cos\theta \\
\mu'_z &= -sin\theta cos\phi\sqrt{1-\mu_z{}^2} + \mu_z cos\theta
\end{aligned} \tag{5.6}$$

The Heyney-Greenstein defines the probability factor of a photon being scattered to a particular

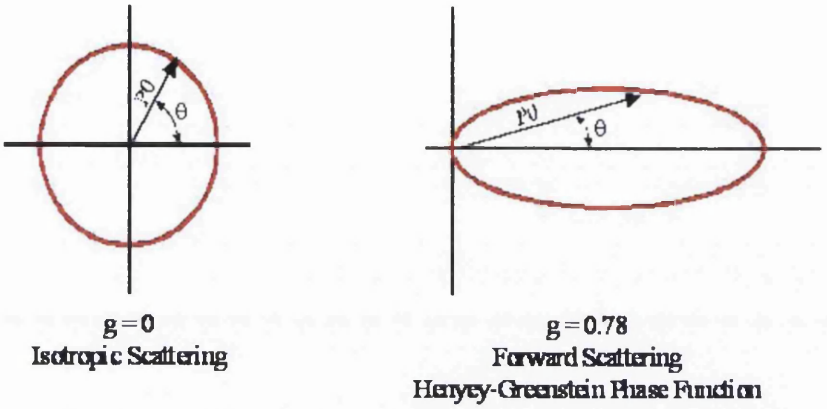

Figure 5.4: Graphical Representation of the Anisotropy Factor.

angle θ. Rearrangement of the equation leads to the angle of scatter being determined, i.e.

$$\theta = \cos^{-1} \frac{1}{2g} \left(1 - g^2 \left(\frac{1-g}{p(\theta)}\right)\right)^{\frac{3}{2}} \tag{5.7}$$

The mean free path, defined as the distance travelled between successive interactions, is given by:

$$L = -\ln\left(\frac{R}{\mu_t}\right) \tag{5.8}$$

Where R is a pseudo-random number $0 < R < 1$, and μ_t is the total extinction coefficient, equal to $\mu_a + \mu_s$. The absorption, scattering and anisotropy values of the skin layers at a wavelength of 1064 nm are shown in the table below. By using 10^7 photons as the incident laser

Table 5.1: Optical Properties of various skin structures at 1064nm

Skin Layer	Absorption Coeff. $[mm^-1]$	Scattering Coeff. $[mm^-1]$	Anisotropy Factor
Epidermis	0.35	260	0.79
Dermis	0.26	130	0.79
Blood Vessel	3.9	470	0.79

light, the path each photon followed through the array was modelled in the following way:

- Each photon is launched into the tissue along the direction of the laser beam. A random

number generates the distance, L, travelled by that photon. A second random number generates the scattered angle, θ, calculated from the Henyey-Greenstein function, that the photon experiences after travelling the distance L.

- The basal layer is incorporated into the epidermis as a piecewise linear distribution of melanin and the absorption and scattering coefficients are then combined in proportion.

The method outlined above is called Monte Carlo method [84]. It refers to a technique first proposed in 1949 by Metropolis and Ulam as a way of simulating physical processes through the use of stochastic model, as shown in [85]. When applied to radiative transport problems, it consists of recording photon histories as they are scattered and absorbed. The method, in its simplest implementation, propagates each photon with a small fixed incremental stepsize. However, this approach is not very efficient. More efficient methods, such as that one used in this thesis, make use of different stepsizes for each photon steps, through the use of randomly generated numbers to feed in to the equations described before. The flowchart in fig. 5.5, adapted from [85], shows the variable stepsize Monte Carlo algorithm. In this method, therefore, the photon undergoes partial absorption in each interaction event by an amount given by the albedo. This technique is well established in laser-tissue modelling and allows the Monte Carlo method to converge more quickly. In this way the energy of a photon will decrease until a minimum threshold value is achieved and then it is deleted. Consequently, each photon will experience significant scattering and the convergence of the statistical method is improved compared to simply deciding whether a photon is entirely absorbed or entirely scattered at each interaction event.

Once the Monte Carlo calculation has been completed, each cell in the 2D computational model will contain a proportion of the photons launched. These locally deposited photons become the source terms , Q(x,y) in the time dependent thermal transport equation described in the next section. The result of this model indicated what percentage of the incident light reached the target vessel after passing through the upper layers of the skin. Taking the physical parameters in 5.2 as being representative for the vascular lesions of interest, the Monte Carlo

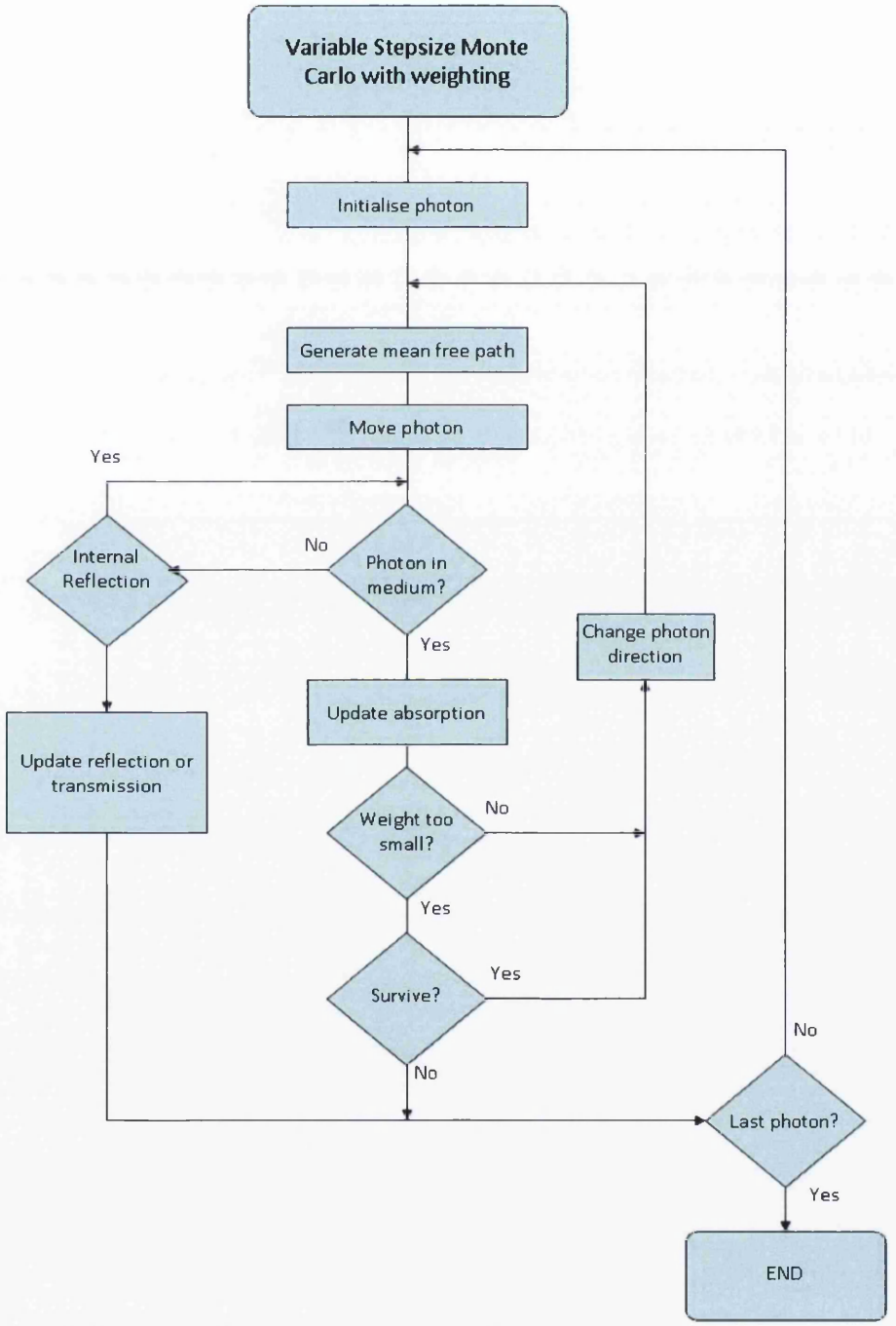

Figure 5.5: Flowchart of the Variable Stepsize Monte Carlo algorithm (from [15])

Skin Structure	Thickness
Epidermis	100μm
Dermis Above Vessel	500μm
Blood Vessel	200-2000μm Diameter
Dermis Below Vessel	1400-3200μm

Table 5.2: Physical Dimensions of the Skin Model

simulation was run to obtain the fluence distribution in the skin. Fig. 5.6 illustrates a typical result from the Monte Carlo model.

5.2 Heat Transport Theory

The computer model is essentially a two stage process:

- Stage 1: Solve for the distribution of photons throughout the tissue using the well-known Monte Carlo statistical technique. The tissue is regarded as a turbid medium, i.e. where absorption and scattering are the principal interaction events.
- Stage 2: Use the volumetric distribution of photons calculated from Stage 1 as heat source terms in the time-dependent thermal diffusion equation.

The temperature of the skin is governed by the following bio-heat equation:

$$\rho c \frac{\partial T}{\partial t} = \nabla(k \nabla T) + Q_s \tag{5.9}$$

where:

- T is the tissue temperature $[K]$

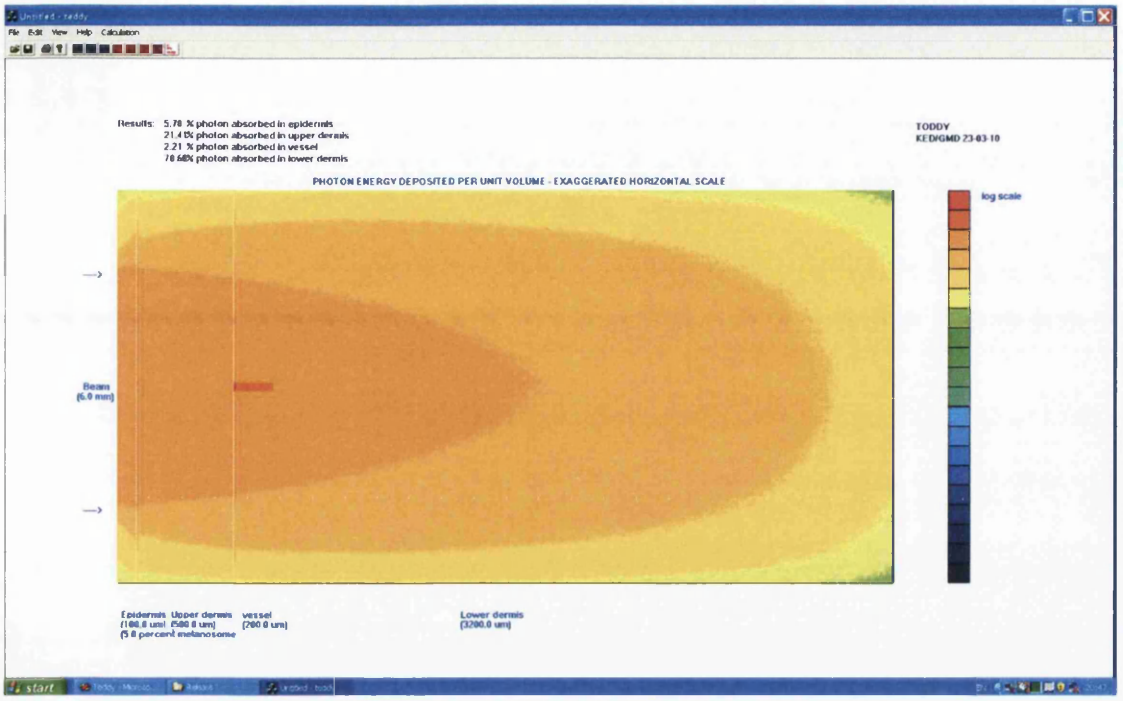

Figure 5.6: Typical output from 2D Monte Carlo model - photon density

- ρ is the tissue density $[kg \times m^{-3}]$,
- c is the specific heat of the tissue $[J \times kg^{-1} \times K^{-1}]$,
- k is the thermal conductivity of the tissue $[W \times m^{-1} \times K^{-1}]$,
- Q_S is the volumetric sub-dermal heat-source term $[W \times m^{-3}]$ representing the laser light absorption, which is derived from the Monte Carlo solution,
- t is the time $[s]$

In these expressions, the metabolic heat generation as well as the heat exchange due to perfusion have been neglected, this is a reasonable assumption for short exposure times relative to the perfusion rate for veins (see [86] and [87]). This model has proved useful in establishing penetration depth, transmitted energy, and variation of laser absorption by blood vessels with depth and diameter and the effect of basal melanin content [88]. The time-dependent thermal

transport equation appropriate for this problem is:

$$\nabla^2 T(x,y,z,t) + \frac{Q(x,y,z,t)}{k} = \frac{1}{\alpha}\frac{\delta T}{\delta t} \tag{5.10}$$

where:

- $T(x,y,z,t)$ is the local temperature in the tissue,
- α is the thermal diffusivity of the tissue $= \frac{k}{\rho c}$ $[W \times m^2]$, where: c is the specific heat, ρ is the mass density, k is the thermal conductivity of the tissue,
- $Q(x,y,z,t)$ is the volumetric thermal source term $[W \times m^{-3}]$.

In the theoretical model, $Q(x,y,z,t)$ represents the heating effects due to the locally deposited photons throughout the tissue. The thermal transport equation is modelled on a two-dimensional mesh and is solved using an implicit integration technique. The well-known Alternating Direction Implicit (ADI) numerical method is used to solve this time-dependent thermal equation. The temporal shape of the laser pulse is modelled using a generic trapezoidal profile, which permits separate values for risetime, holdtime and falltime.

5.2.1 Time Dependent Thermal Model

As we have appreciated from the previous section the results from the Monte Carlo simulation gives an indication of the light fluence distribution within the skin and vasculature. Using this fluence map, the two-dimensional thermal diffusion equation was solved, with the volumetric distribution of photons represented by the heat source term, Q in equation 5.10.

The thermal diffusion equation was given by

$$\frac{\delta^2 T(x,y,z,t)}{\delta x^2} + \frac{Q(x,y,t)}{k} = \frac{1}{\alpha}\frac{\delta T}{\delta t} \tag{5.11}$$

Where

- $T(x)$ is the temperature at penetration depth x;
- α is the thermal diffusivity of the tissue medium;

- k is the thermal conductivity.

The heat source term $Q(x, y, t)$ was derived from the flux distribution as determined from the results of the Monte Carlo simulation. In this equation, the metabolic heat generation as well as the heat exchange due to perfusion have been neglected, this is a reasonable assumption for short exposure times relative to the perfusion rate

The same two-dimensional mesh was used to simulate a 'slice' through the tissue and vasculature.

Each homogeneous layer in the thermal model was given appropriate thermal and physical properties as shown in Fig. 5.7.

The temporal profile of the applied laser pulse was represented as a simple functional form. This allowed the rise, hold and fall time of the applied pulse to be varied whilst maintaining the delivered energy constant (Fig. 5.7 and Fig. 5.8).

The initial temperature characteristic of the tissue layers was chosen to be 37°C. The numerical approximation to the thermal transport equation is based on the well-known Alternative Direction Implicit Method. This permits a time-step that can be much larger than the explicit finite difference method. Although the explicit method is easier to implement, the time step is limited by the Fourier Stability Criterion. However, in the implicit method, although the method is unconditionally stable for any timestep value, care was taken in choosing a time step that adequately represented the characteristics of the laser temporal profile. Even though implicit methods allow for the use of a large time step, since convergence is ensured, the accuracy of the model needs to be verified. This process involves calibrating the simulator with the use of a small number of simulations to check whether the time step used allows for the level of confidence sought after for the relevant modelling.

Therefore, as a *rule of thumb*, in order to represent the shape of the pulse properly, subdividing the pulse in to ten time steps or more can provide in general a satisfactory accuracy.

The temperature in a given cell at given time is determined by the following factors.

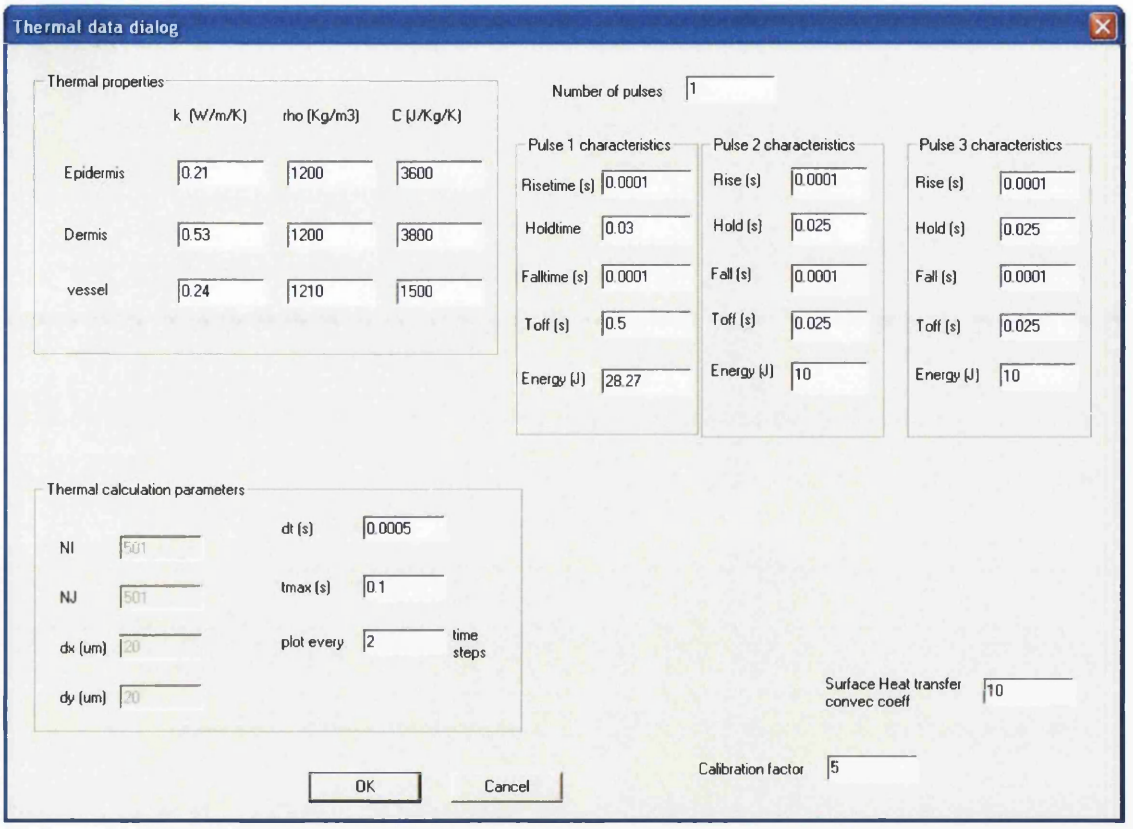

Figure 5.7: Parameters window in the thermal simulator, showing typical Pulse characteristics, Thermal Properties and other simulation parameters

1. The proportion of the total energy in the laser pulse delivered during the time step is calculated. This takes into account the temporal profile of the applied laser pulse.

2. The cell in question only receives a fraction of this energy, the value being determined from the result of the Monte Carlo simulation. This produces a direct heating effect on the particular cell.

3. The temperature in the given cell has a contribution from adjacent cells. This may either be a positive or negative effect.

This is represented graphically in Fig. 5.9 below. Repeating this procedure for the entire

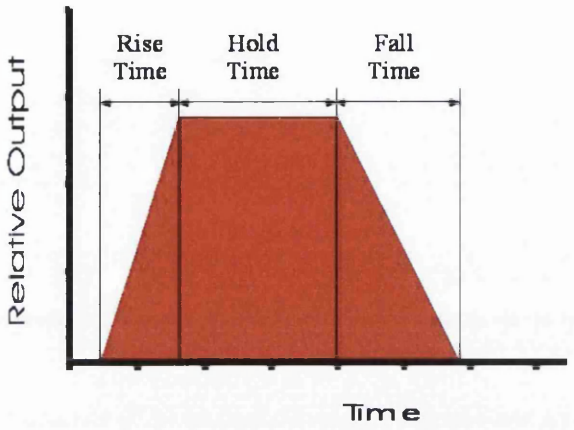

Figure 5.8: Temporal pulse functional form

duration of the laser pulse leads to the temperature profile in the skin and vasculature being determined. As the cooling phase is also of importance to show how the heat diffuses from the target vessel, the model was constructed to allow a substantial cooling phase to be shown.

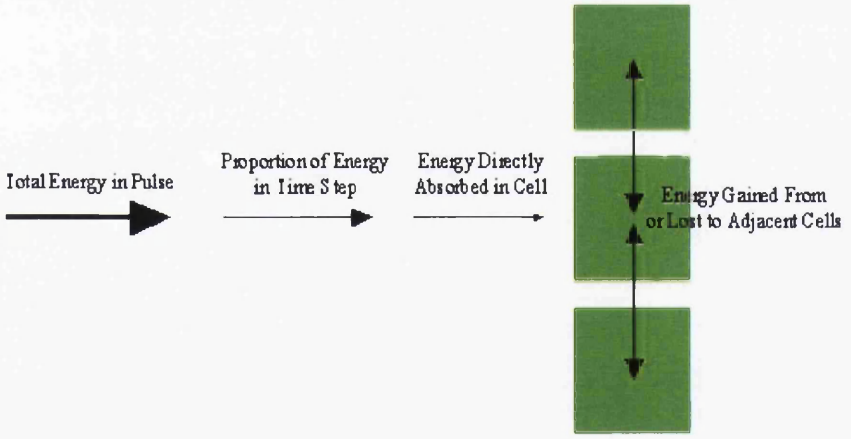

Figure 5.9: Depicted are the effects governing temperature increase in each cell

Taking into account all the factors governing the calculation of the temperature in the cell, the following 3 term equation was used:

$$\begin{pmatrix} Cell \\ Temp \end{pmatrix} = \begin{pmatrix} Heat\ generated\ from \\ direct\ absorption \end{pmatrix} + \begin{pmatrix} Heat\ from \\ adjacent\ Cells \end{pmatrix} - \begin{pmatrix} Heat\ lost\ during \\ time\ step \end{pmatrix} \quad (5.12)$$

The model was designed to output the temperature of any given cell at any time period, during the laser pulse and in the cooling phase.

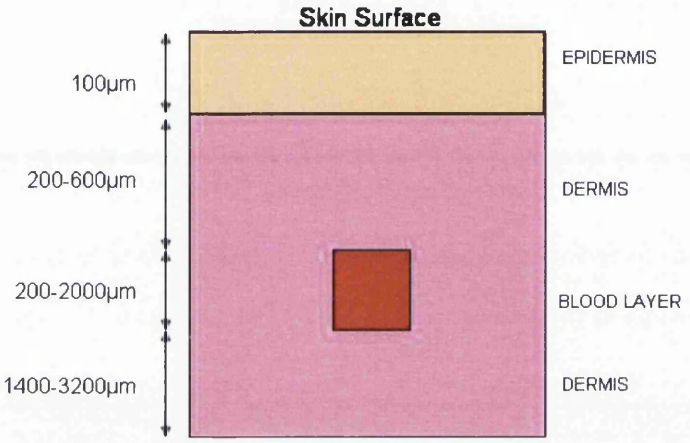

Figure 5.10: Representation of the 2D Monte Carlo model

5.3 Monte Carlo Modelling - Photon Distribution

As explained in the theoretical section of this chapter, a 2-step simulator has been used to carry out the theoretical modelling of this research work. This section reports on the modelling of the photon distribution within the skin model utilised. The following section will report on the thermal modelling carried out to support the hypothesis of the need to control the temporal profile and the shape of the laser pulse, which constitutes the research question at the heart of this work.

The simple skin model used throughout the simulation work showed in Fig. 5.1 is reported again, rearranged and showed in Fig. 5.11. Therefore, in accordance to Fig. 5.11, the skin section measures $4mm$ (horizontal axis)$\times 10mm$ (vertical axis) with origin at the bottom left corner of the skin section (i.e., coordinates $(0, 0)$).

The mesh size utilised within this work was kept fixed to a value of 501×501 cells. Although mesh size can be modified, by referring to [89] where typical mesh size used was 200×200, I have taken a mesh size which is, in fact, six-times more dense.

The blood vessel is modelled as having a square section, with a *pseudo-diameter* varying from $200\mu m$ to $2000\mu m$. These two values are chosen accordingly to the size of vessels more commonly treated with Nd:YAG based laser systems, albeit lasers operating at this wavelength have shown to be effective for some venous malformations involving vessels of up to $4mm$ in diameter. Specifically, 4 vessel diameter, namely $200, 500, 1000, 2000\mu m$ have been used during this modelling work. The vessel has been placed with the anterior wall lying $600\mu m$-deep within the dermis(therefore parallel to the epidermis layer and perpendicular to the incident laser beam), with the left side lying at $4900\mu m$ slightly offset from the median incident to the skin (i.e., the blood vessel placed at $600\mu m$ depth from the epidermis would have coordinates $(600, 4900)\mu m$.

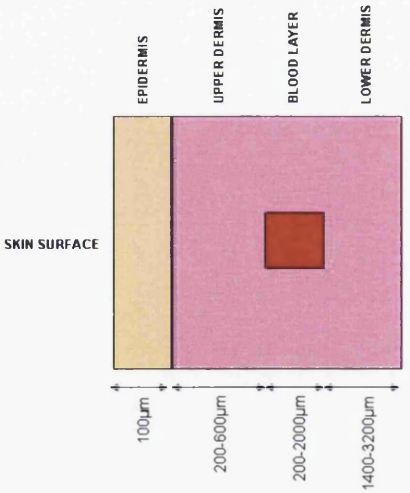

Figure 5.11: Simplified skin model with blood vessel

Photon distribution covering the area of skin irradiated with the Nd:YAG at $1064nm$ has been carried out. A test of sensitivity of the number of photons used in the statistical method

was performed, which acted as a test of statistical convergence with a view of assessing the limitations of the statistical method. The number of photons was varied from 10^5 - 10^6 - 10^7 to model the distribution within the same skin model (vessel diameter equal to $1000\mu m$). Results for the Monte Carlo photon distribution modelling for varying photon number is shown in Fig. 5.12

A $6mm$ spot-size, *top-hat* Nd:YAG laser pulse at the fundamental wavelength of $1064nm$, with a given $t_{rise} = 0.1ms$, hold time $t_{hold} = 30ms$ and fall time $t_{fall} = 0.1ms$ was used, and a laser irradiation with total cumulative energy of $30J$, corresponding to a fluence of $106.12J/cm^2$ (in clinical practice, however, normally higher fluences are needed in order to produce therapeutic results). Temperature values at a defined location within the skin section was compared in order to assess the magnitude of change. It is worth pointing out that the focus of the modelling was on the temperature rise in both the blood and the blood vessel walls.

Table 5.3 reports the results of the tests performed to assess the sensitivity of the modelling approach. Temperature values and the time of occurrence are reported. The graphs in Fig. 5.13 report the thermal behavior of our tissue sample modelled at different volumetric photon densities.

Table 5.3: Effect of Photon Distribution on Thermal modelling

n^o Photons	Tmax[$°C$]@P4	Tmax[$°C$]@P5	Tmax[$°C$]@max vess T	Rel. diff [%]
10^5	104.16	92.93	104.16	0.26
10^6	105.12	94.12	105.12	1.2
10^7	104.39	94.06	104.39	0.22

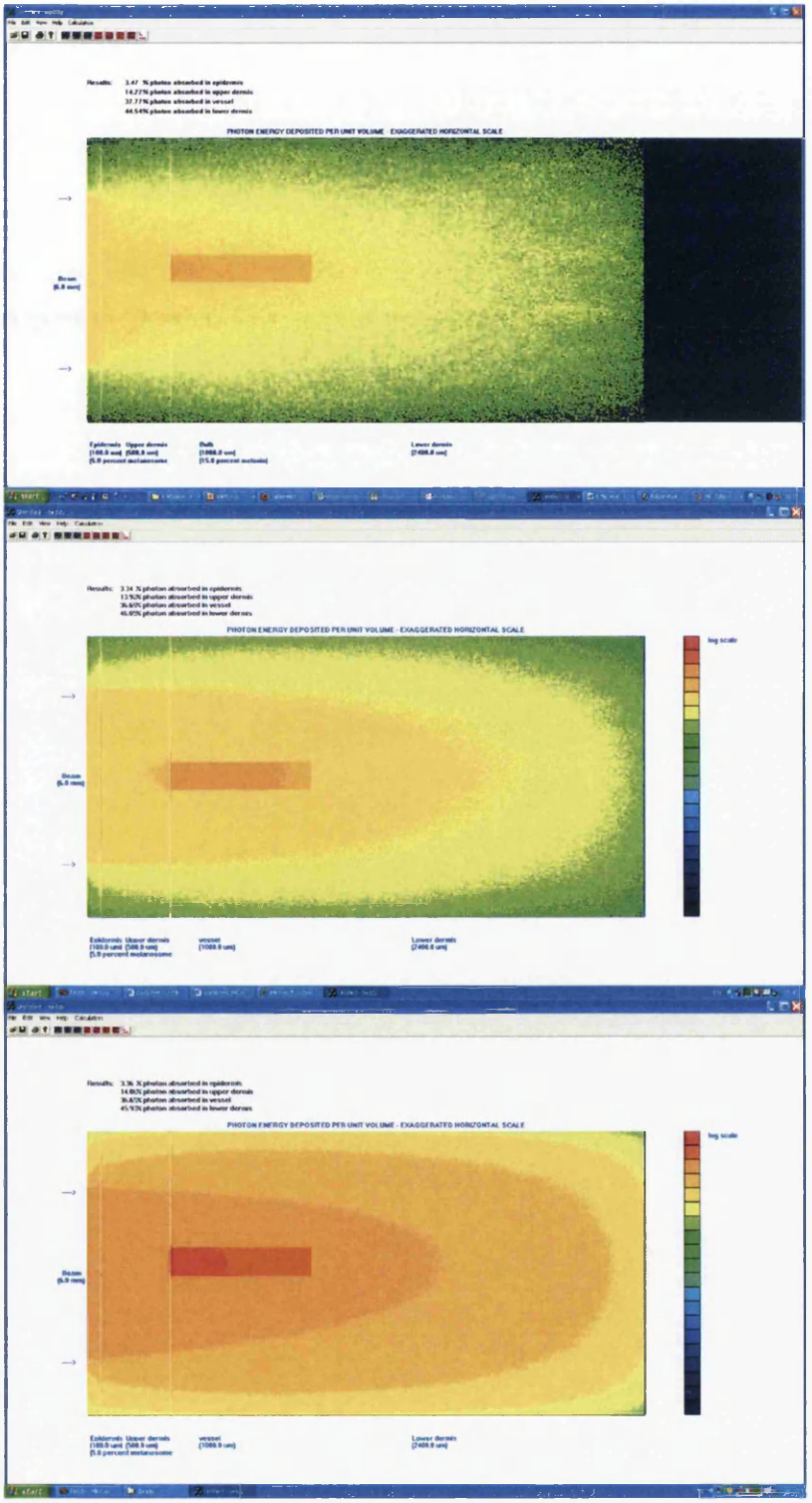

Figure 5.12: Photon Distribution for a skin model incorporating a blood vessel with $D = 1000\mu m$, for varying the number of photons from 10^5 (top plot), 10^6 (middle plot) and 10^7 (bottom plot)

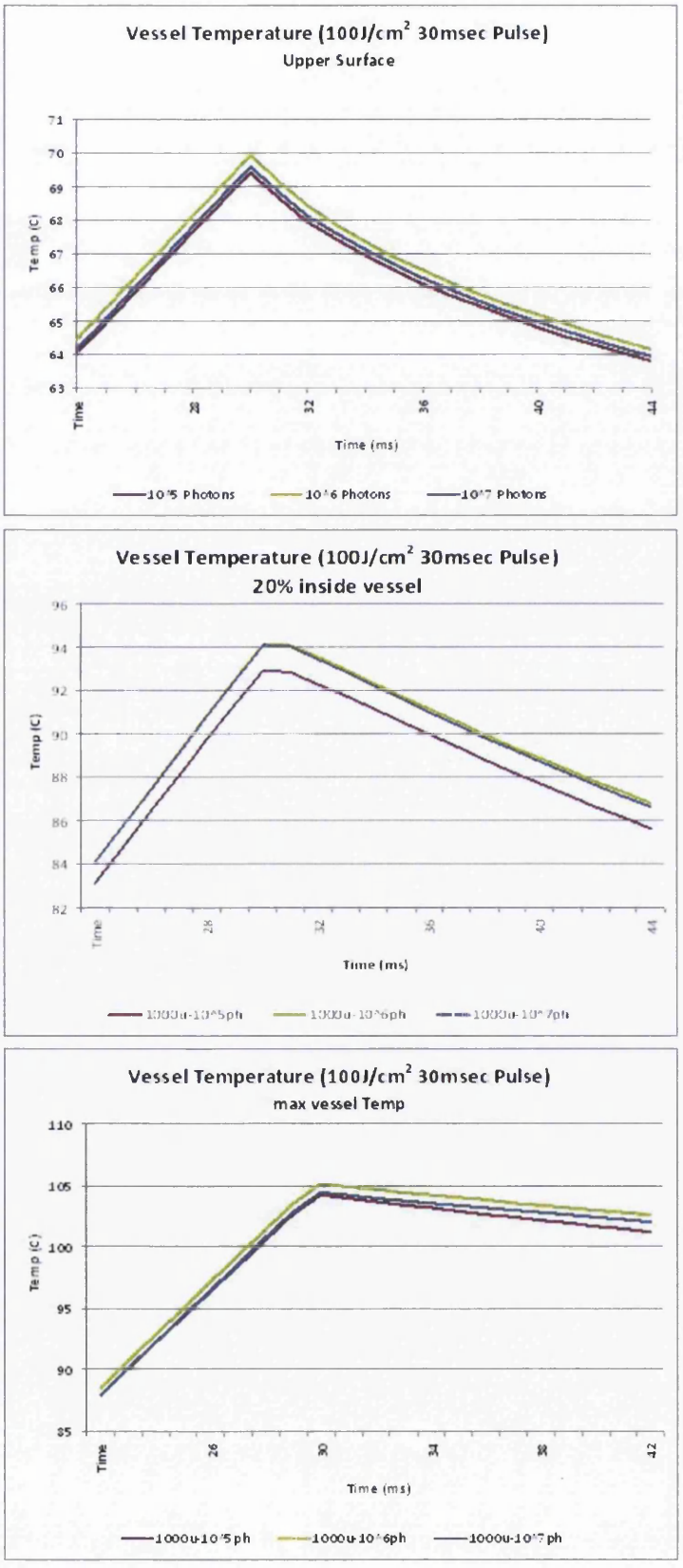

Figure 5.13: Magnified temporal profile for the irradiation of a 1mm blood vessel with Nd:YAG laser. Influence of the Photon Distribution on the Thermal calculations at three points of interest

From the table and the graphs, it is possible to infer that as the number of photons used within the model increases, the maximum temperature at the blood vessel converges. There is only a small oscillation for point P4 which is however of a not relevant entity. The relative percentage differences to the values for the 10^7 photon distribution can be considered satisfactory. These observations support the accuracy of the modelling approach chosen.

Slight variations may be induced from different seeding of the random number generator.

As a subsequent step, modelling efforts have been directed at characterising the photon distribution for the four chosen vessel diameters. Results are shown in Figures 5.14 and 5.15.

A number of considerations can be made with regards to the modelling with reference to Figures 5.13, 5.14 and 5.15.

The Monte Carlo simulations are displayed in a logarithmic photon distribution plot, which factor accounts for the sharp difference in colours characterising adjacent distribution regions. Furthermore, as it appears from the plot, although the region corresponding to the lower dermis is not shown on the plots, calculations have been carried out throughout the skin model including the abovementioned lower dermis layer.

The horizontal scale is expanded, as emphasised in the plot. This means that the vessel, albeit having in reality a square section, appears elongated and therefore of a rectangular shape. This factor, although it may create some level of discomfort to the viewer at first, has to be valued not negatively from a modelling perspective. In fact, having the depth axis expanded provides more useful information on the influence of the radiation through the depth of the skin model and especially the vessel.

Although a piecewise linear variation of melanin concentration can be modelled, for the purposes of the calculations performed and reported in this chapter, I have taken the representative concentration of 5% melanin corresponding to *fair skin*, based on the Fitzpatrick scale thus modelling what effectively is an uniform melanin concentration for the epidermal layer.

The mean free path in the dermis region is significantly higher than that in the epidermis region and it is a widely accepted factor that for a $1064nm$ wavelenght scattering dominates the

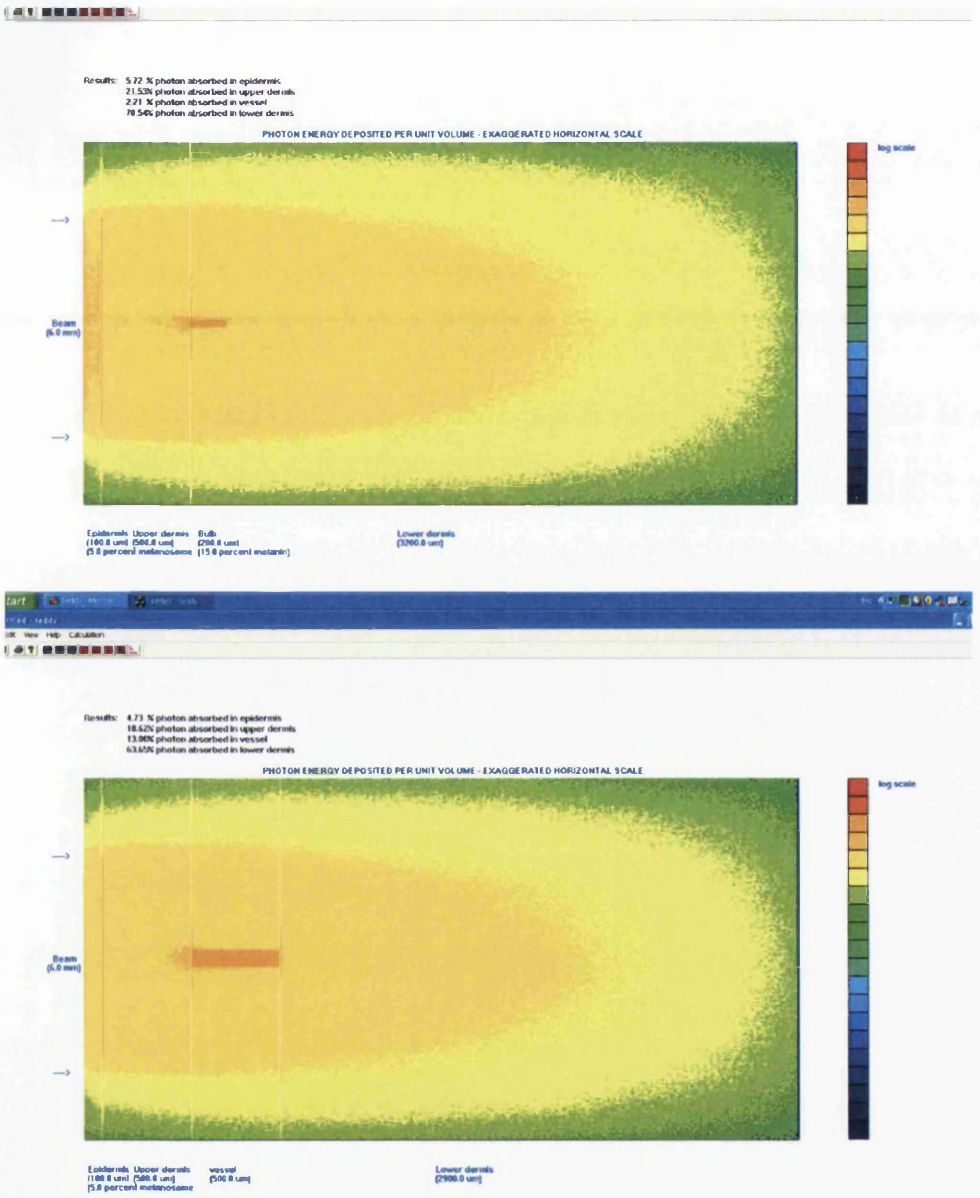

Figure 5.14: Photon Distribution for vessel sizes of $D = 200\mu m$ and $D = 500\mu m$

absorption. Furthermore, as photons move from the epidermis, which is relatively transparent to the $1064nm$ wavelength, down to the upper dermis, vessel and lower dermis layers, due to the highly scattering behaviour of the wavelength of the laser under investigation, photon

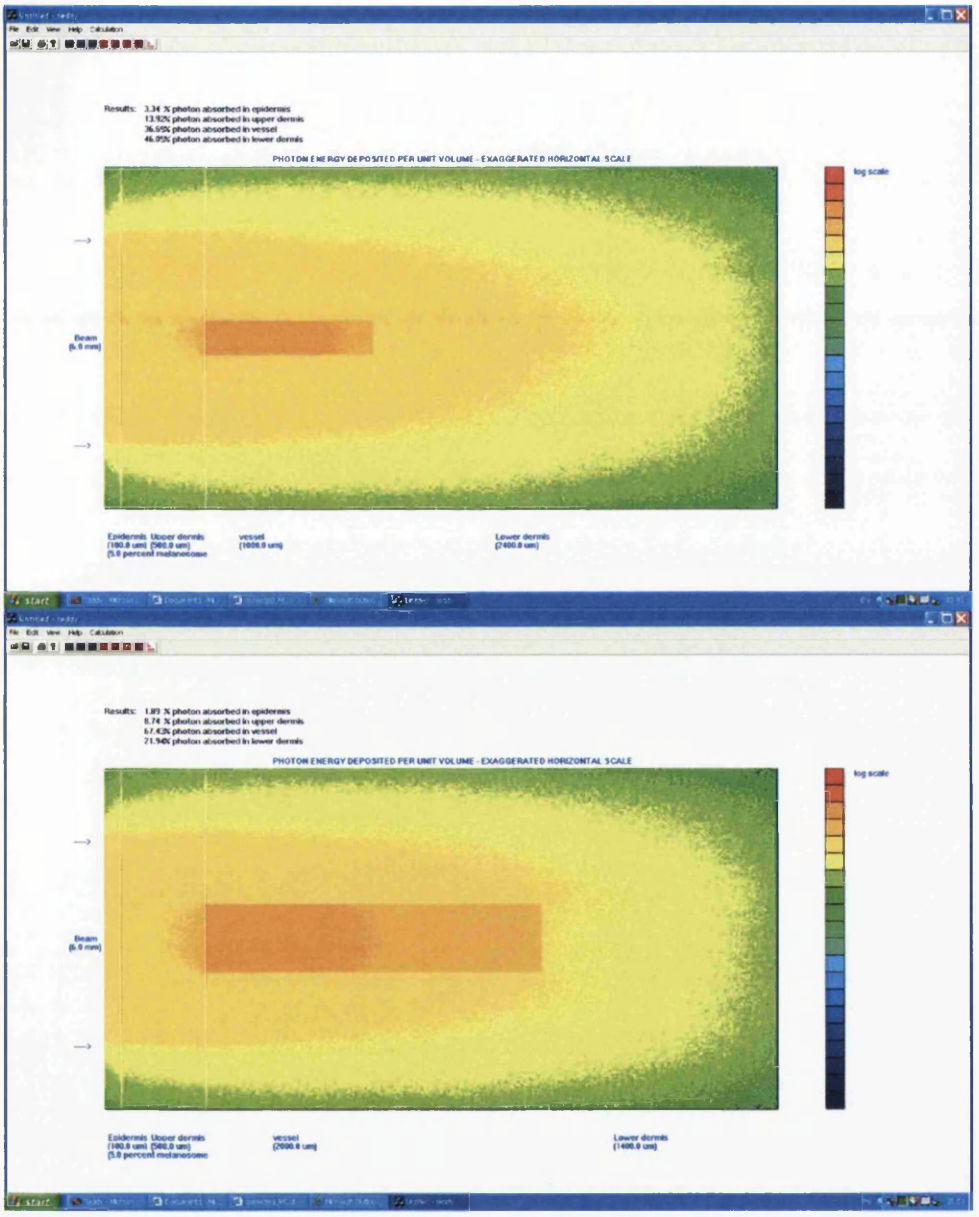

Figure 5.15: Photon Distribution for vessel sizes of $D = 1000\mu m$ and $D = 2000\mu m$

distribution experiences lateral broadening inside the skin. This result is supported by the clinical evidence - found in literature, of the higher efficacy of Nd:YAG-based therapy. As broadening effects take place, a smaller laser beam size of lower energy would be sufficient to

treat a given vessel. This is in agreement with the indications from clinicians of the need to match the beam diameter with the vessel size as much as possible, in order to avoid un-specific heat of the tissue surrrounding the target vessel ad excess pain, effects that can arise for the 1064nm wavelength, which is within the absorption spectrum of water.

These observations are consistent with findings from literature. Longer wavelenghts penetrate more deeply in to the skin than shorter wavelengths. Furthermore, Nd:YAG light in the fundamental wavelength of 1064nm is well known to experience strong scattering in the skin, with end effect being that thanks to scattering the photons have statistically higher chances to penetrate further before they get annihilated.

5.4 Time-dependent Thermal Profile Modelling

The Monte Carlo simulations performed provide the input to the thermal solver. As previously outlined, the thermal calculations are performed by solving the time-dependent thermal diffusion equation. Simulations were carried out in order to evaluate the use of Nd:YAG laser light and specifically to provide early indications to support the hypothesis underlying this piece of work. As recalled at the beginning of this section, it was postulated that the temporal profile of Nd:YAG laser radiation could have influence on the effectiveness of the laser therapy to treat vascular lesions. In order to ascertain this, extensive modelling of the thermal profile of the skin tissue irradiated with the Nd:YAG laser has been performed. The laser spot size was kept fixed for all the simulations to $6mm$ diameter, incident to the epidermis. Three main sets of modelling experiments have been performed, in order to characterise the effect of fluence, shape and duration of the laser radiation on a human skin model for vessel sizes of diameter D=500μm, 1000μm and 2000μm. The graphs show how the temperature varies with time for various virtual temperature probes within the tissue (key curves are highlighted). The various probes are numbered in ascending order with the increase in depth, and are given the names of Pi, $i = 1, 2, ..., n$.

Table 5.4: Virtual Probes and position within the tissue model

Probe	Depth [μm]
P1	8
P2	100
P3	350
P4	600+C
P5	(600+0.2*D)
P6	600+D-C

Table 5.4 illustrates the various probe points together with their respective depth. D is the blood vessel diameter [μm], C is the cell size (8μm). The figures provide spot temperatures at different points as time evolves. Probe P3 is located in the middle of the Upper Dermis region, whereas probe P4 is located at 1 mesh Cell inside the blood vessel. A 501 $\times$ 501 elements mesh

was used. An accumulated thermal damage in the vessel is evaluated and displayed within the thermal calculation, using the Arrhenius integral [90]

$$\Omega(x,y,z,t) = A\int_0^{\tau} \exp\left(\frac{E_a}{RT(x,y,z,t)}\right) dt \tag{5.13}$$

where A is the molecular collision rate equal to $1.98 \times 10^6[s^-1]$, E_a is the activation energy equal to $6.676 \times 10^4[Jmole^{-1}]$, R is the universal gas constant equal to $8.314[J \times mole^{-1} \times K^{-1}]$, and T the temperature in K.

The temperature at the surface of the skin was kept at an initial value of $37°C$.

Results and discussions for the studies carried out are reported on the following subsections.

5.4.1 Effect of Fluence

In this section modelling was performed to assess the effect of the increased radiated energy to various vessel sizes. Three vessels with different diameter D, out of the original 4 were chosen, with $D = 500\mu m, 1000\mu m, 2000\mu m$.

The reference tissue model and standard optical and thermal properties at the $1064nm$ wavelenght were used. Fluence was varied in steps of 50, 100, 200 J/cm^2. The values of the

Table 5.5: Pulse shape parameters - Fluence Investigation

Pulse parameter	Value
t_{rise}	$0.1ms$
t_{hold}	$30ms$
t_{fall}	$0.1ms$

fluence were chosen as they have resemblance to values used clinically to treat vessels of the size under investigation. The irradiation duration was kept constant at a value of 30ms, by means of a *top-hat* square pulse. Table 5.5 provides the characteristics of the pulse used. Results showing the thermal plots for the various probe points for all the three vessels for varying fluence are provided in Figg. 5.16, 5.17 and 5.18.

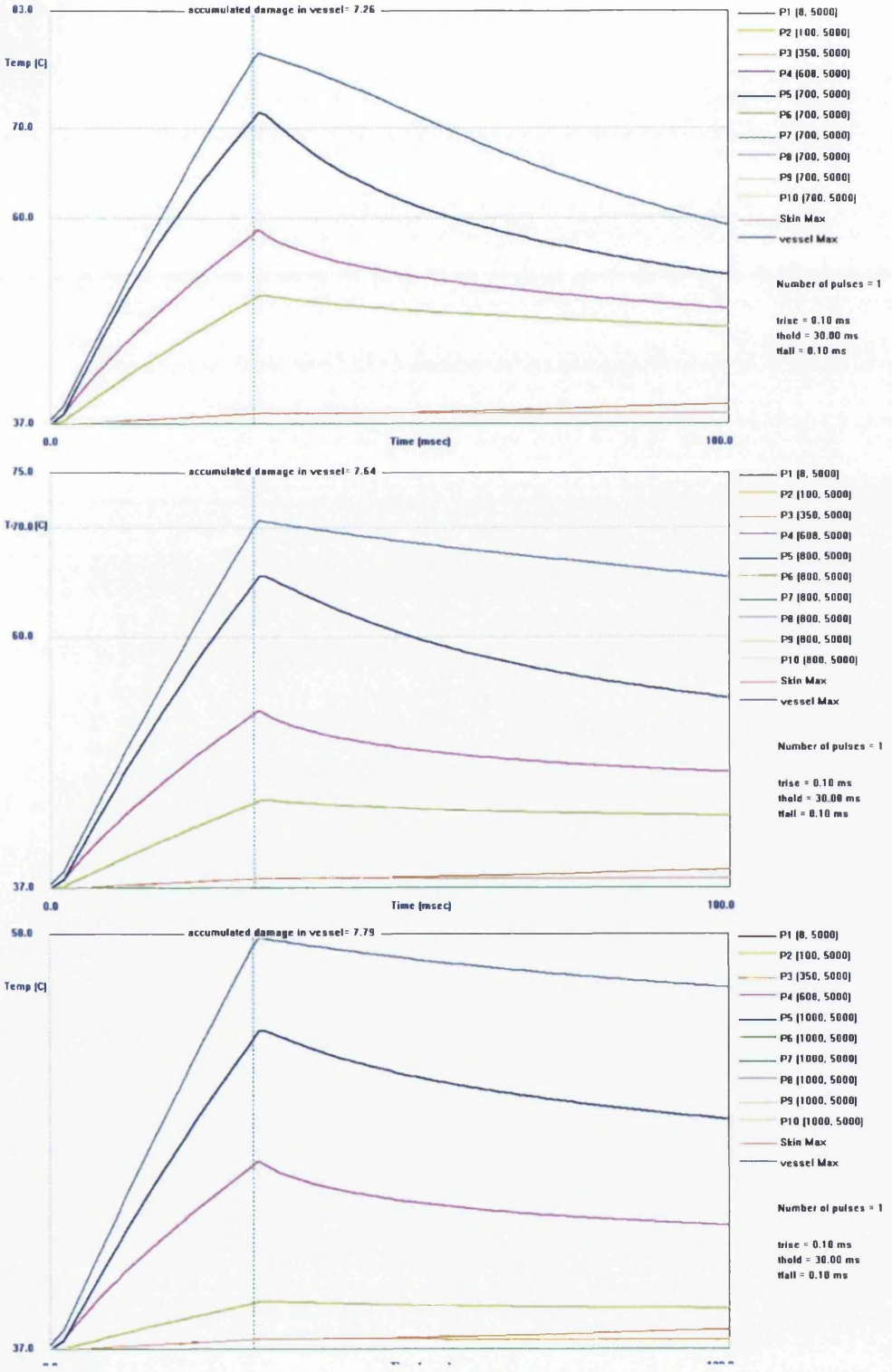

Figure 5.16: Effect of the fluence for varying vessel sizes - Fluence: $50J/cm^2$. Top - $500\mu m$; Middle - $1000\mu m$; Bottom - $2000\mu m$ respectively

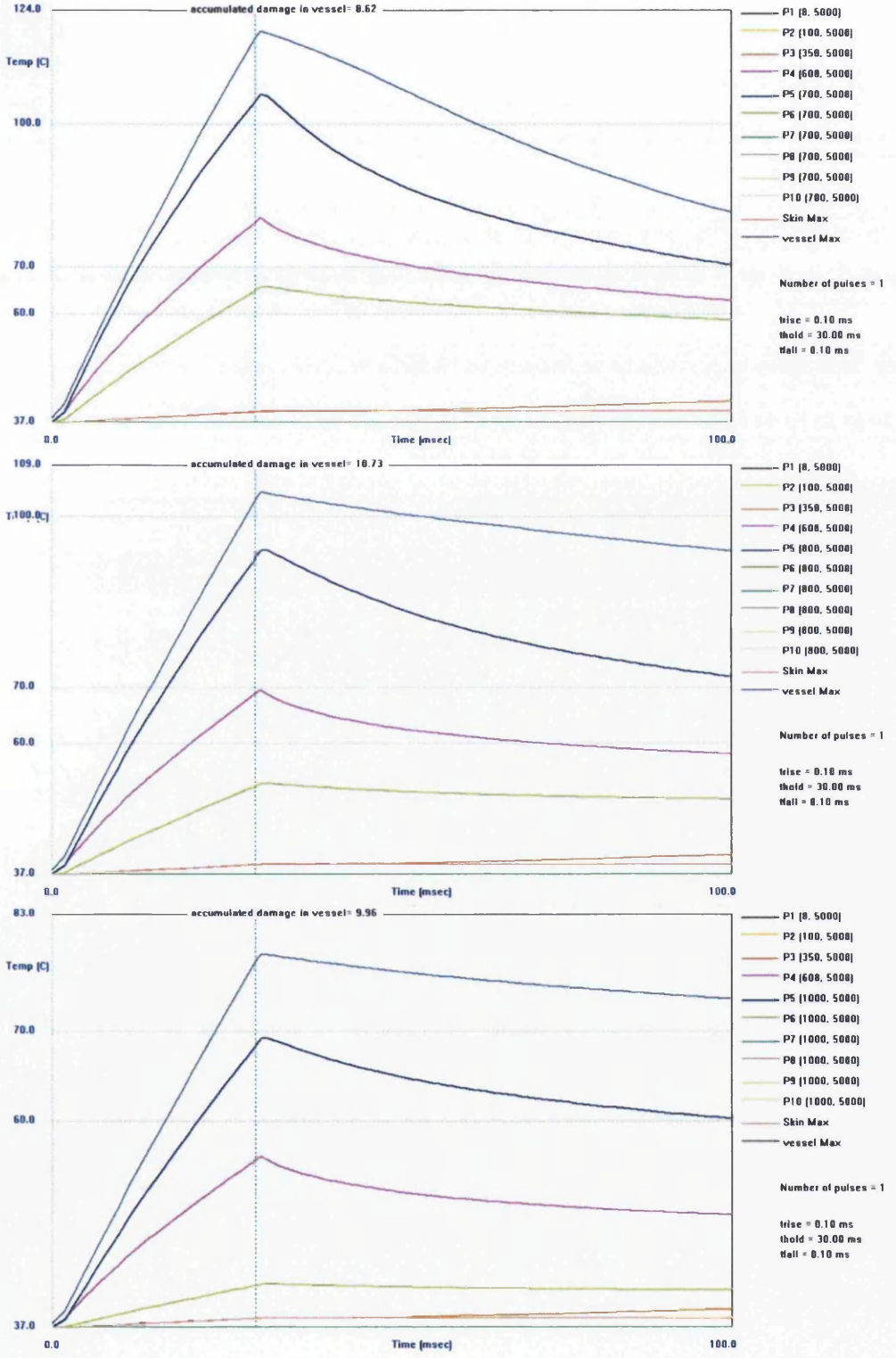

Figure 5.17: Effect of the fluence for varying vessel sizes - Fluence: $100 J/cm^2$. Top - $500 \mu m$; Middle - $1000 \mu m$; Bottom - $2000 \mu m$ respectively

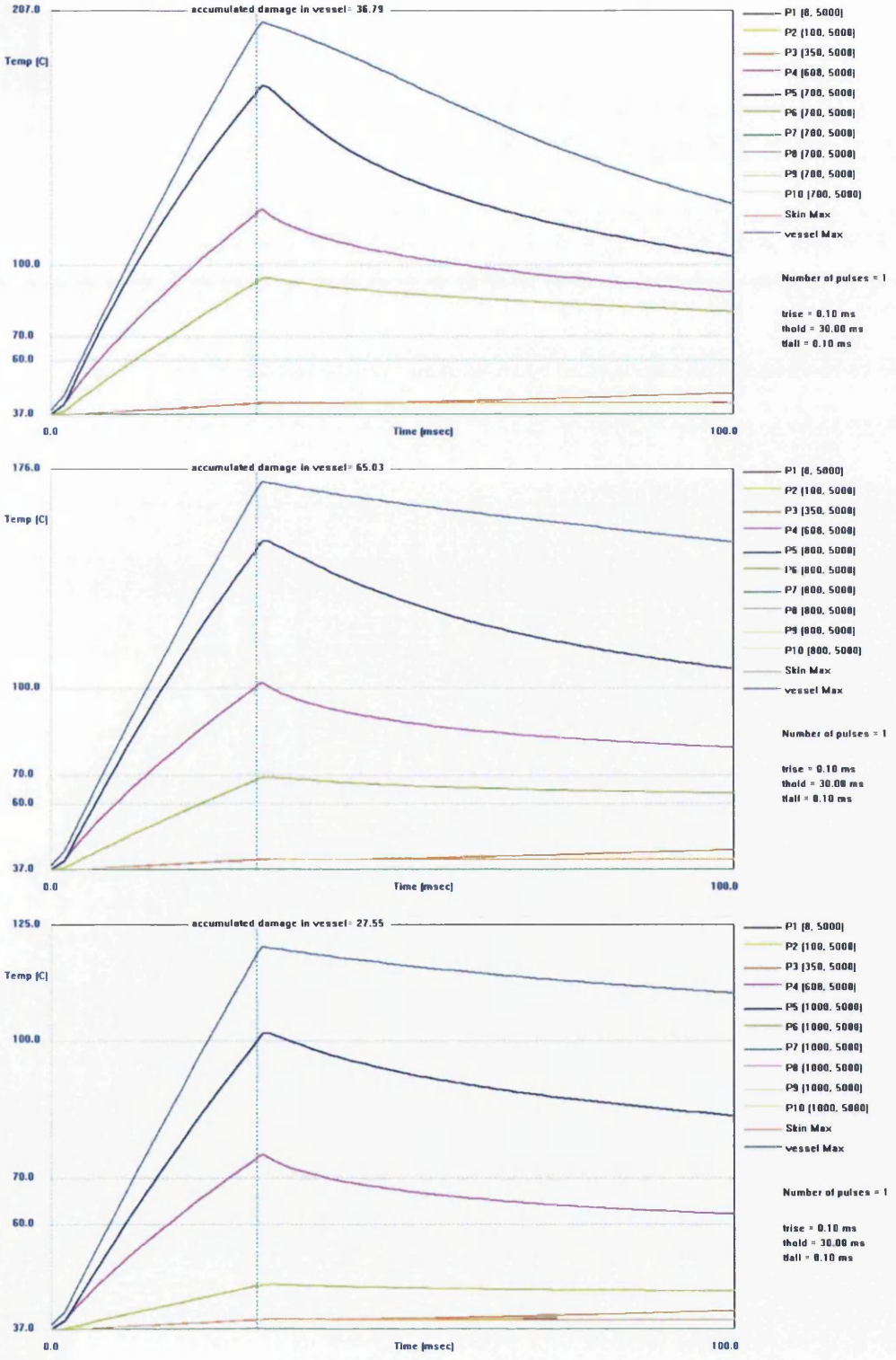

Figure 5.18: Effect of the fluence for varying vessel sizes - Fluence: $200 J/cm^2$. Top - $500 \mu m$; Middle - $1000 \mu m$; Bottom - $2000 \mu m$ respectively

Fluence - Observations

Based upon observation of the graphs, we can notice the following:

- results show a steady increase in the temperature profile as the fluence is raised.

- the temperature also increases with decreasing vessel size, from $2000\mu m$ down to $500\mu m$.

- the temperature difference experienced by the anterior versus the posterior wall of the vessel increased with increasing fluence.

- at $50Jcm^{-2}$ none of the vessels experiences a temperature approaching $70°C$, therefore there is no predicted necrosis.

- at $100Jcm^{-2}$ the $500\mu m$ vessel exceeds $70°C$ for 30ms and therefore the upper surface will experience necrosis. The other vessels do not approach the $70°C$ threshold.

- at $200Jcm^{-2}$ all three vessel sizes exceed the $70°C$ and will therefore experience various degrees of injury (however, it is important to emphasise that unless the entire vessel is not coagulated, it will recover and re-canalise, thus resulting - in clinical terms, in a treatment failure).

- at $200Jcm^{-2}$, the $500\mu m$ blood vessel exceeds $100°C$ and explosive cavitation may result.

- Temperature at the epidermis, as expected, does not change much within the simulated time, and it experiences a higher increase for decreasing size of the vessel.

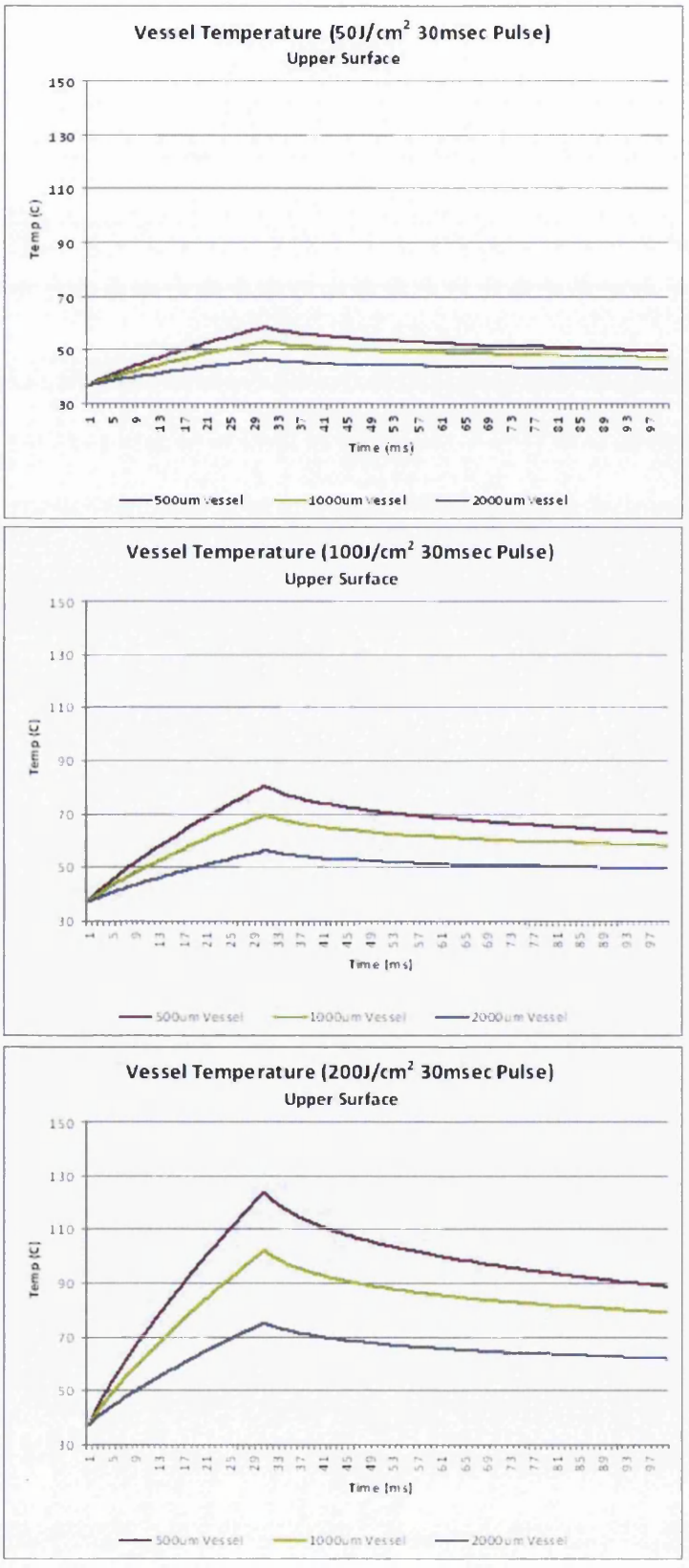

Figure 5.19: Influence of varying the laser fluence on the temperature at the upper surface of blood vessels of diameter $D = 500, 1000, 2000 \mu m$

5.4.2 Results - Pulse Shape

This paragraph brings us to the heart of the modelling performed. The following studies were in fact carried out to evaluate whether controlling the shape of the pulse can have an influence on the thermal response of the target tissue, and specifically of the target structure within the tissue, namely the blood vessel.

Modelling and simulation have been carried out as follows.

Two pulse shapes have been tested:

- a *top-hat* square pulse;
- a ramp pulse.

Total duration of the two pulses has been kept constant. The temporal profile of the two pulses is provided in Table 5.6

Table 5.6: Parameters for the square and the ramp pulses

Pulse	t_{rise}	t_{hold}	t_{fall}
Square	$0.1ms$	$30ms$	$0.1ms$
Ramp	$30ms$	$0.1ms$	$0.1ms$

Fluence was varied from 50, 100, $200J/cm^2$, corresponding to energies of around $14.134J$, $28.27J$ and $56.54J$.

The calculations were performed for a simulated time of $100ms$.

Graphical results of the simulations are shown in Figg. 5.20, 5.21 and 5.22.

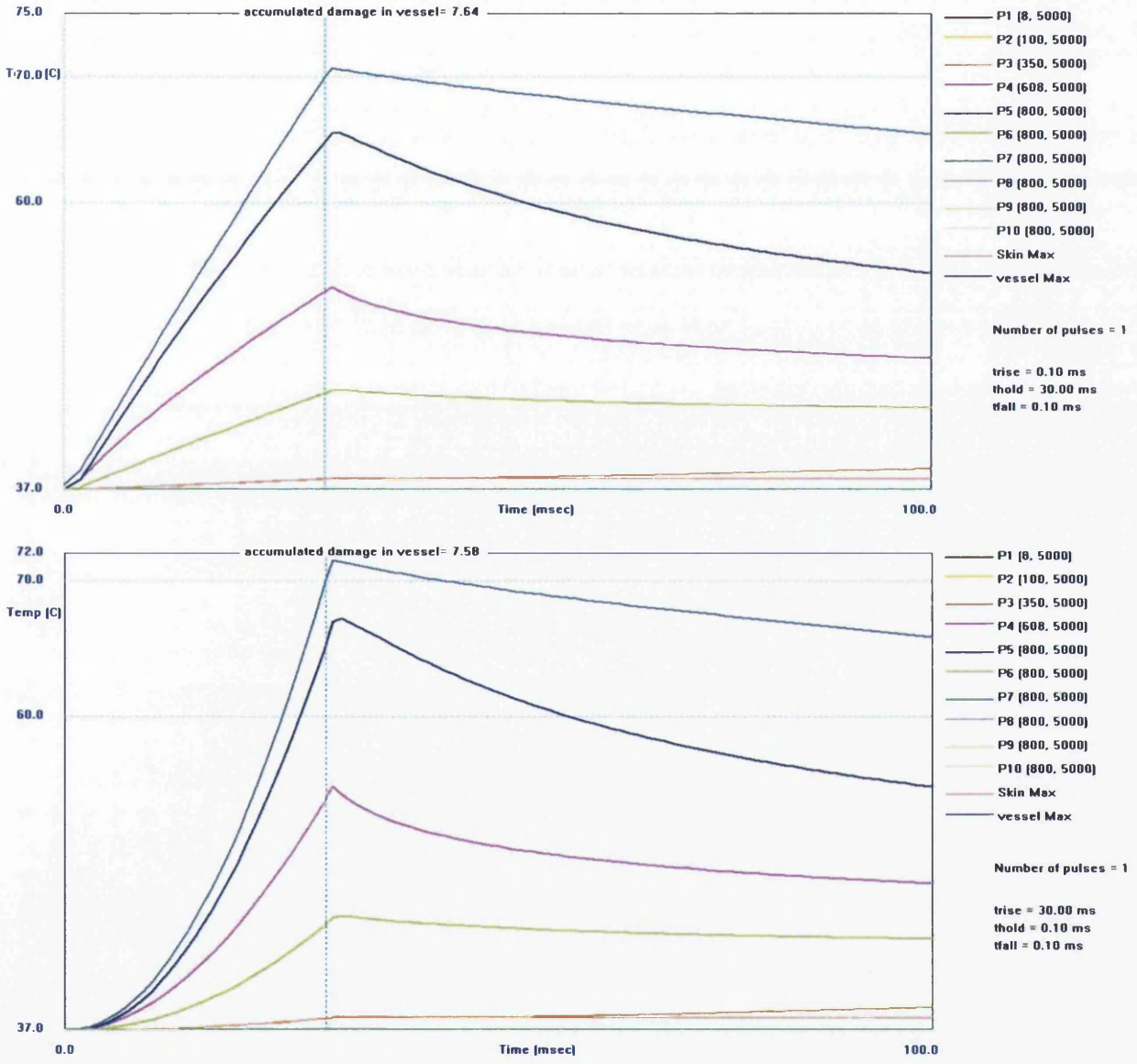

Figure 5.20: Influence of the pulse shape on the temperature profile for virtual-probe points. Square pulse (top) versus Ramp pulse (bottom). Fuence=$50 J/cm^2$

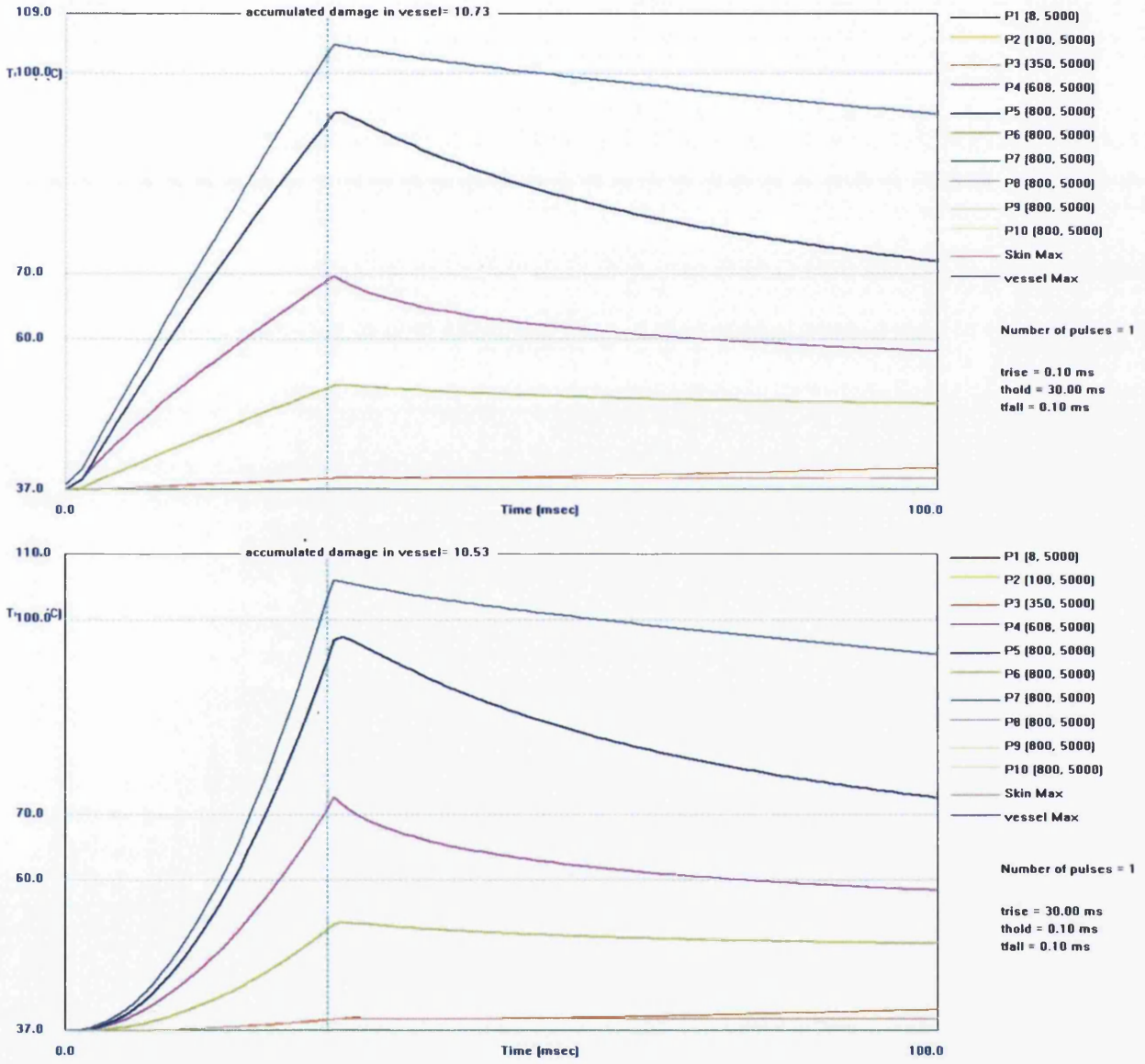

Figure 5.21: Influence of the pulse shape on the temperature profile for virtual-probed points. Square pulse (top) versus Ramp pulse (bottom). Fuence=$100 J/cm^2$

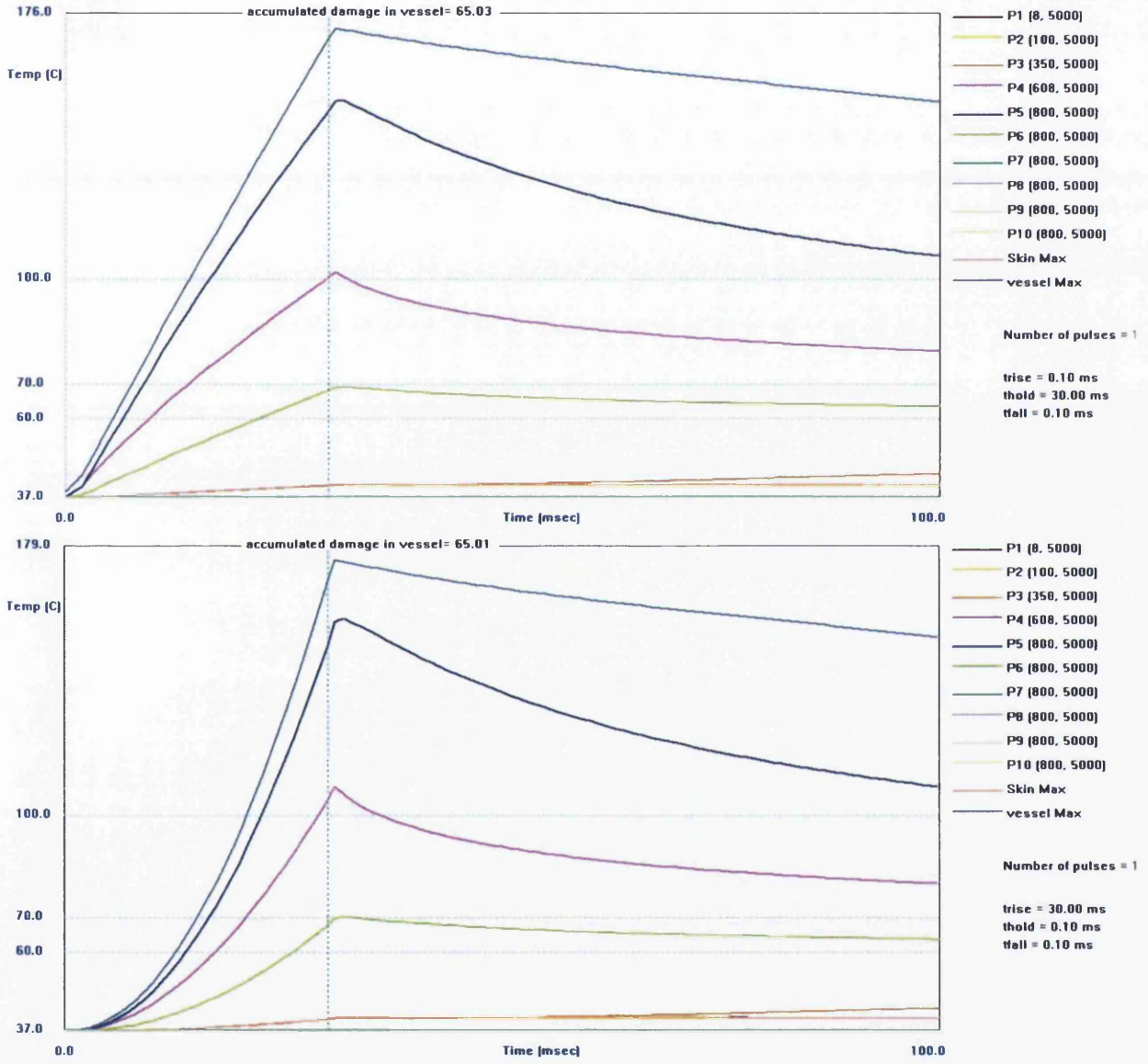

Figure 5.22: Influence of the pulse shape on the temperature profile for virtual-probed points. Square pulse (top) versus Ramp pulse (bottom). Fuence=$200 J/cm^2$

Shape - Observations

Based on observations of the graphs:

- results show a steady increase in the temperature profile as the fluence is raised.

- at $50Jcm^{-2}$, there is no predicted necrosis for either pulse shape and the peak temperature is similar for both.

- at $100Jcm^{-2}$, the ramp profile temperature exceeds $70°C$ for four to five milliseconds, and therefore necrosis is predicted. The corresponding square pulse does not predict necrosis.

- at $200Jcm^{-2}$, both profiles predict necrosis with the ramped profile predicting a peak temperature at the upper surface exceeding the square pulse by $10°C$.

From the three figures above we can distinguish two main trends in the temperature behaviour of our tissue model in response to the two different laser pulses. - In the inner regions of the tissue, the Square pulse originates a response from the tissue which, due to the linear rise during t_{rise}, can be modelled with a quadratic relationship, in the form of:

$$y = ax^2 + bx + c \tag{5.14}$$

with $a > 0$ for $t \leq 0.1ms$. When the pulse reaches its costant value, that is for $01.ms < t \leq 30.1ms$, the curve inverts its slope, and the coefficient a in the polinomial equation becomes slightly negative. This behaviour is experienced throughout the constant region of the pulse. When the pulse starts its descent and enters the t_{fall} region, the temperature in the tissue displays a slight inertia increases for around $50\mu s$, before inverting its slope and starting to decrease with a decaying exponential behavior, dictated by the thermal relaxation time constant of the target tissue. - In the inner regions of the tissue, the Ramp pulse originates a quadratic rise in temperature following the linear rise of the energy delivered by the pulse. Therefore, the same fitting equation used for the square pulse holds for the rising area of the ramp pulse (that is, for $0 < t \leq 30ms$), albeit with different coefficients. When the pulse reaches the constant energy region, which is only held for $0.1ms$, the temperature curve inverts its slope, and for $t > 30.1ms$

the curve assumes an exponential behaviour similar to that experienced by the square pulse. Figure 5.23 provides a direct comparison of the temperature output from the two pulses. As it is clear, the two very different behaviours of the pulses demonstrate a radically different behaviour of the tissue in response to the irradiation modality. This behaviour is magnified as the fluence is increased. However, as the pulse ceases, the exponential tail of the two curves tend to overlap for the highest fluence ($200 J/cm^2$).

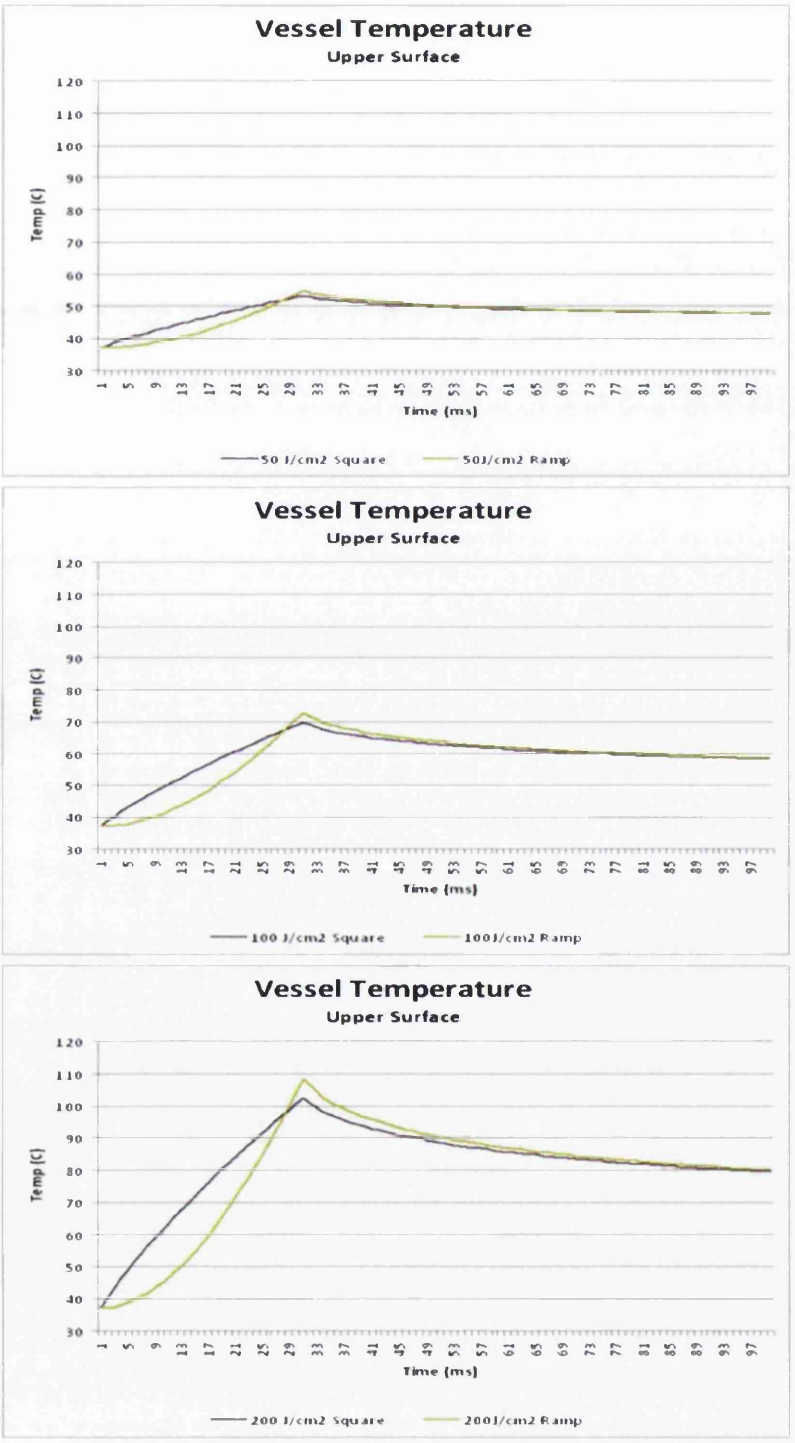

Figure 5.23: Vessel Temperature at the upper wall of the blood vessel, for a Square vs Ramp pulse, at different fluences

5.4.3 Results - Effects of the pulse duration

The effects of the duration of the pulse is now taken in to consideration for varying pulse shape. The same tissue model is used, with reference to Fig. 5.11. Two model pulses, a *top-hat* square pulse and the Ramp Pulse were again used for these studies. The modelled pulses characteristics are shown in Table 5.7. Fluence is kept fixed at a value of $100J/cm^2$.

Table 5.7: Square and Ramp pulses - Effect of pulse duration

Pulse	t_{rise}	t_{hold}	t_{fall}
Square	$0.1ms$	$10, 30, 50ms$	$0.1ms$
Ramp	$10, 30, 50ms$	$0.1ms$	$0.1ms$

The simulated time was kept once more to a total of $100ms$. This, although it may appear to be a limiting factor, is purely functional to aiding in the evaluation of the effect of the different pulses in the temperature area that is relevant. This observation is expanded in the discussion section of the chapter.

Simulated results are plotted and displayed in Fig. 5.24 and Fig. 5.25.

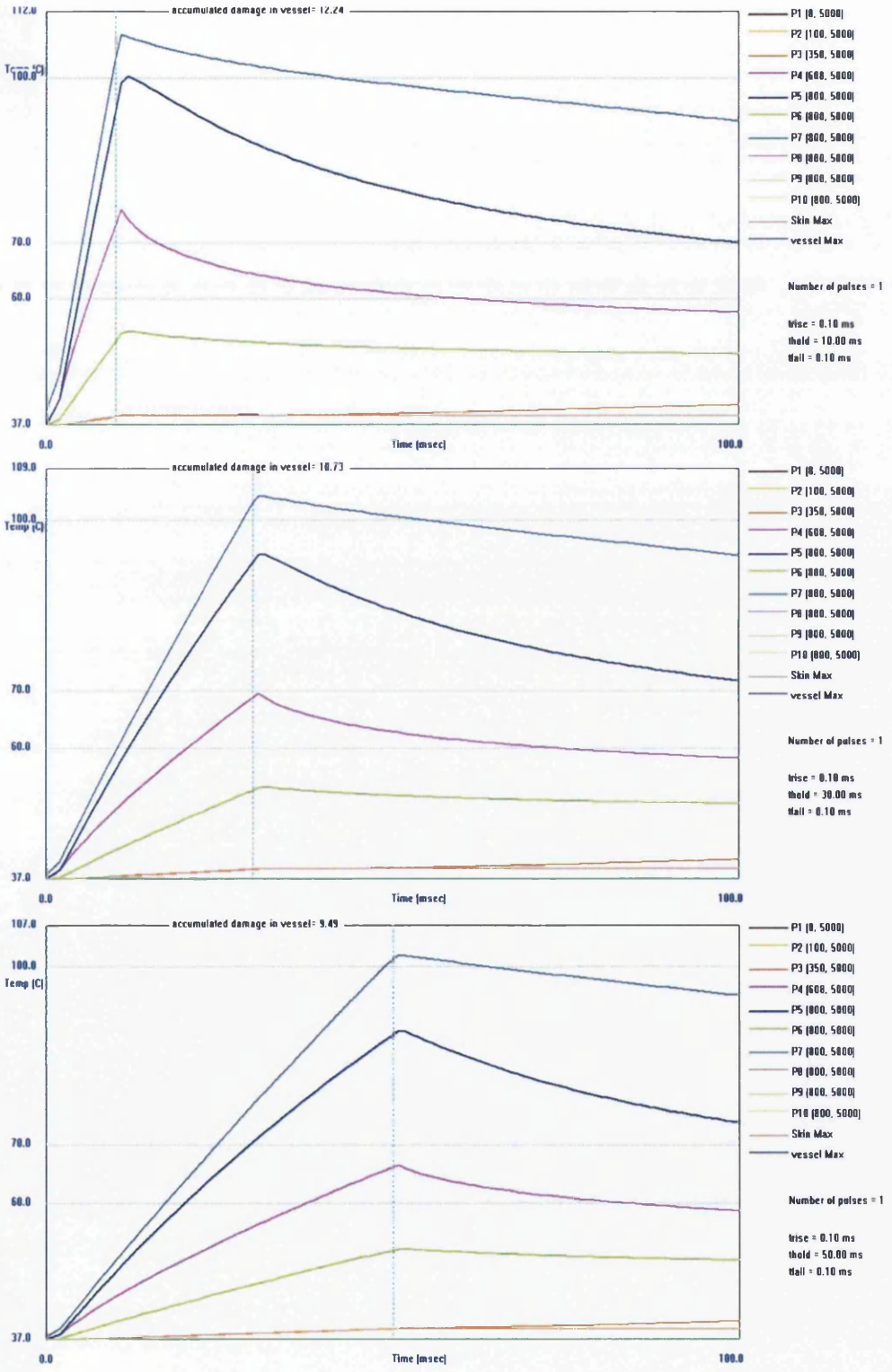

Figure 5.24: Thermal diffusion for tissue model incorporating a blood vessel with $D = 1000\mu m$ - effect of varying the duration of a top-hat (square) pulse: $10ms$ - top; $30ms$ - middle; $50ms$ - bottom, t_{hold}, respectively

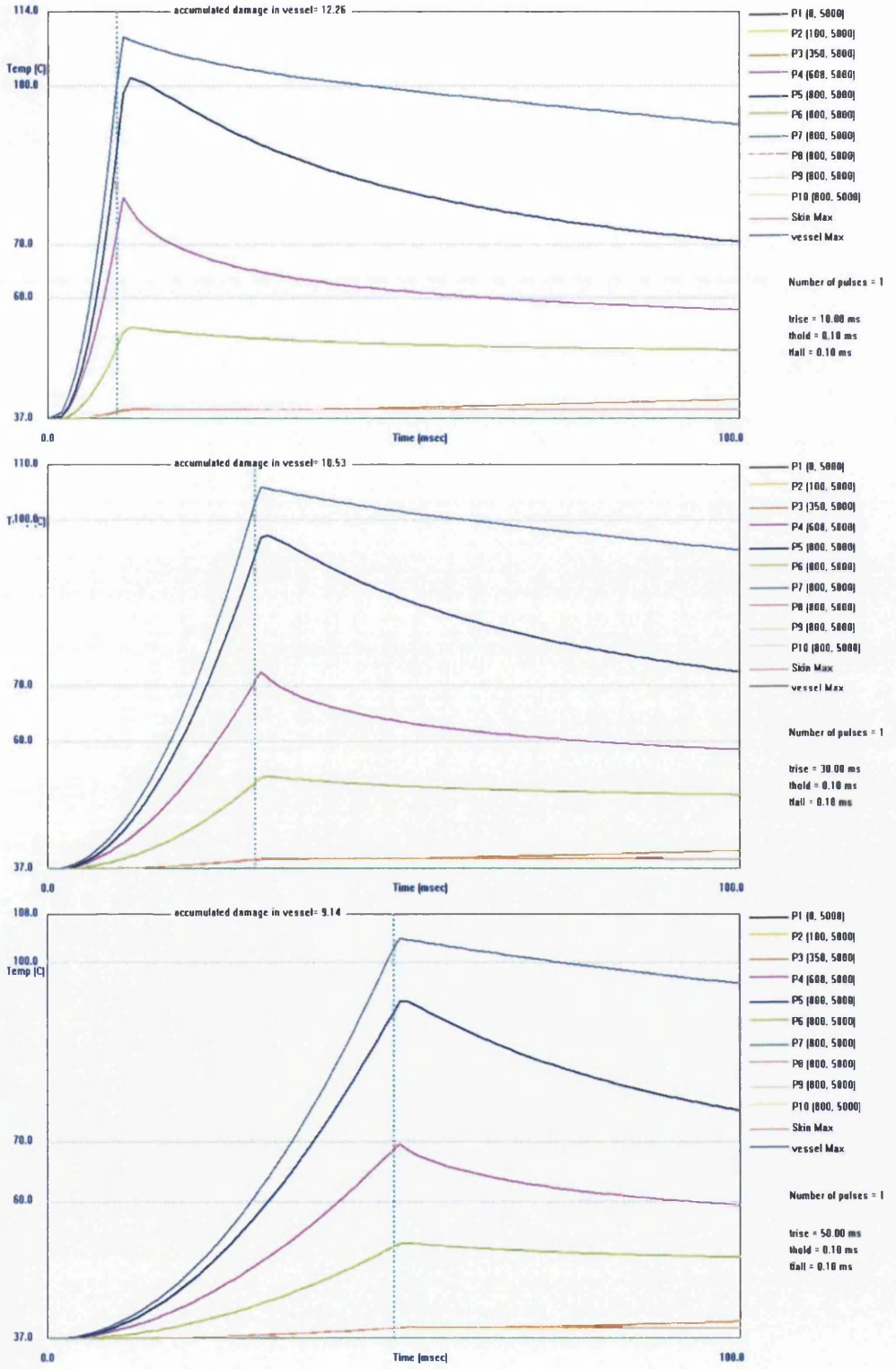

Figure 5.25: Thermal diffusion for tissue model incorporating a blood vessel with $D = 1000\mu m$, effect of varying the duration of a ramp pulse: $10ms$ - top; $30ms$ - middle; $50ms$ - bottom, t_{rise}, respectively

Duration - Observations

Based on observations of the graphs:

- results show a modest decrease in peak temperature at the upper vessel wall as the duration increases.

- at $10ms$, both profiles exceed $70°C$ for $10ms$, therefore necrosis is predicted.

- at $30ms$, only the ramped profile predicts necrosis.

- at $50ms$, neither profile exceeds the $70°C$.

- the Ramp pulse appears to yield to a higher temperature increase in the tissue. All the probe points within the skin model show a monotonal increase in temperature with decreasing duration of the pulse, with values for the ramp pulse always above the square counterpart. If we consider now two points of interest, namely P4 (i.e., the anterior wall of the vessel) and vessel Max, as highlighted in Fig. 5.26 and Fig. 5.27 respectively, we can more clearly evidence these results. Fig. 5.27, which shows the behaviour of the point at maximum temperature inside the vessel, we can clearly see that the Ramp pulse temperature curve shows a higher peak value compared to the Square pulse. Furthermore, the difference between the peaks increases for increased duration of the pulses.

- particularly important are the values corresponding to the point P4 ($8\mu m$ inside the blood vessel). This point, as evidenced more clearly in Fig. 5.26, experiences substantial increase in temperature for the irradiation profile corresponding to the ramp, as opposed to the square pulse.

- from Fig. 5.24 and 5.25 we can infer that the relative temperature difference between points P4 and P5 for the Square pulse is smaller than for the Ramp pulse.

- point P3, which is placed at a depth of $350\mu m$ from the skin surface, shows a decrease in temperature for increasing pulse duration. Furthermore, the rate of decrease is more sustained for the Ramp pulse than for the Square pulse.

- Temperature values for the skin surface experience a small increase for the duration of the simulated time for both the square and the ramp pulses.

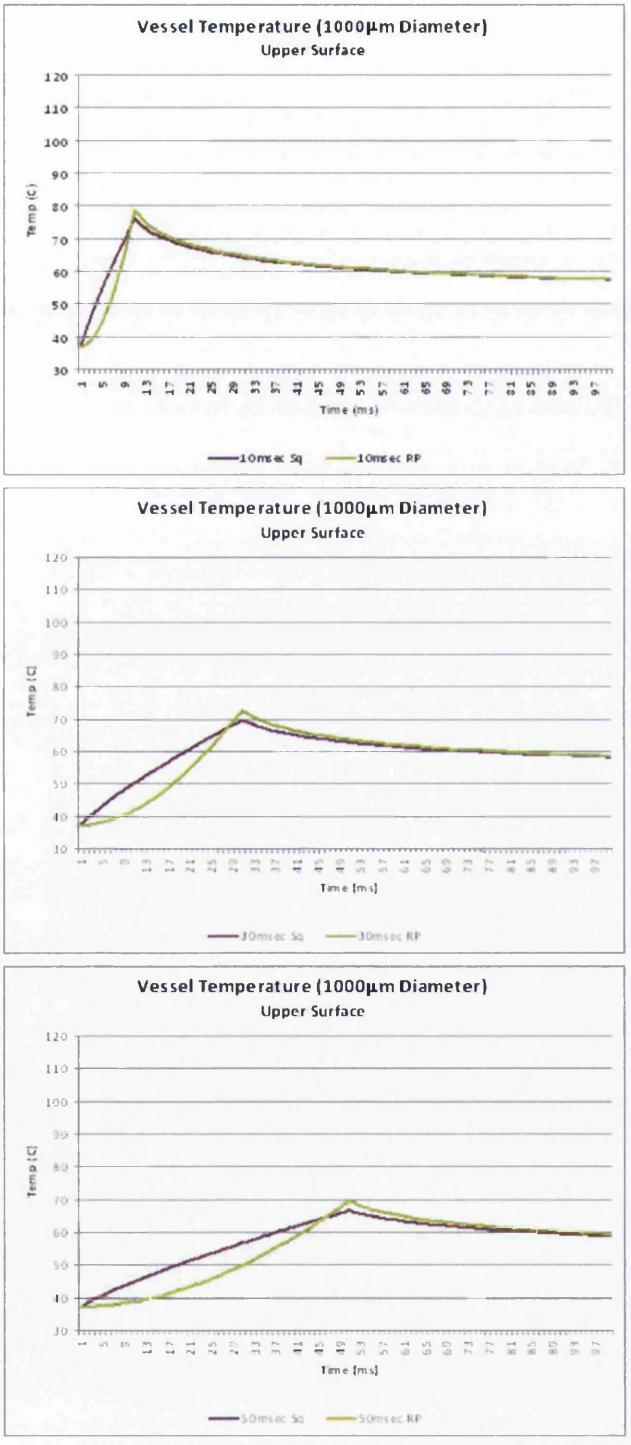

Figure 5.26: Thermal diffusion for tissue model incorporating a blood vessel with $D = 1000\mu m$, fluence $100Jcm^{-2}$ - effect of varying the duration of a pulse on a point at the upper wall vessel's temperature

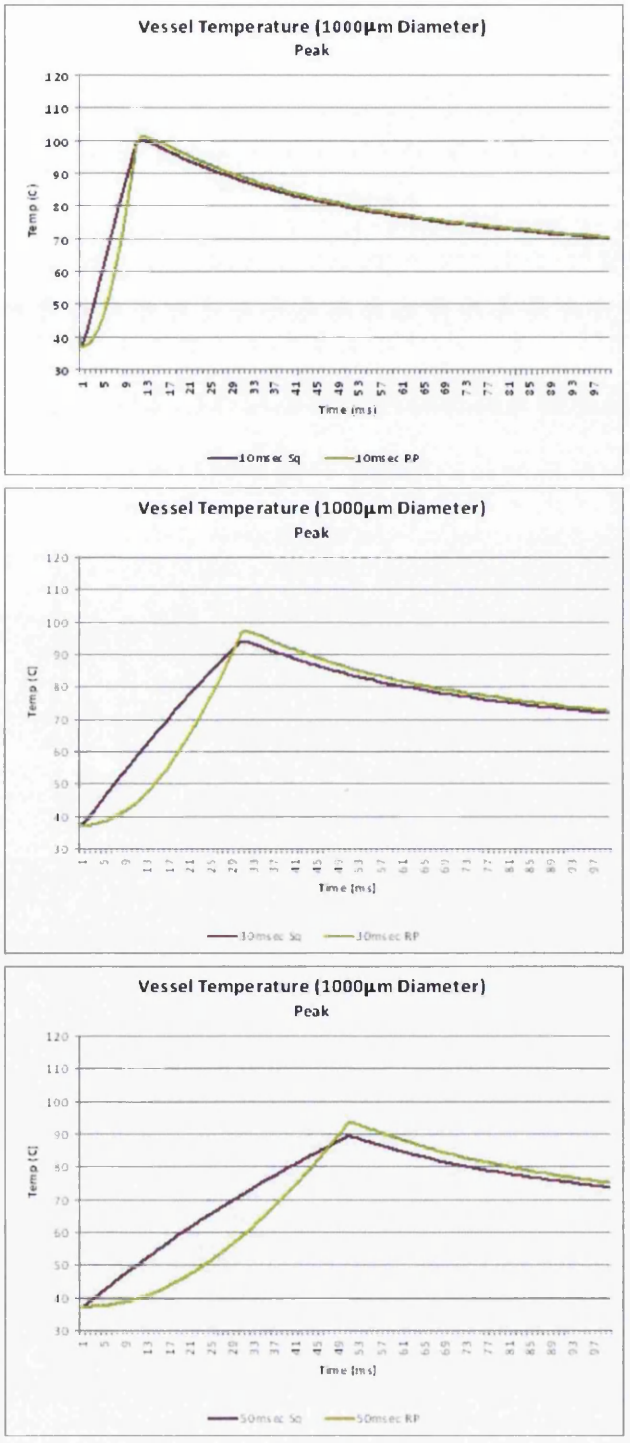

Figure 5.27: Thermal diffusion for tissue model incorporating a blood vessel with $D = 1000\mu m$, effect of varying the duration of a pulse on the maximum temperature point within the vessel;simulated time $t = 2000ms$

5.5 Modelling - Discussion

The computer modelling study undertaken proves the following points:

- that a YAG laser targeted at human skin can deliver significant energy to the blood vessel without raising the temperature of the epidermis when parameters are controlled carefully

- that larger blood vessels $500, 1000, 2000\mu m$ experience increased temperature as the fluence increases, eventually exceeding the $70°C$ threshold, therefore predicting necrosis. All vessels require fluence in excess of $100Jcm^{-2}$, with the $2000\mu m$ vessel requiring more than $200Jcm^{-2}$.

- pulse duration is a critical factor and has a direct impact on therapeutic outcome. As the pulse duration increases, a greater fluence is required to compensate for thermal losses.

- pulse shape has been demonstrated to be an important factor, with the ramped pulse delivering a greater temperature increase than a square pulse of equal duration and fluence.

5.5.1 Limitations of the model

Modelling work has been carried out in order to investigate the response of skin tissue to the irradiation with monochromatic Nd:YAG laser light at $1064nm$. Specific emphasis has been given to the evaluation of Fluence, Shape and Duration of the laser pulse on the target tissue within the skin, i.e., the blood vessel, whilst paying attention to include the investigation of the surrounding tissue.

As for every modelling effort, every model carries its own limitations and constraints which are introduced in order to keep the complexity under control, whilst allowing satisfactory investigation of the parameters core to the research work.

The main purpose of this modelling work was to investigate the hypothesis of the importance of the temporal profile of the laser pulse, factor that is mostly overlooked at both technological and clinical level - in favour of the other more traditional parameters such as fluence and duration, for the treatment of vascular lesions. Therefore results are meant to provide indications and trends rather than absolute values, which would require *in-field* testing and accurate measurements of tissue response *in-vivo* in order to accurately calibrate the model.

A number of assumptions have been made throughout this modelling work:

- The model is a two-dimensional (2D) model. Although a three-dimensional model is somewhat preferable because of aesthetic considerations and true volumetric calculations characteristics, for the purposes of these studies a 2D model was deemed to be adequate. In fact, in a three-dimensional model, each cell of the mesh would be surrounded in the three dimensions by other cells, as in within a cube. During the thermal calculations, and according to the three term equation as previously outlined, each cell would receive a component of heat from the neighbouring cells surrounding it; this would give rise to a better result in terms of temperature rise for the points of interest especially for the upper and lower walls of the vessel, with even greater temperature increase and increased difference in results between the two pulse shapes under investigation.

- the model performs a statistically convergent Monte Carlo calculation to obtain a steady-state distribution of photons. For a typical Monte Carlo run as used in this thesis (e.g., see Fig. 5.14), the code shows that most of the photons are absorbed in the dermis and the Monte Carlo code terminates a photon when its energy is less than 10^{-4} of its original energy. Since the energy left at any interaction is $1 - \mu_a/\mu_t = 0.998$, then we can estimate the approximate number of interactions a photon would undergo in the dermis, for the conditions set in this thesis, from the relationship: $0.998^n = 10^{-4}$. Taking the logarithm of each side gives $n = (-4/log_{10}(0.998)) = 4600$ events. If we take the average distance travelled between interactions to be $1/\mu_t$, this gives a typical distance of $35mm$ travelled by a photon, which in turn gives a typical time of flight $\approx 10^{-10}s$. This time is many orders of magnitude less than both the laser pulse and the thermal diffusion time.

  This approach allows for a considerably reduced simulation time, without sacrificing the accuracy, as the local photon flux is weighted by the temporal profile of the pulse in order to take in to consideration the temporal distribution of the laser pulse. Therefore, whilst avoiding the costs of subdividing the photons both spatially and temporally during the

calculation (we must consider that each bundle of photons is first divided according to a division in bands of the pulse, then subdivided within cells of the grid), a much efficient use of processor time can be achieved.

- As outlined in 5.2, the model does not include the effect of perfusion rate within the blood vessel. It has been shown in [86] that perfusion is not a significant factor in the thermal response of tissue for typical therapeutic laser irradiations for these tissues. This is not applicable to convective heat loss by blood flow in major vessels or profuse bleeding. However, in this work we have decided not to include the blood flow among the modelling parameters. The vascular lesions under investigation are predominantly veins, as opposed to arteries. Venous blood flow rate is substantially lower compared to the arterial flow, for the duration of the pulses chosen, therefore in first approximation the effect of perfusion has been neglected.

- The blood vessel has been modelled with infinitesimal vessel wall thickness, i.e., the thickness of the vessel has not been considered.

- As outlined in the previous subsection, simulated time has been kept to a total of $100ms$. This was done in order to keep the total processing time to a reasonable value and also to allow the investigation to concentrate of the regions of main interest for the analysis of performance on the target tissue.

  In order to assess the effect of the radiation *post-thermal relaxation* of the target tissue, simulations have subsequently been carried out to for a total simulated time of $2000ms$ to serve both as a test and also to evaluate the longer term effects of the heat diffusion to the tissue surrounding the target vessel, with emphasis on the points between the vessel and the skin surface. Results from the simulator are shown in Fig. 5.28. As we can see from the Figure, the temperature in point P3 increases steadily during the off-time after the pulse.

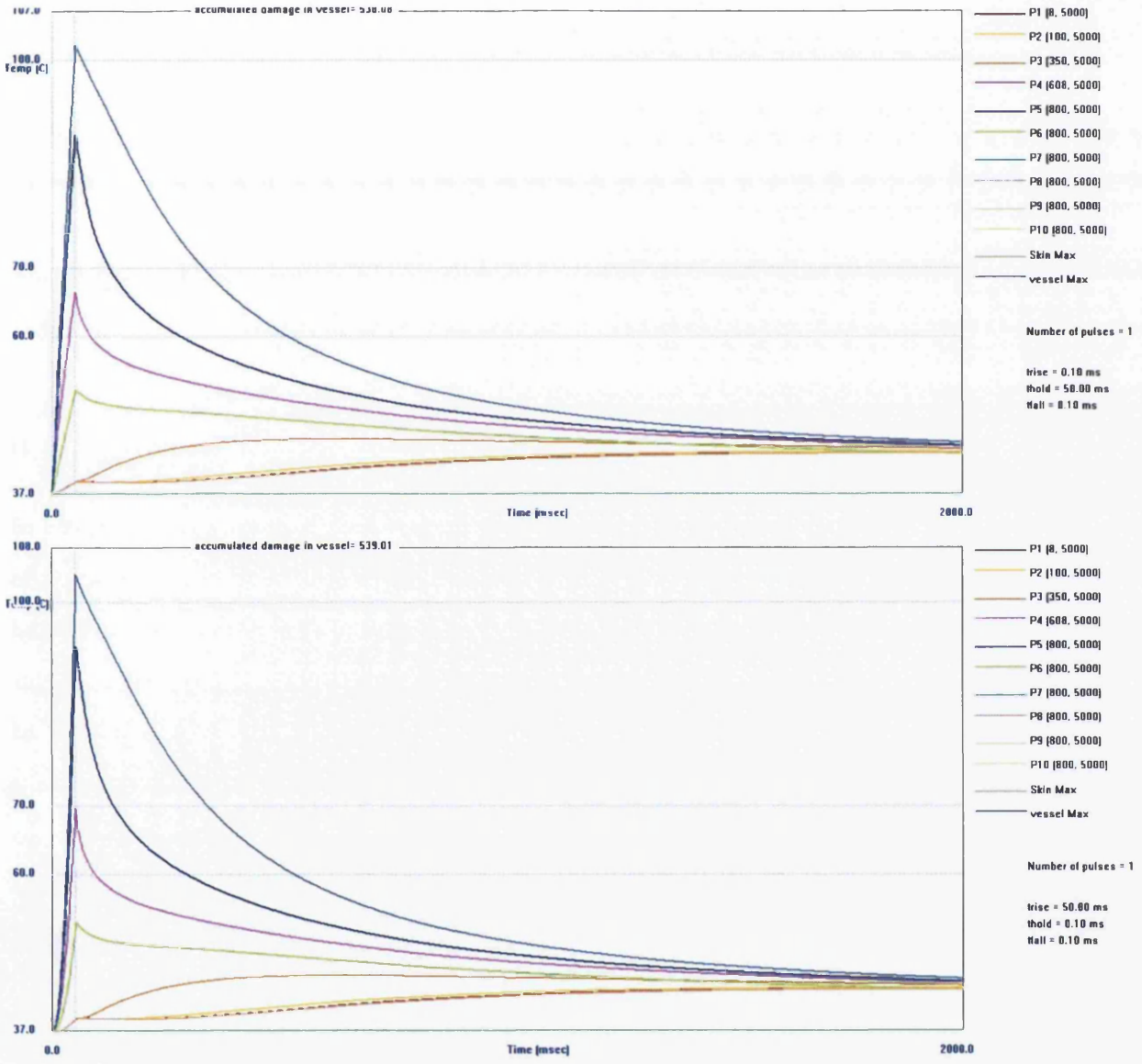

Figure 5.28: Thermal diffusion for tissue model incorporating a blood vessel with $D = 1000\mu m$, effect of varying the duration of a pulse on the maximum temperature point within the vessel

Chapter 6

New Technology

6.1 Introduction

In Chapter 5, thermal modelling of a tissue sample comprising of varying blood vessels by means of a two-step simulation method was carried out. Results showed the potential therapeutic benefits of controlling the temporal profile of the pulse. Thermal damage to the vessel has been shown to be affected by the use of different pulse shapes, the effect of whom has been shown to be independent from other parameters such as fluence and pulse duration. In this chapter, a novel technology and a system are described. The system combines technology originally conceived to provide controllability of the temporal profile of a flashlamp output within a novel apparatus with the aim of addressing the need for controlling the output of a solid state laser. In this chapter the importance of pulse control and shaping for applications in the medical field, which has been outlined in the previous chapter, will be translated in to a physical system. Explanations of the technology needs and limitations behind effective control of the output will also be outlined.

6.2 The Background Innovation

As explained in 1.1 no major innovation in the power supply section of solid state lasers had happened. However, recently, advances in non invasive, non-laser light based treatment devices for cosmetics use are bringing to market novel units with *intelligence on board* that have allowed an astonishing reduction in device weight and volume, whilst providing semi-professional results in the fields of use. The real innovation that these units are bringing to the market is multi-fold. Firstly, concepts in electrical and electronics engineering have been adapted and developed which had (in a more primitive form) been generated to originally serve other fields, such as the professional reprographic technology (description of circuits and methods of work are found for example in [82]). Secondly, these concepts have been supported with advances in control and system design. Thirdly, the first two aspects have been coupled with the availability of more affordable solid-state semiconductor devices (transistors diodes and microprocessor). Lastly, all these aspects have been embedded within an effective business model to allow quality assurance in manufacturing. The following subsections will address the aforementioned four aspects.

6.2.1 Innovation in Electrical and Electronics Engineering

To address the first aspect, the need in fields such as the mentioned reprographic and photocopy technology for illuminating documents had given rise to developments in flashlamp technology long before its use, and related technology developments thereof, was to be envisaged for dermatology and generally speaking, cosmetics use. As reported in said patent, back in 1983, dedicated circuitries which would accomplish the charge and discharge of capacitors to provide incremental energy inputs to a flashlamp as well as separate circuitry to also recharging the capacitors were provided. The embodiment was in such a way as to provide two different circuits to switch between, one to provide the energy to the lamp in incremental steps, and the other one to provide restoration of the energy to the capacitors, also in packets of energy, which were small compared to the total amount of energy required by the lamp. The concept of incremental steps in the provision of energy is crucial to the subsequent developments of the technology for this

work, whereas the hardware realisation of separate circuits to manage the charge and discharge will eventually be abandoned to allow saving in weight, size and ultimately cost, and is directly linked to the second and third aspects of the innovation behind the unit employed within this work, as it will be evident from the following considerations.

6.2.2 Innovation in Control

The availability of processing power at extremely low cost is a direct consequence of the semiconductor roadmap following the so-called Moore's law. For the purpose of avoiding any trivial discussions, it is worth noting that what the Law described as a trend in the scaling up of processing power in relation to the number of transistors per square centimeter of silicon, and more precisely the doubling of this number approximately every 20 months, in a paper by Moore back in 1965 [91] is what has kept the technological developments in computing and in general in semiconductor processing and manufacturing possible, but it also is what has made the development what effectively is a slave of the law itself: that being the fact that designers and manufacturers have been forced to "do the impossible" in order to keep up with the law itself (a comprehensive treatment of this matter involves a more philosophical approach to reviewing technology and science developments, and therefore is beyond the scope of this work, however, arguments to support this line of thought can be found extensively in literature, amongst which, for example, in the book: "Getting New Technologies Together: Studies In Making Socio Technical Order", by Cornelis Disco and Barend van der Meulen [92], citing the lines: "They (chipmakers) direct their efforts toward achieving the predicted values," and thus the law is described/titled a "Self-Fulfilling Prophecy" and also: "This prediction has come true so beautifully, that nowadays we speak of Moore's Law as if it were a law of nature.").

Pulse Width Modulation

Pulse Width Modulation, or PWM, refers in principle to a waveform control technique. The main applications for PWM are in digitally creating an analog waveform for control functions

and power supplies, as well as in digital creation of analog signals for generation of arbitrary waveforms, sounds, etc. From the applications mentioned, it is clear that PWM techniques could be used for power delivery control, to provide intermediate amounts of electrical power between an "'on"' and an "'off"' state, thereby precisely controlling the amount of energy delivered at each point in time. PWM is a relatively recent technique, made practical by modern electronic power switches and microprocessor control. Modulation is performed through the alteration of the so called "'duty-cycle"' (DC) of a square waveform at a certain frequency. The duty cycle is a parameter defined as the percentage of time where a electrical parameter (usually Voltage) level is at its full-on value compared to the entire cycle of the waveform (see Fig. 6.1.

Figure 6.1: Pulse-Width-Modulated signal showing progressive increase of the duty-cycle

PWM techniques allow for a control of the variation of the duty-cycle, thereby making the duty-cycle a function. Often, control and alteration of duty cycle is used to create an analog signal from a digital signal by extracting the average value of the waveform through filtering (for example, if we consider the voltage as our electrical variable between $0V$ and $+5V$, a duty-cycle of 0.5 will give an average output of 2.5V after passing through a filter). A duty-cycle of 0.50 gives a standard square wave, whereas altered duty-cycles provide for a higher average signal. The PWM technique is extensively used in telecommunication and in power electronics control, as it provides for a finer control of power delivery thereby increasing the overall efficiency of the system. Within this research work, PWM principles are employed in an innovative and simple yet effective implementation, to modulate the energy delivered to the pumping medium of the laser system (i.e., the flashlamp), in order to achieve control of the flashlamp output.

6.2.3 Semiconductor Technology Evolution

Inexpensive processing power allows control of ever more affordable high speed semiconductor switches and components, the maturity of technology of which means that circuits can be designed to work reliably. It also means that it is possible to encode the control strategy somewhere within the system in order to instruct the processor(s) to execute a certain operation. There are many strategies to instruct a processor, with the main discriminating factor being once more the conundrum of reconciling cost with flexibility and accuracy/precision of the desired output. The preferred strategy will be explained in more detail in the proceedings of this work (see 6.3.2).

6.2.4 Innovation in Business Model and Manufacturing

The unit used in this work was an iPulse development unit. This unit combines the positive aspects outlined by the four aspects as described above. It is worth noting that the adoption of an effective business model by the company was instrumental in allowing the development of the product in-house, whilst meeting the quality requirements and costs through outsourcing the manufacturing of the components to a leading and reliable manufacturer (again, a complete and exhaustive discussion regarding these matters involves areas such as business development which is outside the scope of this work, however interestingly, and contrary to the current trend, the outsourcing strategy for manufacturing, as adopted by the company did not involve any overseas manufacturing, but rather an UK-based branch of a leading high tech manufacturer; exploitation of a global market would likely involve links with far-east players to keep up with the demand).

The various components of the system are described in the following section.

6.3 Design Concepts

A system to test the hypothesis of controllability of a solid state laser with the digital control of a flashlamp output has been assembled. A more detailed explanation of the standard components

was given in 4.6.2. The system subject of this work comprises of the following subsystems:

- laser head
- digitally controllable power supply
- additional microprocessor unit
- trigger subsystem
- mains transformer
- additional circuitry

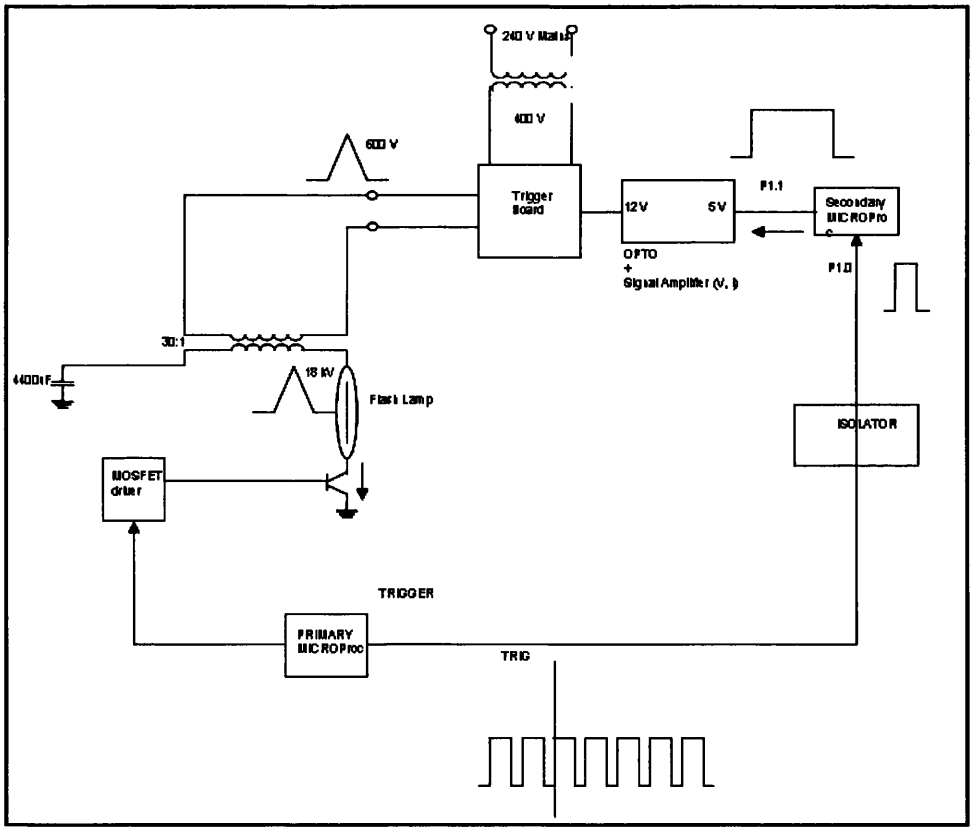

Figure 6.2: The designed System Under Test

A more detailed explanation of the concepts in the design of the aforementioned system is given in the following section.

Figure 6.3: Components of the Nd:YAG Laser head used during the design and experiments, with the YAG laser medium (pink crystal bar). The flashlamp is not shown

6.3.1 Laser Head

The laser head used within this work was an alluminium unit. As we can see from Fig. 6.3, the head is an assembly comprised of a central main body housing the optical cavity which in turn houses the flashlamp and the YAG laser bar; two extremities screw on to the main body. The two extremities have the dual function of sealing the optical cavity (with the use of o-ring seals) for water-cooled operation, and of providing the support for external optics and Q-switch module, which was removed for the purposes of this work.

6.3.2 Digitally-controlled Power Supply Unit

The digital power supply subsystem is essentially an integrated control unit comprising of a microprocessor, a digital signal processing unit, a semiconductors driving circuit, charging and discharging circuits comprising of storage capacitors and other conditioning circuitry. The unit

is a constituent part of a broadband radiation spectrum light based therapeutic device for hair removal, which has been very recently market-piloted in the UK market. The unit was originally designed to drive a dual compact flashlamp, with each of the lamps measuring $4cm$.

In such design fashion, the energy storage elements are in essence reduced down to one main capacitor, and two secondary capacitors of a very small value. All these capacitors are housed within the main power supply unit. The flashlamps would be energised by the secondary capacitors, which have a small capacitance compared to the primary capacitor, and such capacitors would be connected in series with the flashlamps. The microprocessor controls the release of energy to the flashlamp via high speed semiconductor switches, specifically Cool-MOS (Metal-Oxide Semiconductor) FETs (Field Effect Transitors). Release of energy happens in a controlled manner, where it is possible to predetermine the duration of the pulses and the trend of the pulse train. Specifically, the switches' activity is modulated at relatively high frequency by selectively opening and closing them throughout the predetermined time interval thus releasing the energy from the storage capacitor in the form of packets of energy, whose duration is only a small fraction of the total time interval.

The unit is mains powered with a switch mode power supply supplying the system with a $+19V_{DC}$.

Detailed Description of the power supply

The digitally controlled power supply is comprised of the following main sub systems:

- microprocessor unit
- capacitor charging circuit
- MOSFETs driver

Figure 6.4 shows a schematic view of the driver circuit. The circuit is constituted by two identical mirrored subcircuits. Each circuit comprises of:

- a semiconductor driver element
- an inductor
- a high speed semiconductor switch (MOSFET)

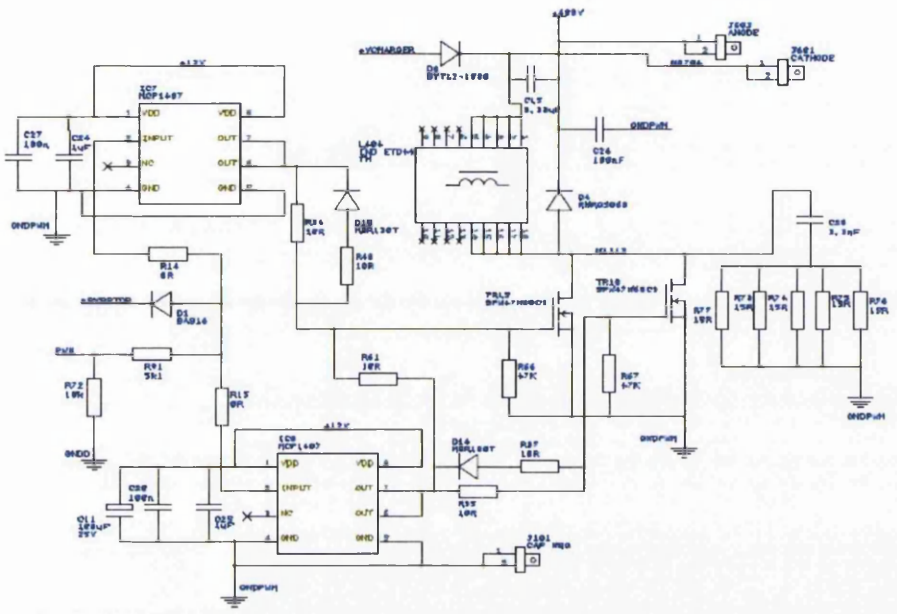

Figure 6.4: The gate drive circuit of the Digital Power Supply

- other passive components within the circuit network

The semiconductor driver element is controlled through PWM signals originating as output from the main processor unit, as per Fig. 6.2. Principles of PWM have been given in 6.2.2. Modulation is performed according to the following relationships:

$$\frac{T_{on}}{T} = n \tag{6.1}$$

T is the period of each PWM segment, which has been set to $4\mu s$. This time is dependent on the switching frequency of the MOSFETs.

T_on is the total on-time of the discharge phase, that is, the sum of the periods T of the pulse train to operate the MOSFETS. therefore, $T_{on}/T = n$, with n equal to the number of periods.

S is a function of a parameter called δ, and its numerical value ranges from 0 to N. S stands for START and it models how the duty-cycle increases within the pulse train and in effect it

is mapped in a look up table (LUT) within the microprocessor memory, thus representing a coded form of the duty-cycle. N is a constant of value 65535, which represents the number of increments which each segment of period T, of the pulse train is divided in to, and corresponds to a duty-cycle of 100per cent. This as we will see will dictate the effective total number of PWM signals in output from the main microprocessor to the MOSFETs drivers.

δ is a slope factor and essentially is a parameter which accounts for the drop in the Voltage level of the main capacitor capturing the ϵ increase at each full cycle of the wave and δ and S are the critical values dictating the level of energy output. For each combination of parameters, there is a value, namely δ_{MAX}, which is equal to

$$\frac{\delta_{MAX}}{256}n = N - S \tag{6.2}$$

At each period T, S will vary during the pulse operation of the laser, by increasing its value by a $\epsilon = S + \delta/256$. This value has to be $\leq N$. When a value exceeds N, the microprocessor will interrupt the delivery of PWM pulses thereby interrupting the operation of the switches.

Storage Element

The energy storage elements of our interest in the proceedings of this work are the Storage Capacitor and the inductor part of the flashlamp trigger transformer.

The storage capacitor is a $4400\mu F$, $400V$ Electrolytic Capacitor. With regards to the inductor, the following subsection will provide a more detailed explaination.

Trigger Subsystem

The trigger subsystem comprises of a trigger card, a step-up transformer and related wiring.

The trigger circuit comprises of circuitry to generate the high voltage trigger necessary to ionise the gas inside the flashlamp. The trigger circuit receives input signal from the secondary microprocessor unit. This signal is then used to trigger an output pulse at the primary winding of a trigger transformer.

Further explanation regarding the rationale for the use of a separate unit are found in section 6.3.

The trigger transformer is a purpose-built hand made inductor. The inductor has a ferrite core, and copper windings. In order to achieve a step up Voltage in excess of $10kV$ in order to initiate the breakdown of the Xenon gas within the lamp, the transformer has to satisfy the following design rules:

If we consider N_1 to be the number of windings at the primary of the transformer, and N_2 to be the number of windings at the secondary of the transformer ((which is connected to the anode of the lamp), then:

$$n = \frac{N_1}{N_2} \tag{6.3}$$

then the Voltage at the secondary, V_2, will be equal to:

$$V_2 = \frac{n}{V_1} \tag{6.4}$$

With $N_1 = 60$ and $N_2 = 2$, $n = 30$, $V_1 = 600$ and therefore $V_2 = 18kV$.

The trigger transformer whilst of rudimentary manual construction, proved to be effective.

6.4 Operation of the circuit

This section will describe the drive circuit to operate the flashlamp and therefore the laser system.

The control circuit provides a pulsed electrical input to a flash lamp, comprising of a charge pathway for charging a capacitor, and a discharge pathway for discharging the capacitor to the flash lamp. The charge pathway comprises of a path including a sequence of conductors and electronic components which are common to and shared with part of the discharge pathway. The control circuit includes means for selectively channelling current flow either from an electrical potential supply via the charge pathway including the path, or from the capacitor via the

discharge pathway including the path, wherein the electrical potential supply is less than a potential at a cathode terminal of the discharge tube during the discharge of the capacitor.

Each of the components used in the path of the charge pathway used to charge the capacitor is common to and shared with the part of the discharge pathway and vice versa.

The charge and discharge pathways includes a shared transistor which comprises of a source terminal connected to the electrical potential supply for the control circuit. Such a transistor is arranged to be controlled using a drive signal from a drive circuit. The control circuit is used to control the operation of the flash lamp.

The drive signal to the transistor may be varied during the optical output of such a flash lamp. In this way it is possible to provide a substantially constant current flow through the flash lamp.

The control circuit is powered using a supply voltage at $+19V$. Rectification is provided by an ac/dc converter. Alternatively, the supply voltage may be provided from a battery or other dc supply.

In use when the control circuit is used to control a flash lamp, the voltage is applied at the cathode terminal of the flash lamp.

The drive signal is pre-calculated before the charging and discharging of the capacitor (alternatively, a drive signal may be dynamically calculated during the charge and discharge of the capacitor).

In order to provide a pulsed electrical input to a flash lamp to produce an optical flash (intense pulsed light), selective charge of the capacitor for a first pre-determined time interval using the charge pathway, and selective discharge of the capacitor to the flash lamp for a second predetermined time interval using the discharge pathway, are performed. The first and second pre-determined time intervals occur at different (non-overlapping) times.

The optical flash of the flashlamp has a predetermined time interval and a predetermined total electrical energy input for the optical flash, in combination with the control circuit for providing a pulsed electrical input to the flash lamp for producing the optical flash.

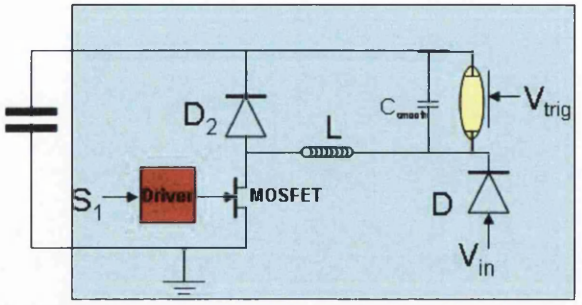

Figure 6.5: Diagram of the flashlamp driving circuit

Fig. 6.5 is a circuit diagram of the control circuit in accordance with the aforementioned description.

The control circuit comprises a drive circuit, which receives signals S1 as input from a microprocessor (not shown) and outputs signals as control signals to a MOSFET. The microprocessor controls when the control circuit operates as a charging circuit and as a discharging circuit.

The input voltage Vin to the circuit is a 19V dc supply which may be provided from a battery, or be derived from a mains supply, for example, by rectifying an alternating current (ac) using an ac/dc converter (not shown). The input voltage Vin is applied at the cathode terminal of a flash lamp via a diode. The diode avoids conduction to the power supply for the input voltage during the firing (pulsing) of the flash lamp.

The circuit operates in two distinct modes, namely charging and discharging modes, which occur at different (non-overlapping) times. It either operates in a charging mode or a discharging mode, but not both at the same time.

As a charging circuit, the current path is from the diode through an inductor and to ground through the MOSFET, when the MOSFET is "ON". When the MOSFET is "OFF", the current is again directed from the diode, through the inductor, and then to a capacitor via a second diode D2. Current is prevented from passing through the flash lamp since the supply potential is insufficient to ionise the gas atoms within the flash lamp to thereby create a conduction path between the separated electrodes. The current from the supply is supplemented with the current

derived from the collapse of the magnetic field in the inductor which thus causes a high voltage spike to be applied across the capacitor.

During the collapse of the inductor current, only an incremental charge and thus voltage is applied to the capacitor. Accordingly, after the inductor current has completely decayed to zero, the MOSFET is then switched back "ON" for a pre-determined time and then "OFF" again, so as to add more charge to the capacitor and thus further increase the voltage across the terminals of the capacitor. At each charging step, the capacitor is prevented from discharging back across the inductor due to the diode and so the only other route for discharge is across the flash lamp. The charging process is repeated for a predetermined time until there is a sufficient potential difference across the terminals of the capacitor to create an optical output pulse from the flash lamp.

As a discharging circuit, the current derives from the capacitor and passes through the flash lamp, then the inductor and to ground through the MOSFET when it is "ON". However, the MOSFET is only switched "ON" for a limited time to prevent the inductor current increasing to saturation.

Before the inductor current reaches saturation, the MOSFET is switched "OFF", thereby preventing further discharge of the capacitor, to enable the current in the inductor to subsequently decay and thus create a voltage spike. The collapse of the magnetic field within the inductor causes a current to flow through the diode and then back through the flash lamp so as to try to maintain the discharge and thus an optical output.

After the current in the inductor has fully decayed to zero, the MOSFET is then switched back "ON" to further discharge the capacitor and thus maintain the voltage across the flash lamp. The discharging process is repeated for a pre-determined time with each successive step involving a small reduction in the charge stored on the capacitor.

During the discharge process, a smoothing capacitor C_{smooth} smoothes the output voltage across the flash lamp, to provide a substantially constant optical output from the flash lamp.

The microprocessor (not shown) maintains a voltage of at least 90V at the cathode terminal

of the flash lamp to maintain the gas atoms within the flash lamp in partially excited state. This further prevents current flowing from the supply voltage through the flash lamp, but maintains a plasma discharge within the flash lamp, which is evident as a low intensity glow. Before the control circuit enables the discharge of the capacitor to produce an intense discharge arc however, the microprocessor (not shown) causes a trigger voltage to be applied across the flash lamp to ionise the gas atoms therein. The microprocessor (not shown) controls the timing of the trigger voltage to the lamp (using signal S2 - not shown) and the subsequent discharge of the capacitor across the discharge lamp (using signal S1) to ensure that they take place at the correct time.

During discharge, - i.e., when an an output pulse event is occurring, the drive signal to the MOSFET is continually changed to ensure that a constant current flows in the flash lamp even though the capacitor voltage decreases due to discharge. This continual change to the drive signal to the MOSFET follows a pre-calculated (but theoretically it could be dynamically calculated) algorithm which is based upon the input parameters such as the capacitor value, required pulse duration load characteristics and voltage.

From this description is therefore evident that this control circuit requires only one drive circuit, inductor and transistor as compared with other control circuits which require duplication of such components. In addition, the transistor, inductor and diodes of the control circuit can lead to a shorter charge time and increased reliability due to de-rating of charging components.

Chapter 7

Testing and Results

7.1 Introduction

In the previous chapter a novel system has been described which has been hypotesised to allow control of the temporal profile of the pulse of a solid state laser.

This chapter will describe the experimental efforts of this research work. The experiments subject of this chapter have been carried out with the aim of demonstrating and proving a concept, which was the main engine behind the entire research work. The type of experimental work carried out has therefore taken a decisive investigational pathway which will be described in the following sections. When dealing with High Voltage, High Current equipment safety aspects have to be taken in to account. If, on the other hand, these elements are coupled to the operation of laser, further safety considerations have to be taken in to account. Safety aspects involved in this research work are the subject of Section 7.3. Section 7.4 will then describe the conditions under which the tests were performed; limitations and benefits of the proposed approach are given. Section 7.5 describes the methodology used for the tests, and related analysis, focussing on the objective of the tests.

7.2 Test setup

Testing has been performed within a laboratory environment, using commercial electronic test equipment. In order to perform the tests, the following equipment was used:

- oscilloscope
- energy meter
- regulated power supply unit (PSU) with photodetector circuit

7.2.1 Oscilloscope

The oscilloscope used was a Tektronix TPS2024 digital oscilloscope, with 200 MHz Bandwidth, Sample Rates up to 2 Giga-Samples/s (GS/s) Real Time, four fully isolated channels and LCD screen, manufactured by Tektronix Inc., Beaverton, OR 97077, USA [93]. The chosen oscilloscope is specifically designed to allow power measurements. The oscilloscope was equipped with a series of different sets of probes to suit the different requirements of the measurements to be undertaken. Specifically:

- A622 1000A clamp on current probe
- high-voltage voltage probe
- P5120 600V probes

all from Tektronix Inc. Before each test session, the oscilloscope probes were calibrated through the standard calibration procedure suggested by the manufacturer. The procedure consist in connecting the probe to a "'Ground"' pin and to a 5kHz waveform pin; by adjusting a screw on the probe and monitoring the displayed waveform on the screen, it was possible to offset possible distortions in the acquired waveform (see Tektronix TPS2000 Manual). The result is a probe matched to the specific channel to which it is connected. This factor is important in reducing the amount of ripple present at the output and therefore limiting the noise at the output.

7.2.2 Energy meter

The energy meter used was an Ophir Inc. Two different detectors were used in combination with the meter, in order to be able to monitor different ranges of energy outputs. Readouts of

the detected cumulative optical energy of the laser pulse was through an integrated display.

7.2.3 PSU + Photodetection

The Power supply unit used was a Tektronix T355 with multiple outputs at $\pm 35V$ on 3A and 0-5V on 5A. Regulation of voltage and current was through potentiometers on the front panel. The unit was calibrated. One of the voltage outputs of the PSU provided a voltage V_{cc} of +32V between the Emitter E of a near-infra-red (NIR) phototransistor and a current limiting resistor placed in series between the Collector C of the transistor and V_{cc}. The photodetector used was a silicon NPN Phototransistor model SFH-300 manufactured by Siemens. The low voltage output was used during the design phase of the pulse conversion circuitry to test the circuit and the external circuit boards.

7.3 Safety aspects

The work subject of this research involved operation of potentially hazardous equipment. Risks to be considered with specific regards to this work fall primarily within two categories:

- Laser radiation hazards: these are the risks associated with the exposure to *non-ionising* radiation. Specific hazards can be identified to be:
  - Eye Hazards
  - Skin Hazards
- Electrical hazards

7.3.1 Laser radiation Hazards

Eye Hazards

Several different structures of the eye can be affected by coherent radiation. Retinal injury can happen for radiation in the visible and infrared spectral region. The focussing effect of the cornea and lens means that even a direct or a reflected beam of small intensity will be intensified to a

factor of up to 100000 and form a very small image in the retina. Corneal effects are produced primarily by radiation outside the visible and near infrared regions. Damage to the lens is also possible within this region. For radiation at 1064nm, retinal damage is the main risk, as this wavelength is transmitted through the ocular media with very little attenuation, therefore reaching the retina with high energy density over a very small spot (due to the lensing effects already mentioned). This can cause permanent retinal damage even for exposures of $< 1\mu s$ at fluences in the μJ domain. A serious hazard is constituted by the fact that infrared radiation falls outside of the visible spectral region, therefore it does not cause the eye to automatically self-protect through mechanisms such as the blink reflex.

Skin Hazards

Skin hazards can be considered of secondary importance within this work, as the radiation spectrum involved does not include the ultraviolet regions which is potentially carcinogenic; however, possible effects of exposure to infrared radiation will be skin burns and excessive dry skin.

7.3.2 Electrical Hazards

These are the most lethal hazards from the use of lasers. They come from the inappropriate use and handling of the high-voltage components of the laser systems, and can cause electrocution, as well as fire hazard and risk of explosion of the energy storage/charge subsystems.

7.3.3 Laser protection

In order to limit the possible dangers which exposure to and operation of laser system present, a set of standard measures and a classification based upon the potential hazards presented by lasers has been developed by the accredited standards committee (Z136); see for example, *Z136.1 Safe Use of Lasers*, which is employed by the *American National Standards Institute* (ANSI). The ANSI Z136.1 recognises 4 Classes of lasers, based upon the level of hazard caused.

The laser subject of this work would fall within the Class 4, therefore protective goggles for the specific wavelength were used during the experiments.

It is emphsised that protective goggles are wavelength-specific, therefore care must be taken in ensuring that the right eyewear is used to match the laser wavelength.

Furthermore, care has been taken in avoiding risks of direct exposure to the high voltage section of the experimental setup.

7.4 Testing conditions and considerations

Testing Conditions reflect the main aim of the testing phase, that being of providing evidence of the controllability of the solid-state laser pulse shape through the control of the flashlamp pulse.

The maximum energy that the system could provide is limited ultimately by the capacitance of the main storage element (Capacitor, $4400\mu F$), together with the performances of the switching elements within the circuit. Therefore, emphasis was given to show the optical output through the acquisition of the laser output pulses over the acquisition of the energy output. This also means that absolute values of the optical energy were only monitored for a limited set of variations of parameters, whilst main focus of this work has been towards investigating possible optimisation of the pulse shaping.

Factors influencing this choice were also the nature of the equipment used. The number of acquisition channels on the oscilloscope was 4, which limits the amount of information (in terms of outputs) that are simultaneously available to be monitored; therefore, secondary aspects such as electrical parameter drift within for example the switching transistors were not monitored; the combination of energy meter and photodetecting circuit used means that optical measurements and energy measurements, for a given set of parameters, were performed separately; however a protocol taking in to account this factor is presented below.

- Two types of measurements have been performed for the laser system:

  - optical measurements - these measurements were performed using the optical detecting circuit
  - energy measurements - these measurements were performed using the Ophyr energy/power meter.

- A cooling time of 2 minutes between each operation of the laser was used. The explanation for this involves two considerations:

  - the laser head normally requires liquid cooling for normal continuous wave or Q-switched operation; however, operation within the normal settings was, albeit of some interest, not of relevance for the purposes of this study; liquid (water) cooled operation also required an additional pumping system which was not available at the time of testing, albeit it could be implemented in a commercial system in a variety of relatively cheap embodiments;
  - the power switching driving elements within the electronics were passively cooled through a small metal heat sink embedded within the body of the system; at a later stage a small electric fan was directed on to the switches to aid the heat spreading; however, operation of the laser without insufficient cooling time could cause temperature-related effects on to the switches with transient electrical parameters drift as well as, if the maximum junction temperature is exceeded, potential permanent damage to them through catastrophic failure (punch-through).

    Temperature of the switches was manually checked throughout the testing to ascertain the correct operation and cooling of the devices.

- for each set of parameters, the protocol followed for the measurements consisted of:

  - optical measurement
  - cool-down period (2min)
  - energy measurement
  - cool down period (2min)

- second optical measurement
- cool down period (2min)

The second optical measurement and the second energy measurement were taken in order to check the optical and energy outputs for performance consistency within each test.

- Electrical current measurements of the current output on the flashlamp was also performed in parallel to each measurements, to obtain the reference flashlamp pulse shape for comparison with the laser pulse shape. This is a type of high current measurements, which required the use of the HC probe connected to the oscilloscope.

In parallel to these sets of measurements, the flashlamp output was monitored against the Laser output (both during optical measurements and energy measurements). The optical measurement provides the pulse shape of the laser pulse detected by the optical detector circuit. When the optical radiation reaches the base B of the transistor, it causes the Junction between base and emitter to be polarised, therefore causing V_CE to drop. A oscilloscope probe between ground and the collector C will detect this voltage drop which is proportional to the optical energy that reaches the detector, thus producing an output corresponding to a certain pulse shape.

The detector was positioned at a fixed distance from the YAG laser head of $180cm$, in line with the direction of the laser beam. In order to avoid saturation, the detector was shielded by using white paper-based attenuating filters. The laser head was kept at non variant direction respective of the photodetector, in order to avoid misalignment between laser and detector. As it is clear from the previous comments, attenuating the optical energy of the pulse provides for the ability to display the pulse shape and to concentrate on this aspect of the work which is critical to prove the principle.

The effect of the artificial light in the laboratory - provided by standard fluorescent lighting tubes, was considered to be negligible according to the following considerations:

- the detector was tested through the standard acquisition routine and showed a output null when the laser was not fired, i.e., the Voltage level at its collector remained equal to V_{CC};

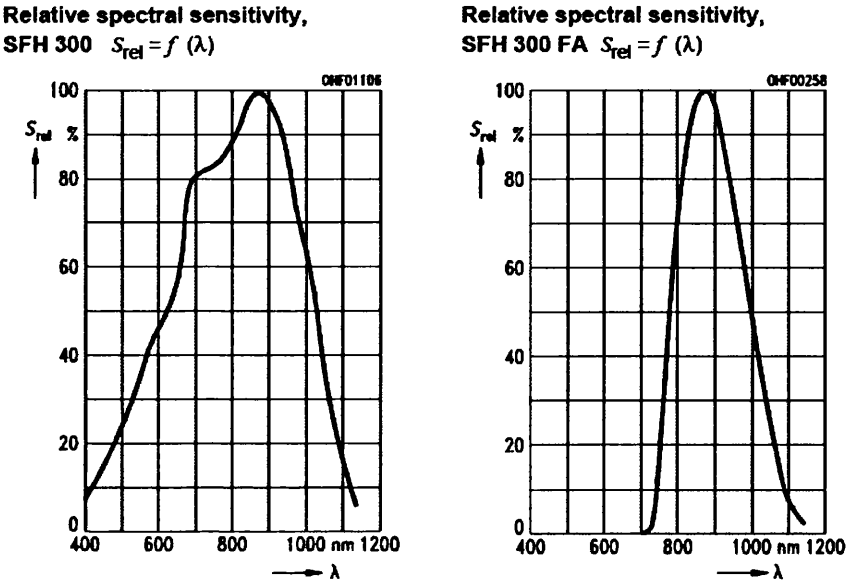

Figure 7.1: Comparison between relative spectral sensitivity of two models of the phototransistor used to detect laser pulses: unfiltered (left) vs filtered (right) diode (from [16])

the output did not change when test was performed in darkened conditions. Alternatively it is possible to use phototransistors packaged with daylight filter, however, as it can be inferred from Fig. 7.1, the spectral sensitivity S of the un-filtered detector is better for the wavelength of interest (1064nm).

- the laser crystal is within the laser cavity in the laser head, and it is not affected by external radiation; the only exposed parts of the bar are the two ends, however, as the energy necessary to create the carrier inversion within the crystal is several orders of magnitude higher than the radiated energy from the fluorescent tubes, their effect is negligible

The broadband light escaping from the laser head was screened using an enclosure to avoid the detector picking up longer wavelength components of the flashlamp light; however, the system was also tested to ascertain the influence of this factor on the optical and energy outputs readouts, and those were both negligible and smaller than the sensitivity of both the detector and energy measurement systems.

7.5 Testing Methodology

Following on from the considerations on 7.1, extensive testing was performed in order to answer essentially to questions:

- ascertain the feasibility of operating a solid state laser using a compact-size digitally controlled power supply
- demonstrate the controllability of the temporal profile through the use of digital control

The first part of the test phase aims therefore at answering the initial fundamental question, i.e.: is it possible to fire the solid state laser with a system not originally conceived for use with solid state laser?

The second part of the test phase aims at providing evidence of the controllability of the laser pulse to obtain arbitrary pulse shapes. This phase provides experimental evidence and the rationale behind this research work.

7.5.1 Feasibility of operation

To ascertain the first fundamental condition to enable the proceedings of this research work to be carried out, preliminary feasibility tests were performed. These tests aimed at verifying that the proposed system could in effect operate the laser. This implies that essentially three conditions needed to be satisfied:

- the current supplied to the flashlamp is adeguate to initiate the breakdown of the gas fill necessary in order to allow the flashlamp operation
- a sufficient amount of energy be delivered to the Nd:YAG laser bar to initiate and sustain a level of carrier inversion sufficient to fire; and
- the amount of energy that could be delivered in output by the YAG is detectable by the photodetector and the energy meter

This type of testing involves operation of the system in a operation mode that can be described as *free-discharge.* The free discharge operation can be defined as the operation of the lamp (and therefore of the laser) with no control over the drive circuit, i.e., the capacitor discharges its energy according to the time constant of the circuit at the terminals of the capacitor. The circuit "seen" by the capacitor can be modelled as a resistance of value equal to R_{eq}, which is the Equivalent Resistance of the circuit at the capacitor's ends. Under this condition, the discharge of energy happens to follow an exponential law:

$$e^{-\frac{t}{\tau}} \tag{7.1}$$

with a time constant, $\tau = R_{eq} \times C$. Measurements were performed in order to ascertain the effective laser output, in accordance with the parameters associated with it.

Observations

The first tests to be conducted were to confirm that the system successfully triggered the discharge of the lamp.

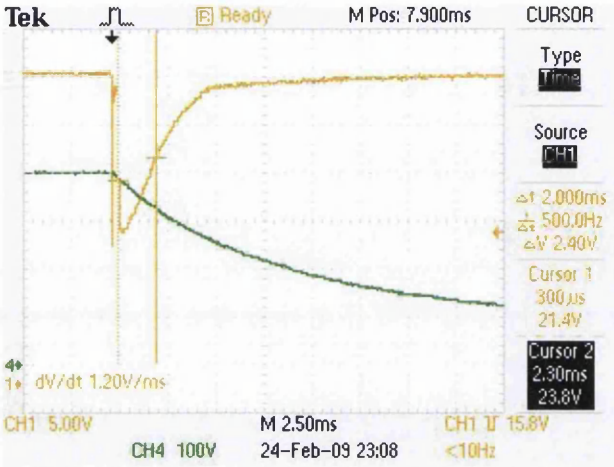

Figure 7.2: Flashlamp output with capacitor discharge curve

Fig. 7.2 shows a flashlamp discharge of $2ms$ Full-Width Half-Maximum (FWHM) which contains optical energy of $203J$

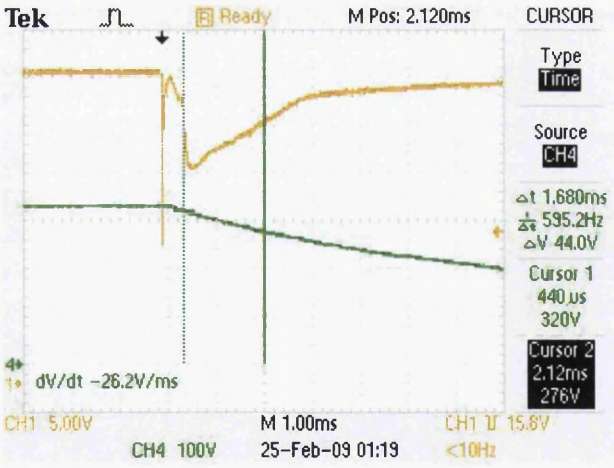

Figure 7.3: Laser output with capacitor discharge curve

Fig 7.3 shows the laser output pulse relative to the same capacitor discharge pulse. The laser output pulse contained $2J$ of optical energy and was of $2.4ms$ FWHM. A useful tool that is normally used during laser experiments is the so-called *ZAP-IT Paper*. It is a black

coated paper which when subject to incident laser light pulse, gives a permanent visual record, corresponding to the energy distribution within the laser beam. With the *ZAP-IT Paper* it is possible to analyse the Beam shape Mode, Intensity, Divergence and Energy Distribution of the laser pulse (see [94]).

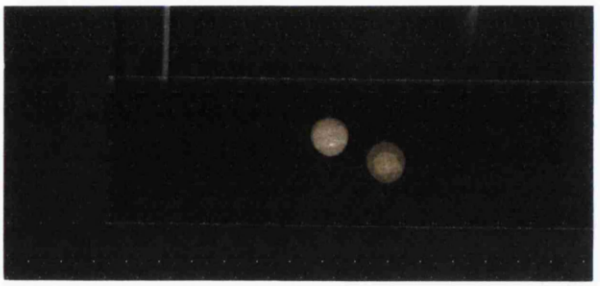

Figure 7.4: Nd:YAG pulse using the Digital Power Supply Unit (DPSU) in free discharge mode

Fig. 7.4 shows two Nd:YAG laser pulses obtained with the system in free discharge.

Within this section we have demonstrated the feasibility of producing a laser output from our system under test. This result is non trivial, given the nature of the technology under evaluation.

7.5.2 Controlled Laser Operation

In the previous section feasibility of laser output from our substem has been shown. This section investigates the attempt at controlling the laser pulse to produce pulses with arbitrary shape and duration.

Fig 7.5 shows direct control of the YAG laser output following digital control of the discharge. The orange curve is the capacitor discharge, the blue curve is the flashlamp discharge, and the green cuve is the laser output.

The left hand trace of Fig 7.5 shows a laser pulse of $1.75ms$ and the right hand trace a laser pulse of $2.75ms$

Fig. 7.6 demonstrates the ability of the techniuque to control ont only the duration of the YAG laser pulse, but also the shape. The figure shows a sequence taking at the outset a near triangular or ramp form and resulting, in five step, in a near top-hat form. In this sequence, the energy of the pulse has been allowed to increase from $1.65J$ to $1.85J$.

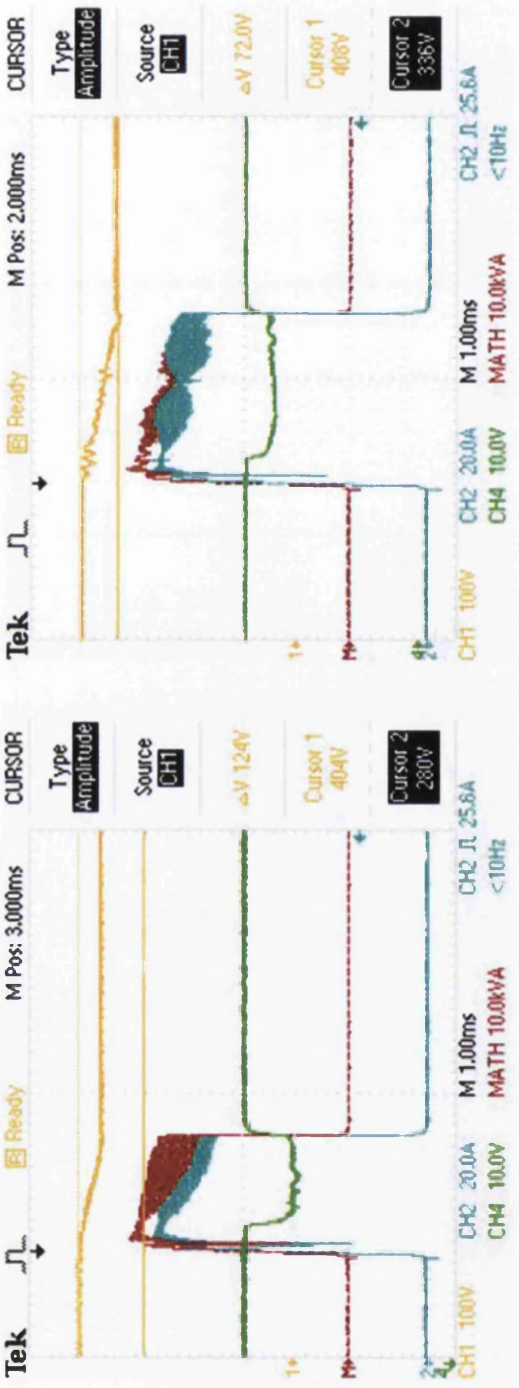

Figure 7.5: Direct digital control of the time duration of a square laser pulse

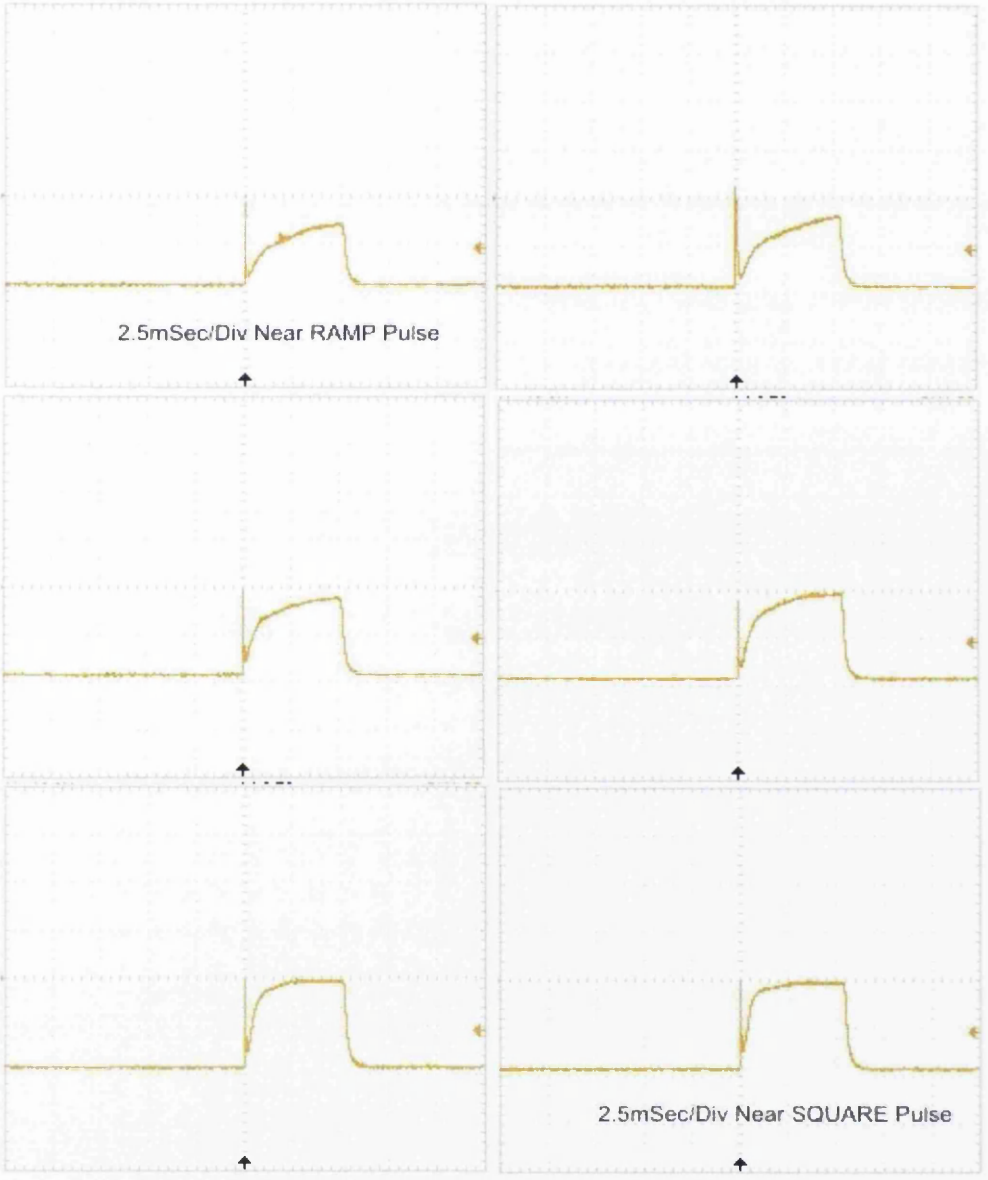

Figure 7.6: Sequence showing the ability of the developed technique to change the temporal shape of a laser pulse

Fig. 7.7 shows a sequence of eight pulses controlled to deliver equal energy with the rise time of the leading edge adjusted, enabling accurate control of the laser-tissue interaction which can be explosive for fast-rise times.

Fig. 7.8 shows the application of pulse shaping techniques for the arbitrary shaping of a YAG pulse.

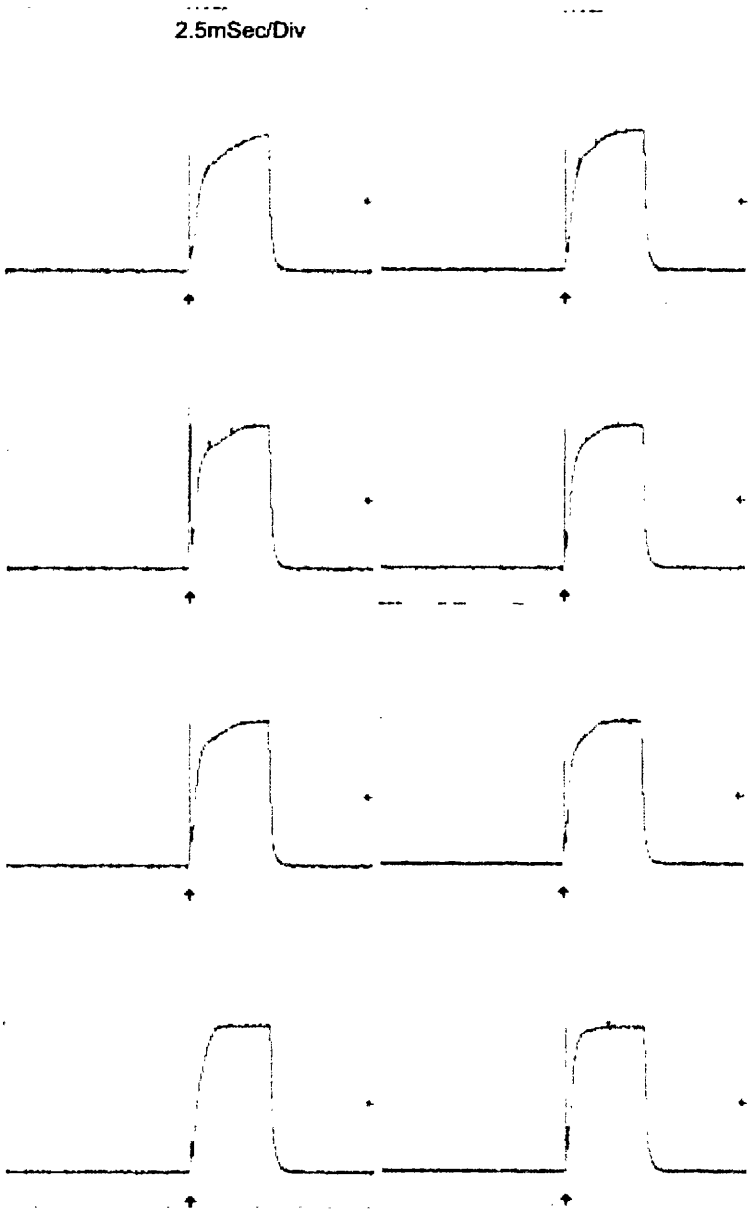

Figure 7.7: A sequence of light pulses of equal energy showing accurate control of the leading edge

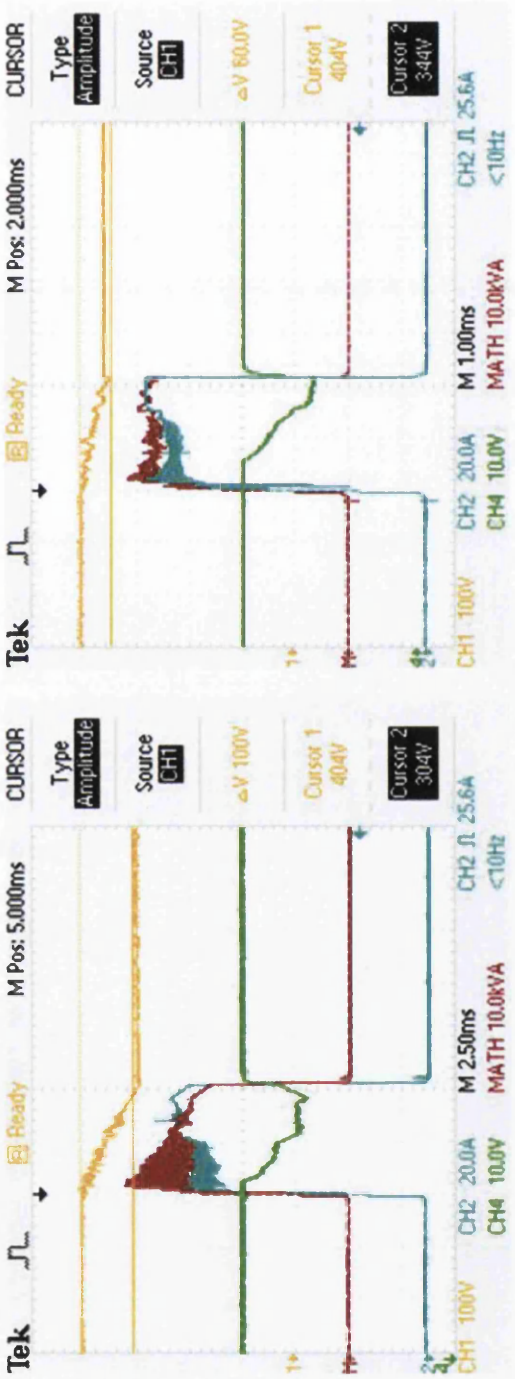

Figure 7.8: Direct digital control of the shape and rise time of a triangular laser pulse

Chapter 8

Discussion

Vascular lesions, be they thread veins, telangiectasia or Port Wine Stains, are difficult to treat when the vessels increase in size. Laser technology is by far the most promising treatment modality but it itself has been in need of new innovation to achieve the desired therapeutic and cosmetic output.

Wavelengths of the order of $1\mu m$, fluences of up to $200Jcm^2$ and beyond with pulse durations in the 10's of milliseconds are accepted to be the parameters of choice. Despite many advances in optical device technology, the traditional Nd:YAG laser still seems to be the best candidate technology. However, with traditional approaches, the temporal control of the Nd:YAG laser output has been problematic.

This study has challenged, through advanced computer modelling, the basic premise that temporal control of the Nd:YAG can enhance therapeutic benefit. The results of that modelling has shown that control of the pulse duration, together with the temporal shape of the pulse, does in theory have the capability of enhancing therapeutic output by increasing vessel necrosis without damaging the skin surface or surrounding tissue structures.

Following theoretical confirmation of the hypothesis, and building on the work of others, a system capable of digitally controlling the laser output was designed, developed and tested. Earlier workers had shown that digital control of the discharge of a capacitor allowed the accurate

control of the output of a flashlamp. This study took that work a stage further and showed that controlling the light output from the flashlamp had direct influence on the Nd:YAG laser output pumped by that discharge.

The approach adopted allowed the user to control the pulse duration but went further and allowed the temporal shape of the pulse to be adjusted as required. This temporal control was achieved without any need for major hardware redesign as the adjustment means was incorporated into a software driven system.

This innovative approach is yet to be tested clinically. The work has shown that the technique can deliver the desired temporal profile; if applied to a scaled-up system it can also be able to deliver the desired fluence for effective clinical applications; all this with almost unlimited flexibility. The next logical steps would be to conduct clinical trials on vascular lesions which have been shown to respond positively to the Nd:YAG wavelength. Those trials could include a personalisation of the temporal profile of the target patient. Having studied the impact on efficacy, both therapeutically and cosmetically, the technique could be combined with real-time measurement systems that would define treatment parameters not only specific to the lesion but to individual areas of the treatment site.

Chapter 9

Conclusions and future work

This thesis, at the outset, defined two research questions, namely:

- Can the accurate control of the temporal form of a Nd:YAG laser in principle deliver improved therapeutic benefit when analysed theoretically?
- Can the necessary level of control of the optical output of the Nd:YAG laser be achieved utilising sophisticated digital control techniques?

These two research questions have been studied and investigated through literature survey, computer modelling and the design, construction and testing of an innovative technical solution.

The study has concluded that:

- In theory, the temporal control of the Nd:YAG laser can increase damage to, and necrosis of, vascular lesions without increase in side effects;
- The digital control of the discharge of a flashlamp pump of a YAG laser can lead to the accurate control of laser output and delivery of optical parameters that have been proven to be beneficial for the clinical application under consideration.

Bibliography

[1] Sobotta (2001) *Atlas of Human Anatomy*, vol. Volume 1. Lippincott Williams & Wilkins, 13th edition edn.

[2] Ash, C. (2009) *Optimising Output Dosimetry of a Broadband Pulsed Light Source for the Removal of Unwanted Hair*. Ph.D. thesis, School of Medicine.

[3] Viator, J., Komadina, J., Svaasand, L., Aguilar, G., Choi, B., and Nelson, S. (2004) A comparative study of photoacoustic and reflectance methods for determination of epidermal melanin content. *Journal of Investigative Dermatology*, **vol. 122**, 14321439.

[4] Jacques, S. and Prahl, S. (1987) Modelling optical and thermal distributions in tissue during laser irradiation. *Lasers in Surgery and Medicine*, **vol. 6**, 494–503.

[5] Kauvar, A. and Khrom, T. (2005) Laser treatment of leg veins. *Semin Cutan Med Surg*, **vol. 24**, 184–192.

[6] Kiernan, M. (1997) *An Analysis of the Optimal Laser Parameters Necessary for the Treatment of Vascular Lesions*. Ph.D. thesis, University of the West of England - Swansea Institute of Higher Education.

[7] Source: http://fgmdb.kakuda.jaxa.jp/sspshtml/e-001st1.html.

[8] Source: http://cord.org/step_online/st1-5/st15ei3.htm.

[9] VLOC Yttrium aluminium garnet laser materials. Tech. rep., VLOC, 7826 Photonics Drive, New Port Richey, FL 34655.

[10] Source: en.wikipedia.org/wiki/file:various_laser_pump.

[11] Koechner, W. and Bass, M. (2003) *Solid-State Lasers*. Springer.

[12] Goncz, J. (1966) *Instr. Soc. Am. Trans.*, **vol. 5**.

[13] Ash, C. (2008) In-vivo measurements of stimulated transient cyanosis using rgb histogram and a spectrometer irradiated with intense broadband light. *CyDen Private Communication*.

[14] Perkin-Elmer, Application notes - trigger circuits, technical report. http://www.perkinelmer.co.uk.

[15] Prahl, S., Keijzer, M., Jacques, S., and Welch, A. (1989) A monte carlo model of light propagation in tissue. *SPIE Intitute Series*, **vol. IS 5**, 102–111.

[16] Siemens, Sfh-300 / sfh-300fa npn-silizium-fototransistor [datasheet]. Source: http://www.datasheetarchive.com/SFH2030-datasheet.html.

[17] Townes, C. H. (2003) *A Century of Nature: Twenty-One Discoveries that Changed Science and the World*, chap. The First Laser, pp. 107–112. University of Chicago Press.

[18] Einstein, A. (1917) Zur quantentheorie der strahlung (on the quantum theory of radiation). *Physika Zeitschrift*, **vol. 18**, 121–128.

[19] Hecht, J. (1992) *The Laser Guidebook*. McGraw-Hill, 2nd edn.

[20] Goldberg, D. J. (2005) *Laser Dermatology*. Springer.

[21] Campbell, C., Rittler, M., and Koester, C. (1963) The optical maser as a retinal coagulator: an evaluation. *Trans Am Acad Ophthalmol Otolaryngol.*, **vol. 67**, 58–67.

[22] Goldman, L., Blaney, D., D.J.and Kindel, and Franke, E. (1963) Effect of the laser beam on the skin. preliminary report. *J Invest Dermatol.*, **vol. 40**, 121–2.

[23] Muller, G., Berlien, P., and Scholz, C. (1986) Der laser in de medizin. *Umschan*, **vol. 4**, 233–240, English Translation: Medical Laser Application, vol. 21 (006) pp.99-108.

[24] Eichmann, A. (1989) Laser applications in dermatology. *Schweiz Rundsch Med Prax.*, **vol. 78(16)**, 474–6, article in German.

[25] Lask, G. P. and Glassberg, E. (1995) Neodymium:yttrium -aluminum -garnet laser for the treatment of cutaneous lesions. *Clinics in Dermatology*, **vol. 13, issue 1**, 81–86, Cutaneous Laser Therapy.

[26] Greve, B. and Raulin, C. (2000) The neodymium yag laser: its application in dermatology. *Hautarzt*, **vol. 51(3)**, 152–8, article in German.

[27] Kilmer, S. and Garden, J. (2000) Laser treatment of pigmented lesions and tattoos. *Semin Cutan Med Surg.*, **vol. 19(4)**, 232–44.

[28] Kilmer, S. (2002) Laser eradication of pigmented lesions and tattoos. *Dermatol Clin. 2002*, **vol. 20(1)**, 37–53.

[29] Wheeland, R. (1993) Treatment of port-wine stains for the 1990s. *J Dermatol Surg Oncol.*, **vol. 19(4)**, 348–56.

[30] Garden, J. and Bakus, A. (1997) Laser treatment of port-wine stains and hemangiomas. *Dermatol Clin.*, **vol. 15(3)**, 373–83.

[31] Alster, T. and Railan, D. (2006) Laser treatment of vascular birthmarks. *J Craniofac Surg.*, **vol. 17(4)**, 720–3.

[32] Haedersdal, M., Togsverd-Bo, K., and Wulf, H. (2008) Evidence-based review of lasers, light sources and photodynamic therapy in the treatment of acne vulgaris. *J Eur Acad Dermatol Venereol.*, **vol. 22(3)**, 267–78.

[33] Anderson, R. and Parrish, J. (1983) Selective photothermolysis: precise microsurgery by selective absorption of pulsed radiation. *Science*, **vol. 220 issue 4596**, 524–27.

[34] Apfelberg, D., Maser, M., Lash, H., White, D., and Flores, J. (1985) Comparison of the argon and carbon dioxide laser treatment of decorative tattoos: a preliminary report. *Ann Plast Surg*, **vol. 14**, 6–15.

[35] De Coste, S. and Anderson, R. (1991) Comparison of q-switched ruby and q-switched nd:yag laser treatment of tattoos. *Lasers Surg Med Suppl 3*, p. 64.

[36] Kilmer, S., Lee, M., Grevelink, T., J.M. ans Flotte, and Anderson, R. (1993) The q-switched nd:yag effectively treats tattoos: a controlled, dose response study. *Arch Dermatol.*, **vol. 129(8)**, 971–8.

[37] Kilmer, S. and Anderson, R. (1993) Clinical use of the q-switched ruby and the q-switched nd:yag (1064 nm and 532 nm) lasers for treatment of tattoos. *J Dermatol Surg Oncol.*, **vol. 19(4)**, 330–8.

[38] Kilmer, S. (1997) Laser treatment of tattoos. *Dermatol Clin.*, **vol. 15(3)**, 409–17.

[39] Kuperman-Beade, M., Levine, V., and Ashinoff, R. (2001) Laser removal of tattoos. *Am J Clin Dermatol.*, **vol. 2(1)**, 21–25.

[40] Bernstein, E. (2006) Laser treatment of tattoos. *Clin Dermatol.*, **vol. 24(1)**, 43–55.

[41] Watts, M. T., Downes, R. N., Collin, J. R., and Walker, N. P. (1992) The use of q-switched nd: Yag laser for removal of permanent eyeliner tattoo. *Ophthalmic Plastic & Reconstructive Surgery*, **vol. 8, issue 4**, 292–294.

[42] Morelli, J. (1998) Use of lasers in pediatric dermatology. *Dermatol Clin.*, **vol. 16(3)**, 489–95.

[43] Stier, M., Glick, S., and Hirsch, R. (2008) Laser treatment of pediatric vascular lesions: Port wine stains and hemangiomas. *J Am Acad Dermatol.*, **vol. 58(2)**, 261–85.

[44] Cordisco, M. R. (2009) An update on lasers in children. *Curr Opin Pediatr.*, **vol. 21(4)**, 499–504.

[45] Wanner, M. (2005) Laser hair removal. *Dermatol Ther.*, **vol. 18(3)**, 209–16.

[46] Davoudi, S., Behnia, F., Gorouhi, F., Keshavarz, S., Nassiri Kashani, M., Rashighi Firoozabadi, M., and Firooz, A. (2008) Comparison of long-pulsed alexandrite and nd:yag lasers, individually and in combination, for leg hair reduction: an assessor-blinded, randomized trial with 18 months of follow-up. *Arch Dermatol.*, **vol. 144(10)**, 1323–7.

[47] Khoury, J., Saluja, R., and Goldman, M. (2008) Comparative evaluation of long-pulse alexandrite and long-pulse nd:yag laser systems used individually and in combination for axillary hair removal. *Dermatol Surg.*, **vol. 34(5)**, 665–70; discussion 670–1.

[48] Haedersdal, M. and Wulf, H. (2006) Evidence-based review of hair removal using lasers and light sources. *J Eur Acad Dermatol Venereol.*, **vol. 20(1)**, 9–20.

[49] Haedersdal, M. and Goetzsche, P. (2006) Laser and photoepilation for unwanted hair growth. *Cochrane Database Syst Rev.*, **issue 4**.

[50] Civas, E., Koc, E., Aksoy, B., and Aksoy, H. (2009) Clinical experience in the treatment of different vascular lesions using a neodymium-doped yttrium aluminum garnet laser. *Dermatol Surg.*, **vol. 35**, 1933–1941.

[51] Simonsen, I. and Kiernan, M. (2006) *Flashlamp drive circuit*. UK PCT/G05/01977.

[52] Troilius, A. (1999) *Characterisation and Treatment of Patients with Port Wine Stains with Special Reference to the Emotional Impact*. Ph.D. thesis, Lund University.

[53] Moure, C., Reynaert, G., Lehmman, P., Testelin, S., and Devauchelle, B. (2007) Classification of vascular tumors and malformations: basis for classification and clinical purpose. *Rev Stomatol Chir Maxillofac.*, **vol. 108(3)**, 201–9.

[54] Wassef, M., Vanwijck, R., Clapuyt, P., Boon, L., and Magalon, G. (2006) Vascular tumours and malformations, classification, pathology and imaging [article in french]. *Ann Chir Plast Esthet.*, **vol. 51(4-5)**, 263–81.

[55] Mulliken, J. and Glowacki, J. (1982) Hemangiomas and vascular malformations in infants and children: a classification based on endothelial characteristics. *Plast Reconstr Surg.*, **vol. 69(3)**, 412–22.

[56] Haggstrom, A., et al. (2006) Prospective study of infantile hemangiomas: Clinical characteristics predicting complications and treatment. *Pediatrics*, **vol. 118**, 882–887.

[57] Laut-Labrze, C., Dumas de la Roque, E., Hubiche, T., Boralevi, F., Thambo, J., and Taeb, A. (2008) Propanolon for severe haemangiomas of infancy. *N Engl J Med.*, **vol. 358(12)**, 2649–51.

[58] Folkow, B. and Neil, E. (1971) *Circulation*. New York Press.

[59] Guyton, A. (1971) *Basic Human Physiology: Normal Function and Mechanisms of Disease*. W.B. Saunders Co.

[60] Rhodin, J. (1962) Fine structure of vascular walls in mammals with special reference to smooth muscle component. *Physiol Rev*, **vol. 42**.

[61] Barton, J., Pfefer, J., Welch, A., Smithies, D., Nelson, S., and van Gemert, M. (1998) Optical monte carlo modelling of a true port wine stain anatomy. *Opt. Express.*, **vol. 2(9)**, 391–6.

[62] Sardar, D., Mayo, M., and Glickman, R. (2001) Optical characterisation of melanin. *Journal of Biomedical Optics*, **vol. 6(4)**, 404411.

[63] Plaetzer, K., Krammer, B., Berlanda, J., and Berr, T., F.and Kiesslich (2008) Photophysics and photochemistry of photodynamic therapy: fundamental aspects. *Lasers Med Sci*, **vol. 24(2)**, 259–68.

[64] Niemz, M. (2007) *Laser-Tissue Interactions - Fundamentals and Applications*. Biological and Medical Physics, Biomedical Engineering, Springer, 3rd edn.

[65] Sarna, T. (1992) Properties and function of the ocular melanin-a photobiophysical view. *J Photochem Photobiol B.*, **vol. 12(3)**, 215–58.

[66] Chandrasekhar, S. (1960) Radiative transfer. *Dover Publications Inc*, p. 393.

[67] Goldberg, D. J. (2007) *Laser Dermatology: Pearls and Problems*. WileyBlackwell, 1st ed. edn.

[68] Tseng, S., Bargo, P., Durkin, A., and Kollias, N. (2009) Chromophore concentrations, absorption and scattering properties of human skin in-vivo. *Opt Express.*, **vol. 17(17)**, 1459914617.

[69] Altshuler, G., Anderson, R., Manstein, D., Zenzie, H., and Smirnov, M. (2001) Extended theory of selective photothermolysis. *Lasers in Surgery and Medicine*, **vol. 29**, 416–432.

[70] Ross, E. (2001) Extended theory of photothermolysis: a new recipe for hair cooking? *Laser Surg Med*, **vol. 29**, 413–415.

[71] Schawlow, A. and Townes, C. (1960) *Masers and maser communication system*. US Patent 2,929,922.

[72] Schawlow, A. and Townes, C. (1958) Infrared and optical masers. *Phys. Rev.*, **vol. 112**, 1940.

[73] Maiman, T. (1967) *Ruby laser systems*. No. 3,353,115, US Patent 3,353,115.

[74] WAGNER, W. and LENGYEL, B. (1963) Evolution of the giant pulse in a laser. *J. Appl. Phys.*, **34**, 2040–6.

[75] Galeckas, K. (2008) Update on lasers and light devices for the treatment of vascular lesions. *Semin Cutan Med Surg*, **vol. 27**, 276–284.

[76] Ross, E., Smirnov, M., Pankratov, M., and Altshuler, G. (2005) Intense pulsed light and laser treatment of facial telangiectasias and dyspigmentation: some theoretical and practical comparisons. *Dermatol Surg.*, **vol. 31**, 1188–98.

[77] Rogachefsky, A., Silapunt, S., and Goldberg, D. (2002) Nd:yag (1064nm) irradiation for lower extremity telangiectases and small reticular veins: Efficacy as measured by vessel color size. *Dermatol. Surg.*, **vol. 28**, 220–223.

[78] Galeckas, K., Ross, E., and Uebelhoer, N. (2008) A pulsed dye laser with a 10-mm beam diameter and a pigmented lesion window for purpura-free photorejuvenation. *Dermatol Surg*, **vol. 34**, 308–313.

[79] Passeron, T., Olivier, V., Duteil, L., Desruelles, F., Fontas, E., and Ortonne, J. (2003) The new 940-nanometer diode laser: An effective treatment for leg venulectasia. *J Am Acad Dermatol*, **vol. 48**, 768–74.

[80] Perkin-Elmer, Flash lamps. http://www.perkinelmer.co.uk.

[81] Chul Lee, H. and Pyung Kim, Y. (2008) Output characteristics of a flashlamp pumped nd:yag laser at 1444nm. *Optics & Laser Technology*, **vol. 40**, 901–5.

[82] Hammond, T. and Lama, W. (1985) *Flash lamp power supply with reduced capacitance requirements*. US Patent 4524289.

[83] Inochkin, M., Togatov, V. V., and Gnatyuk, P. O. (2003) *Flashlamp drive circuit*. US Patent 20030057875.

[84] Cashwell, E. and Everett, C. (1959) *A practical manual on the Monte Carlo method for random walk problems*. Pergammon Press.

[85] Metropolis, N. and Ulam, S. (1949) The monte carlo method. *J. Am Statistical Association*, **vol. 44**, 335–341.

[86] Welch, A., Wissler, E., and Priebe, L. (1980) Significance of blood flow in calculations of temperature in laser irradiated tissue. *IEEE Trans Biomed Eng.*, **vol. 27**, 164–6.

[87] Jain, K. (1983) Photocoagulation of cerebral arteriovenous malformations and arterial aneurysms with the neodymium: yttrium-aluminum-garnet or argon laser. *Neurosurgery*, **vol. 13**, 734–36.

[88] Donne, K. (2000) Two dimensional computer model of laser tissue interaction - private communication.

[89] Daniels, G. (2002) *Optical and Thermal Transport Modelling of Laser-Tissue interaction.* Ph.D. thesis, University of the West of England, Bristol.

[90] Farrell, T. and Patterson, M. (1992) A diffusion theory model of spatially resolved, steady-state diffuse reflectance for the noninvasive determination of tissue optical properties in vivo. *Medical Physics*, **vol. 19**, 879–888.

[91] Moore, G. E. (1965) Cramming more components onto integrated circuits. *Electronics Magazine*, **vol. 38**.

[92] Disco, C. and van der Meulen, B. (eds.) (1998) *Getting New Technologies Together: Studies In Making Sociotechnical Order*. Walter de Gruyter & Co.

[93] Source: www.tektronix.co./tps2000, pp. 1-8 (2005).

[94] Source: http://www.zap-it.com/.

[95] Altshuler, G. and Zenzie, H. (2008) *System for electromagnetic radiation dermatology and head for use therewith.* US Patent 7431719 B2.

[96] Farnsworth, R. (1987) *Wide Band, High Efficiency Simmer Power Supply For a Laser Flashlamp*. Patent WO87/04038.

[97] Inochkin, M., Togatov, V., and Gnatyuk, P. (2009) *Flashlamp Drive Circuit*. US Patent 7531967B2.

[98] Source: http://www.adeptscience.co.uk/products/dataanal/easyplot/.